

Quantifying the Contributors to Extreme Sea Level Events in the Western Mediterranean at High Spatio-temporal Resolution

Jorge Ramos-Alcántara¹, Miguel Agulles², Damia Gomis³, and Gabriel Jordà¹

¹Centre Oceanogràfic de Balears (IEO-CSIC)

²Mediterranean Institute for Advanced Studies (IMEDEA, University of the Balearic Islands - CSIC)

³IMEDEA, Spain

May 13, 2023

Abstract

A comprehensive characterisation of extreme sea levels at different spatio-temporal scales is presented for the Western Mediterranean. The classical view of extreme sea levels as a consequence of the concurrence of storm events and high tides may lead to an incomplete picture for the Mediterranean coasts, where the tidal regime is small and processes operating at high frequencies can contribute significantly to extreme levels. Our approach bases on the analysis of tide gauge records with a high sampling frequency (1 minute), in order to consider other contributors beyond storm surges and tides. To have a basin-scale view, we first analyse the tide gauges operated by Puertos del Estado, which are distributed over all the Spanish Mediterranean coasts and cover at least from 2010 to 2022. Next, we focus on a more reduced domain to take advantage of the unprecedented spatio-temporal resolution of the VENOM tide gauge network, operating since 2020 in the Balearic archipelago. Last, we analyse the role of waves in local extreme sea level events by propagating waves towards the coast in the Bay of Palma. The wave run-up estimates are calculated considering the type of coastal protection and are used to simulate the potential flooding that could occur in the future under an unfavourable climate change scenario. Our results highlight the importance of high-frequency sea level records to study extreme events, and the key role of processes such as meteotsunamis and waves in the occurrence of extreme sea levels.

1 **Quantifying the Contributors to Extreme Sea Level Events in the Western**
2 **Mediterranean at High Spatio-temporal Resolution**

3
4 **J. Ramos-Alcántara^{1,2}, M. Agulles², D. Gomis² and G. Jordà¹**

5
6 ¹ Centre Oceanogràfic de Balears, C.N. Instituto Español de Oceanografía (CSIC), Palma de
7 Mallorca, 07015, Spain.

8 ² Institut Mediterrani d'Estudis Avançats, IMEDEA (UIB-CSIC), Esporles (Mallorca), 07190,
9 Spain.

10 Corresponding author: Jorge Ramos Alcántara (jorge.ramos@ieo.csic.es), Gabriel Jordà
11 (gabriel.jorda@ieo.csic.es)

12
13 **Key Points:**

- 14 • High frequency sea level records are needed to get a complete view of the processes
15 contributing to extreme sea levels.
- 16 • Sub-hourly processes can be a major contributor to extreme levels in some locations,
17 although they usually have a local scale.
- 18 • The contribution of waves to total sea level is highly dependent on the coastal
19 morphology, and can lead to a rise of several meters.

20 **Abstract**

21 A comprehensive characterisation of extreme sea levels at different spatio-temporal scales is
22 presented for the Western Mediterranean. The classical view of extreme sea levels as a
23 consequence of the concurrence of storm events and high tides may lead to an incomplete picture
24 for the Mediterranean coasts, where the tidal regime is small and processes operating at high
25 frequencies can contribute significantly to extreme levels. Our approach bases on the analysis of
26 tide gauge records with a high sampling frequency (1 minute), in order to consider other
27 contributors beyond storm surges and tides. To have a basin-scale view, we first analyse the tide
28 gauges operated by Puertos del Estado, which are distributed over all the Spanish Mediterranean
29 coasts and cover at least from 2010 to 2022. Next, we focus on a more reduced domain to take
30 advantage of the unprecedented spatio-temporal resolution of the VENOM tide gauge network,
31 opening since 2020 in the Balearic archipelago. Last, we analyse the role of waves in local
32 extreme sea level events by propagating waves towards the coast in the Bay of Palma. The wave
33 run-up estimates are calculated considering the type of coastal protection and are used to
34 simulate the potential flooding that could occur in the future under an unfavourable climate
35 change scenario. Our results highlight the importance of high-frequency sea level records to
36 study extreme events, and the key role of processes such as meteotsunamis and waves in the
37 occurrence of extreme sea levels.

38 **Plain Language Summary**

39 Sea level extremes can cause significant environmental damage and affect the well-being of
40 populations living in coastal regions. It is therefore essential to understand and quantify the
41 mechanisms behind these extreme events. Storms are often considered to be the only cause of
42 extreme sea levels; however, in this work we show that in some Mediterranean harbours there
43 are other processes taking place at local scale and over short periods of time than can contribute
44 to sea level extremes. We also show that the contribution of waves to coastal sea extreme
45 elevations can be very significant, though it largely depends on the type of coastline. In
46 particular, we show an example of the areas that could be flooded due to the wave contribution
47 under an unfavourable scenario of sea level rise due to global warming. Overall, we show that
48 for the study of extreme sea levels in the Mediterranean, using tide gauge series reporting at least

49 one datum per minute is essential, in order to consider the contribution of processes that are not
50 usually taken into account.

51 **1 Introduction**

52 Extreme sea level events in coastal regions occur as a consequence of the overlapping of
53 different processes that can act at different spatial and temporal scales. Extreme high waters can
54 cause significant environmental damage and affect the well-being of populations living in coastal
55 regions. Coastal flooding is one of the most common natural disasters (Noji, 1991) and can lead
56 to erosion, damage to infrastructures and even loss of lifes (Ruggiero et al., 2001; Wolf, 2009).
57 Moreover, in a context of global warming and projected sea level rise, the intensity of coastal
58 impacts associated with extreme sea level events is expected to increase significantly (Nicholls et
59 al., 2014; Wahl et al., 2017). In order to make proper assessments of the associated risks and
60 hazards, it is necessary to characterise extreme sea level events, analysing in detail their spatio-
61 temporal variability and quantifying the different processes contributing to extreme values (Del-
62 Rosal-Salido et al., 2021).

63 In the Mediterranean coastal zone, the absolute magnitude of extreme events is small compared
64 to other coastal regions, in part due to the microtidal regime of the basin (Muis et al., 2016).
65 However, the microtidal regime also makes that coastal infrastructures are not as well adapted to
66 large sea level anomalies as in other regions with larger tidal ranges. Furthermore, an important
67 part of the economy of Mediterranean regions depends on coastal activities (e.g. tourism, trading
68 and transport, ...), making this region particularly vulnerable to the consequences of extreme sea
69 levels (Agulles et al., 2021; Gomis et al., 2012).

70 Coastal sea level variability results from the overlapping of many physical processes operating
71 over a wide range of frequencies and spatial scales. Those taking place on long time scales (e.g.
72 seasonal to multidecadal) are assumed to behave similarly in the coastal zone and in the open
73 ocean. On the other hand, coastal areas are also affected by other contributions with shorter
74 temporal and spatial scales, such as storm surges, seiches and wave runup (Woodworth et al.,
75 2019). In practice, extreme sea level events are often quantified as the result of just two
76 processes: tides and storm surges (Menéndez & Woodworth, 2010; Middleton & Thompson,
77 1986; Muis et al., 2016). However, up to our knowledge the accuracy of this approach has not

78 been assessed in the Mediterranean Sea, where there are clues suggesting the significant
79 contribution of other processes.

80 One of the coastal phenomena that may contribute to Mediterranean extreme events are
81 meteotsunamis, atmospherically-induced waves in the tsunami frequency band (2-120 min) that
82 can cause considerable damage to infrastructure and ships (see e.g. Monserrat et al., 2006;
83 Rabinovich, 2020). Vilibić & Šepić (2017) suggested that the contribution of such high
84 frequency phenomena to extreme coastal sea level events could be of up to 50%. Another
85 important driver of coastal sea level is the effect of waves reaching the coast, which can lead to
86 an elevation of sea level over the still water level (referred to as wave runup). The wave runup is
87 in fact the sum of the wave setup elevation onshore and the effect of swash fluctuations (Melet et
88 al., 2018; Ruggiero et al., 2001). This phenomenon can be a dominant contributor in coastal
89 extreme events causing overtopping of coastal infrastructures (Raby, 2003). Although
90 Mediterranean wave heights are usually smaller than in the large oceans, their role can be
91 important in extreme events such as the storm Gloria, in 2020, when the main impacts on the
92 coast were caused by the large waves associated with strong winds (Amores et al., 2020; de
93 Alfonso et al., 2021).

94 When high frequency processes play an important role, the characterization of extreme sea level
95 contributors requires an adequate temporal sampling. Most of the studies undertaken so far have
96 used hourly time series from tide gauges (see e.g. Calafat et al., 2009; Callahan & Leathers,
97 2021; Tsimplis & Shaw, 2010), mainly because few long records with a higher frequency
98 sampling were available. However, the situation has changed in the recent years, and nowadays
99 it is possible to find tide gauge datasets covering several years with a 1-min resolution (e.g.
100 García-Valdecasas et al., 2021; Pérez Gómez et al., 2022). Another feature to be considered is
101 that most tide gauges are located in sheltered harbours, where the wave set-up signal is
102 diminished or practically not present; as a consequence, many of the operational tide gauges only
103 record what is known as Still Water Level (SWLs) (Lambert et al., 2020; Melet et al., 2018).
104 This makes that the only way to obtain a proper regional characterization of the wave effect on
105 sea level is using numerical models (Holthuijsen, 2007).

106 The main objective of this paper is to understand and quantify the different mechanisms
107 contributing to coastal extreme sea level events in the western Mediterranean. For this purpose,

108 we use 1-min tide gauge records altogether with outputs from storm surge and wave numerical
109 models. The paper is organised as follows: in section 2, we describe the datasets and the
110 methodology used to characterize the different contributors to extreme sea levels. Results are
111 presented in section 3, and consist of a first general characterisation of Western Mediterranean
112 extremes (Sect. 3.1) followed by the quantification of the different contributors (Sect. 3.2).
113 Particular attention is paid to the quantification of sub-hourly processes (sampled by an ultra-
114 dense network of tide gauges operating in the Balearic archipelago, Sect. 3.3) and to the
115 contribution of waves to coastal flooding (for the particular case of the Bay of Palma, Sect. 3.4).
116 Results also include an analysis of the spatial scale of each of the main contributors to extreme
117 sea levels (Sect 3.5). Results are discussed in section 4 and the final remarks given in section 5.

118 **2 Data and Methodology**

119 **2.1 Tide gauges records**

120 Several sets of tide gauges with different time coverages have been used; in a first step we used
121 data from tide gauges operated by Puertos del Estado, the Spanish holding of State Harbours
122 (<https://opendap.puertos.es/thredds/catalog.html>). The REDMAR sea level network of Puertos
123 del Estado operates 40 tide gauge stations and the network has been recently improved with the
124 incorporation of new radar sensors that measure sea level at a frequency of 2 Hz (Pérez et al.,
125 2013). From this dataset, the 17 stations located in the Mediterranean Sea (Fig. 1a) were selected
126 and a minute time vector covering the period from 2010 to 2022 was defined (Table 1). In the
127 framework of the VENOM project (acronym in Spanish of “Spatial Variability of Sea Level in
128 the Western Mediterranean”), a low-cost ultra-dense and self-built tide gauge network has been
129 recently deployed along the coasts of the Balearic Islands. The 20 VENOM tide gauges record
130 sea level variations with a 1-min sampling rate, and add to other 12 tide gauges operated by other
131 institutions and recording at the same frequency rate. Basing on the location, sampling rate and
132 record length, we selected 21 tide gauges (listed in Table 2, Fig. 1b): 10 from the VENOM
133 network, 5 operated by Puertos del Estado, 5 operated by the Balearic Islands Coastal Observing
134 and Forecasting System (SOCIB: <https://www.socib.es/>, Tintoré et al (2013)) and 1 operated by
135 Ports IB (<http://webtrans.geonica.com>). Altogether they constitute a network with an
136 unprecedented high spatial density, which allows to investigate the small scale spatial variability
137 of the different contributors to extreme sea level events. The resulting dataset has an average

Table 1: Mediterranean tide gauges operated by Puertos del Estado, with their Location, Date of the first and last data of the considered series, and the Percentage of Missing Data.

Station	Latitude(°)	Longitude(°)	First data	Last data	Missing values (%)
Tarifa	36.01	-5.60	01 January 2010	09 May 2022	6.47
Algeciras	36.18	-5.40	01 January 2010	09 May 2022	5.53
Málaga	36.71	-4.42	01 January 2010	09 May 2022	8.48
Motril	36.72	-3.52	01 January 2010	09 May 2022	6.58
Melilla	35.29	-2.93	01 January 2010	09 May 2022	9.83
Almería	36.83	-2.48	01 January 2010	09 May 2022	7.41
Carboneras	36.97	-1.90	25 April 2013	09 May 2022	7.89
Gandía	38.99	-0.15	01 January 2010	09 May 2022	4.36
Valencia	39.44	-0.31	01 January 2010	09 May 2022	7.77
Sagunto	39.63	-0.21	01 January 2010	09 May 2022	6.07
Tarragona	41.08	1.21	27 May 2011	09 May 2022	6.09
Barcelona	41.34	2.17	01 January 2010	06 May 2022	5.51
Ibiza	38.91	1.45	01 January 2010	09 May 2022	5.57
Formentera	38.73	1.42	22 January 2010	09 May 2022	8.59
Palma	39.56	2.64	01 January 2010	09 May 2022	16.45
Alcudia	39.83	3.14	01 January 2010	09 May 2022	11.30
Mahón	39.89	4.27	01 January 2010	09 May 2022	10.10

138 separation between stations of 8.7 km, in contrast with the average separation of the REDMAR
 139 tide gauge network in the Western Mediterranean, which is of 58.7 km. The first instruments of
 140 the VENOM network were installed at the beginning of 2020; the period used for the analysis
 141 performed in this work covers two years, from July 2020 to July 2022.

142 Tide gauge measurements are subject to errors of different nature that can affect the consistency
 143 and reliability of the series. Thus, a manual control was first applied to the series in order to
 144 detect and correct eventual discontinuities in the datum, and to discard out-of-range and other
 145 clearly anomalous values. An automatic quality control based on well-established procedures
 146 (see e.g. Reek et al., 1992; Williams et al., 2019) was subsequently applied. That second step
 147 included: (i) the elimination of values outside the interval defined by the average of each series \pm
 148 4 times the standard deviation; (ii) the identification of spikes through the analysis of the
 149 differences between groups of 3 consecutive measurements. Finally, the measurements that

150 passed this quality control were converted into sea level anomalies (SLA) by subtracting the
 151 temporal average of the corresponding series.

Table 2: Selected tide gauges in the Balearic Islands, specifying the Institutions operating them, their Locations, the start and end Dates of the series and the Percentage of missing data.

Station	Institution	Latitude (°)	Longitude (°)	First data	Last data	Missing values (%)
Formentera	Puertos del Estado	38.73	1.42	19 July 2020	19 July 2022	1.41
Sant Antoni	SOCIB	38.98	1.30	19 July 2020	19 July 2022	1.26
Ibiza	Puertos del Estado	38.91	1.45	19 July 2020	19 July 2022	2.55
Santa Eulàlia	VENOM	38.98	1.54	10 March 2021	06 July 2022	34.44
Sa Ràpita	SOCIB	39.54	2.38	19 July 2020	19 July 2022	4.49
S'Arenal	VENOM	39.50	2.75	22 January 2021	17 June 2022	39.38
Palma	Puertos del Estado	39.56	2.64	19 July 2020	19 July 2022	0.29
Palma	VENOM	39.56	2.64	21 January 2021	02 June 2022	31.97
Andratx	SOCIB	39.36	2.95	19 July 2020	19 July 2022	7.18
Port de Sóller	VENOM	39.80	2.69	19 July 2020	15 July 2022	11.50
Alcudia	Puertos del Estado	39.83	3.14	19 July 2020	19 July 2022	1.58
Can Picafort	VENOM	39.77	3.16	03 March 2021	13 July 2022	32.23
Colonia Sant Pere	SOCIB	39.54	3.34	19 July 2020	19 July 2022	34.56
Cala Rajada	VENOM	39.71	3.46	19 July 2020	17 March 2022	23.11
Cala Bona	VENOM	39.61	3.39	24 February 2021	19 July 2022	30.23
Porto Cristo	SOCIB	39.74	3.27	19 July 2020	19 July 2022	0.40
Portocolom	VENOM	39.42	3.26	19 July 2020	19 July 2022	0.87
Portopetro	VENOM	39.36	3.21	19 July 2020	19 July 2022	0.97
Mahón	Puertos del Estado	39.89	4.27	19 July 2020	19 July 2022	1.74
Ciutadella	Ports IB	39.99	3.83	19 July 2020	19 July 2022	0.19
Fornells	VENOM	40.05	4.13	19 August 2020	30 December 2021	33.58

152

153 2.2 Decomposition of sea level records

154 In order to assess the role of the different processes contributing to sea level extremes, the tide
 155 gauge time series were split into several components (Fig. 2):

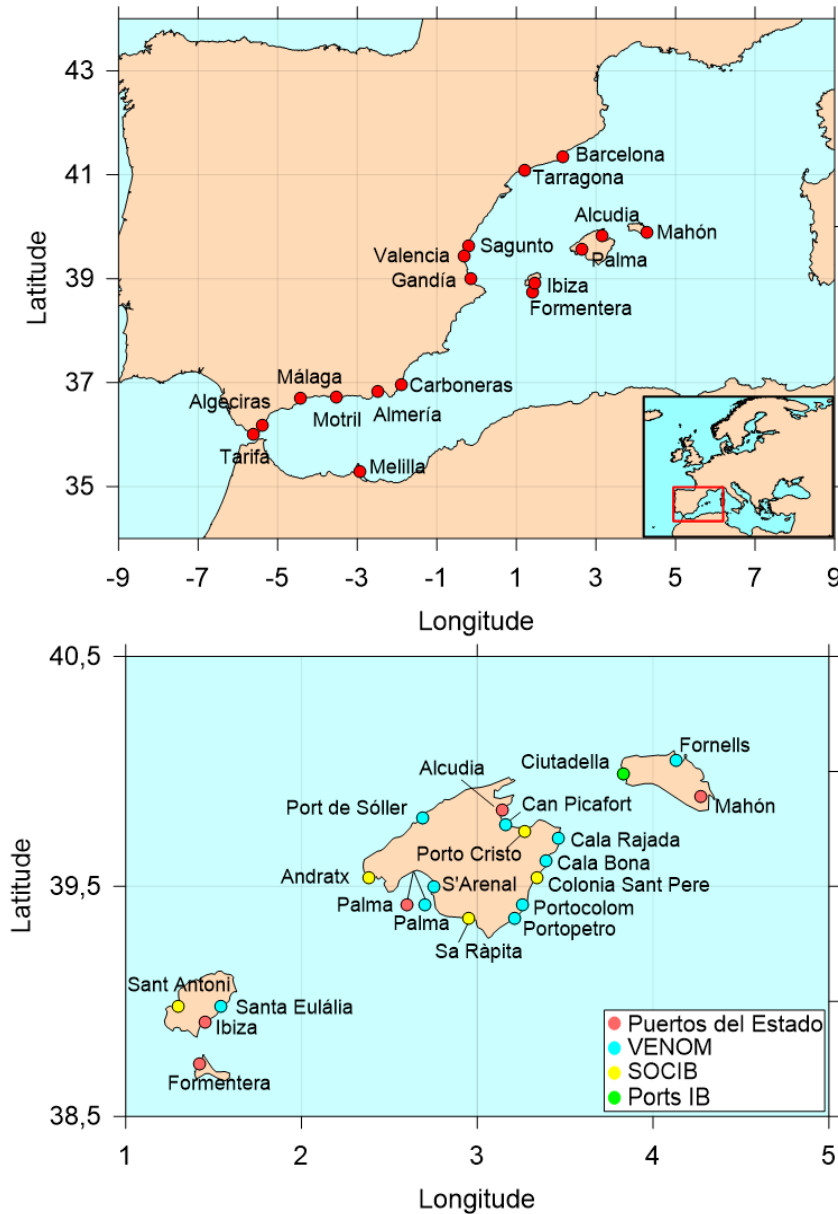


Figure 1: a) Location of the tide gauges from Puertos del Estado available in the Western Mediterranean, b) Location of the selected tide gauges in the Balearic archipelago, with the color indicating the institution operating them.

156 - **Atmospheric component:** Hourly sea level variations caused by changes in the atmospheric
 157 pressure and wind were obtained from the outputs of the NIVMAR forecasting system
 158 (Álvarez Fanjul et al., 2001), which are available from the website of Puertos del Estado
 159 (<http://opendap.puertos.es/thredds/catalog.html>). The NIVMAR system is based on the model
 160 HAMSON (Backhaus, 1985) forced by with wind and sea level pressure data provided by the

161 European Centre for Medium-Range Weather Forecasts (ECMWF, <https://www.ecmwf.int/>).
162 The hourly time series were first converted into 1-min time series using a linear interpolation
163 and then they were split into two frequency bands: $T > 1\text{month}$ and $T < 1\text{month}$, which will
164 hereafter be referred to as the low-frequency atmospheric contribution ($T > 1\text{month}$) and the
165 Storm Surge contribution ($T < 1\text{month}$). It is important to note that this approach differs from
166 other studies where the surge component is simply defined as the non-tidal residual of the
167 original series, without further considerations on the forcing mechanisms of the observed sea
168 level variability (Horsburgh & Wilson, 2007; Menéndez & Woodworth, 2010).

169 - **Seasonal cycle:** Seasonal sea level changes in the Mediterranean are mainly due to steric
170 effects in the upper ocean (Gomis et al., 2012; Tsimplis & Woodworth, 1994) and to seasonal
171 mass transports through the Strait of Gibraltar (Soto-Navarro et al., 2010). The seasonal cycle
172 was obtained by interpolating to 1-min the monthly averages of the tide gauge records once
173 the atmospheric component was removed.

174 - **Astronomical tide:** Once the atmospheric component and seasonal cycle were subtracted
175 from the original series, the remaining sea level signal was adjusted by using the Matlab
176 UTIDE functions (Codiga, 2023).

177 - **Residuals:** the residuals remaining after removing the previous components were separated
178 into three frequency bands: $T > 1\text{month}$, $1\text{hour} < T < 1\text{month}$, $T < 1\text{hour}$. Although these bands do
179 not correspond to specific physical processes, the main drivers of the variability of each band
180 are known. The lower frequency band ($T > 1\text{m}$) is mainly driven by the hydrodynamic
181 structure of the Mediterranean basin (Larnicol et al., 2002) and by changes in the
182 characteristics of the incoming Atlantic waters (Tsimplis et al., 2013). The high frequency
183 band ($T < 1\text{h}$) includes phenomena such as shelf waves or meteotsunamis, which can lead to
184 resonant responses of remarkable magnitude in different inlets and bays of the Western
185 Mediterranean (Monserrat et al., 2006). Finally, the intermediate frequency band ($1\text{h} < T < 1\text{m}$)
186 is the domain of other processes such as wave-induced variability or runoff from rivers
187 (Huthnance et al., 1986; Melet et al., 2018; Woodworth et al., 2019).

188 An example of the splitting of a tide gauge record (Mahón) into the described components is
189 shown in Fig. 2.

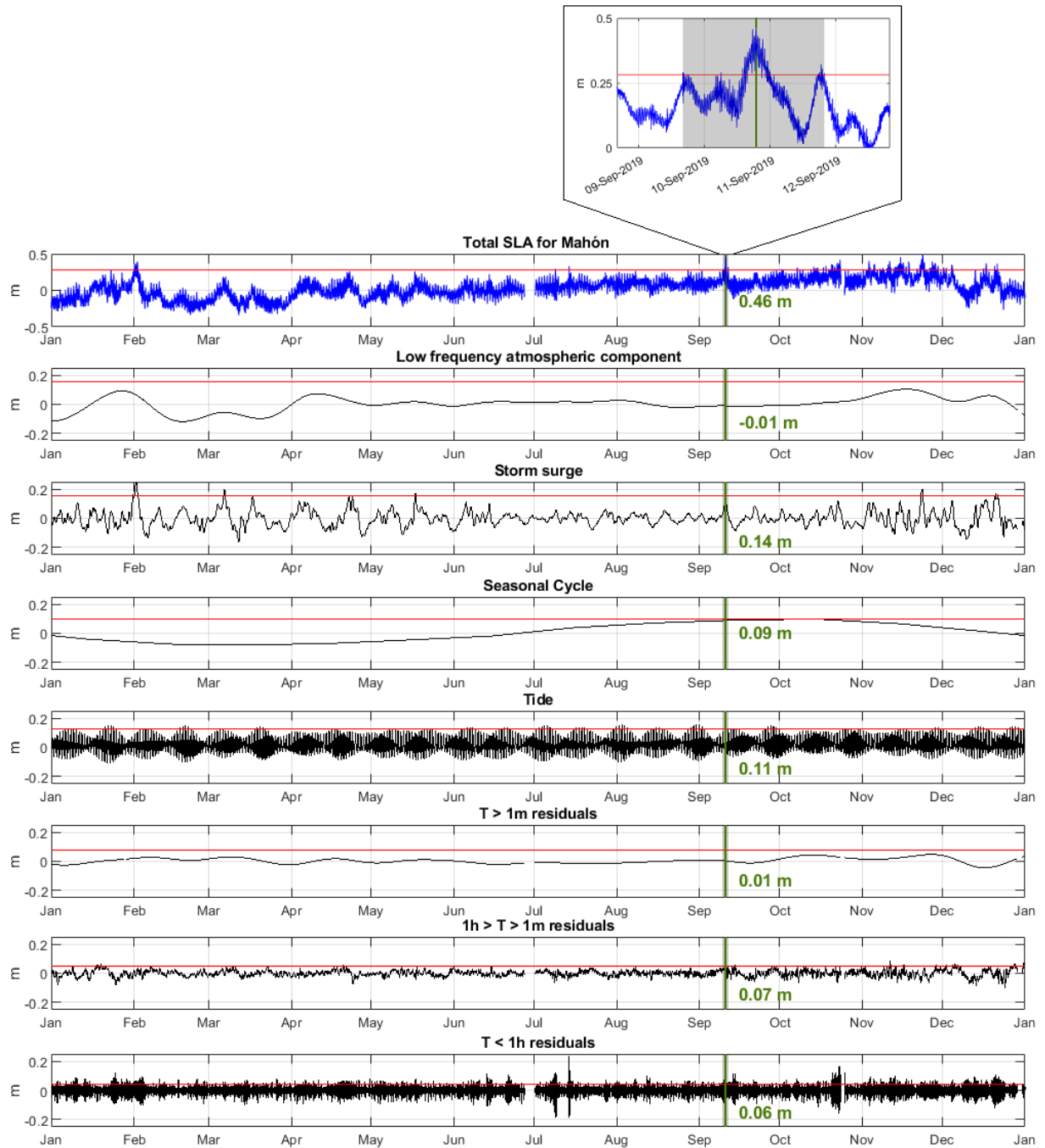


Figure 2: Component decomposition of the Mahón tide gauge record of 2019. For the total series and for each component, the 99th percentile has been marked with a red line. A particular extreme event is selected as example, indicating the time of its peak with a green line. The total sea level anomaly and the value of each component at the time of the peak is shown as green text. A zoom of this event is highlighted at the top of the figure.

190 2.3 Processing of extreme sea level events

191 Extreme sea level events were identified in the tide gauge series on the basis of their 99th
 192 percentile. Following the criteria of other authors (Calafat et al., 2014; Cid et al., 2016; Marcos
 193 & Woodworth, 2017), measurements over this threshold separated by less than 3 days were
 194 considered as a single event, in order to ensure the independence between events. After the
 195 identification, the main characteristics of the event (starting time, ending time, peak value,
 196 instant of maximum height and average value during the event) were determined. The duration
 197 of the event was determined as the time during which sea level was above the 99th percentile,
 198 between the starting and ending times of the event. Another interesting parameter is the intensity
 199 of the event, defined as the area between the series and the 99th percentile, integrated over the
 200 duration of the event. For this calculation we used the numerical integration method of the
 201 trapezoid rule (see e.g. Smyth, 2005).

202 To estimate return levels, we used the classical method of modelling exceedances over a
 203 threshold, through an Extreme-value distribution (Dupuis, 1999). The use of the extremes over a
 204 threshold is an appropriate alternative to modelling from the yearly maximum extremes, which
 205 can lead to a loss of information in the case that the extremes of any year are exceptionally low
 206 (Dey & Das, 2016; Marcos et al., 2009). Thus, if μ is the considered high threshold of a series
 207 (the 99.5th percentile in our case), the cumulative distribution function of the series of excesses
 208 $y = x - \mu$ can be approximated by the generalized Pareto distribution (GPD):

$$209 \quad H(y) = 1 - \left(1 - \frac{\xi y}{\sigma}\right)^{-\frac{1}{\xi}} \quad (1)$$

210 where ξ is the shape parameter and σ (>0) is the scale parameter, both being estimated by
 211 maximum likelihood. In our case the shape parameter must be $\xi \leq 0$, otherwise the distribution
 212 would have no upper limit and the existence of values over the threshold would not be possible.
 213 Fitting the extreme values to a GPD allows the estimation of the 95% confidence intervals for the
 214 parameters of the distribution, which in turn enables to establish confidence intervals for the
 215 calculated return levels.

216 Return levels can be directly calculated from the parameters of the GPD distribution by means of
 217 the following expression:

218

$$R.L.(m) = \mu + \frac{\sigma}{\xi} (m^\xi - 1) \quad (2)$$

219 where $R.L.(m)$ is the level expected to be exceeded once every m years. For each tide gauge,
 220 return levels were calculated both for the original series and for the separate components.
 221 Namely, for each component we analysed the reduction in return levels resulting from fitting the
 222 GPD distribution to the levels corresponding to the instants of the exceedances above the same
 223 threshold used for the original series, but after each component had been subtracted.

224 2.4 Quantification of the component contributions

225 The contribution of each of the identified components to the sea level anomaly series was
 226 quantified through the percentage contribution of each of them to the magnitude of the event
 227 peaks. If we consider for instance the event in the Mahón series highlighted in Fig. 2, the
 228 magnitude of the peak is 46 cm, and the component that contributes the most to it is the Storm
 229 Surge, whose series has a value of 14 cm at the instant of the peak. The contribution of that

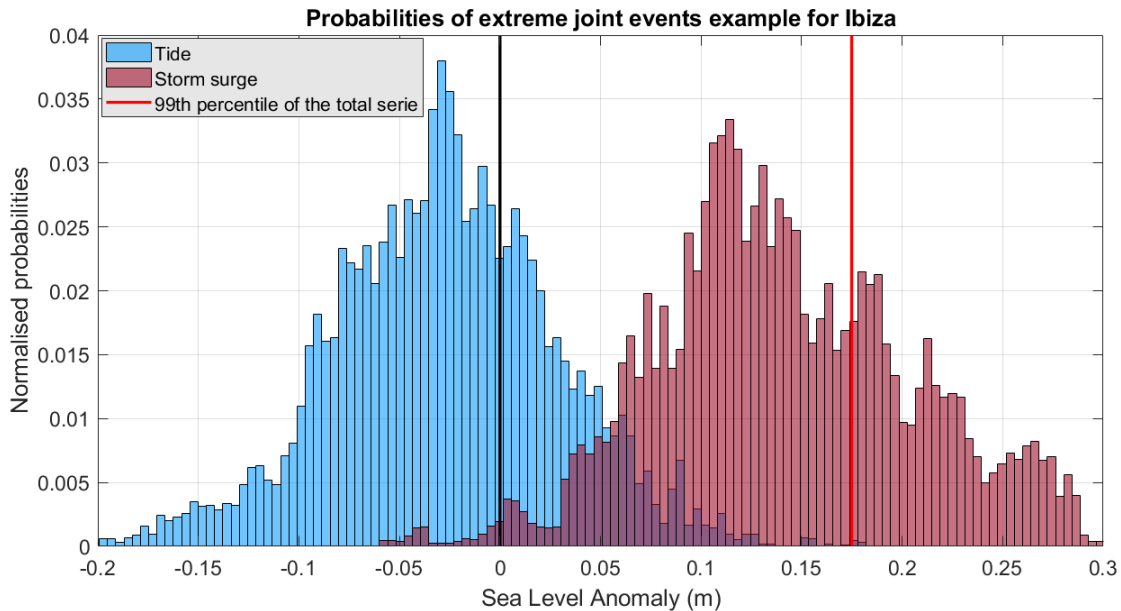


Figure 3: Probability distributions of extreme joint events derived from a synthetic series containing only the tidal and storm surge components. The black line marks the zero level of the total series, while the red line represents its 99th percentile.

230 component would then be evaluated in about 31%. The same procedure was applied to all the
231 events.

232 The probability of extreme joint events was also estimated, as a measure of the dependence of
233 extreme values with respect to each component (i.e., the probability of having an extreme value
234 in a component and in the original SLA series at the same time). This probability can be
235 calculated empirically through the percentage of extreme values of each component that coincide
236 in time with extreme values of the total SLA series. For each component, a probability
237 distribution function (pdf) of the total SLA is computed using the time intervals during which the
238 component is above its own 99th percentile (i.e. when extreme values of that component are
239 observed). If that pdf is centred around zero, this means that the component has no significant
240 impact on the extremes of total SLA (i.e. extreme values of that component do not lead to
241 extreme total SLA values). Conversely, if the pdf is displaced towards positive values, this
242 means that extreme values of that component coincide with larger positive values of total SLA;
243 that is, extreme values of that component significantly contribute to extreme SLA events.

244 For illustrative purposes, we have constructed a synthetic time series by adding only the tidal and
245 storm surge components isolated from the Ibiza tide gauge. Given the microtidal regime of Ibiza,
246 the extreme values of the total synthetic SLA will coincide with the extreme values of the storm
247 surge component, while being independent of the tidal component. Figure 3 shows the synthetic
248 total SLA pdf corresponding to extreme values of both, the tidal and storm surge components.
249 For the tidal component, the distribution is centred slightly before the 0 level (black line),
250 meaning that extreme values of the tides almost never translate into extremes of total SLA. On
251 the contrary, extreme values of the storm surge component show a high coincidence with
252 positive values of total SLA, and a substantial number of them (those to the right of the 99th
253 percentile denoted by the red line) coincide with extreme values of total SLA. Therefore, in this
254 example the storm surge would be the only responsible for the occurrence of extreme values of
255 total SLA.

256 2.5 The role of wind waves

257 Although the contribution of wind waves to sea level within harbors is practically negligible,
258 their contribution to extreme sea levels in exposed coasts can be very relevant. In order to

259 quantify this contribution, the wave runup 2% (hereafter RU2%), which corresponds to the
260 characteristic value of 2% exceeding probability of individual waves reaching the swash zone
261 during a sea state (Stockdon et al., 2006), was calculated along the coast of Palma Bay.

262 The contribution of waves to coastal sea level depends on the characteristics of the incoming
263 offshore waves, but also (and critically) on the morphology of the coast (Dodet et al., 2019). The
264 characterization of wave effects was carried out in two steps. First, the offshore wave regime of
265 the period 2010 to 2022 was obtained from the SIMAR wave hindcast (Pilar et al., 2008)
266 distributed by Puertos del Estado, which covers from 1958 to present. More specifically, the data
267 belong to the WANA subset, which starts in 2006, and is based on WAM (Hasselmann et al.,
268 1988) and Wavewatch (Tolman, 1991) models, forced by hourly wind fields provided by the
269 Spanish State Meteorological Agency (AEMET). These offshore waves were then propagated up
270 to the coast using the SWAN numerical model. SWAN is a third-generation shallow water model
271 that solves the discrete spectral action balance equation (Booij & Holthuijsen, 1987) and has
272 yielded accurate results in many studies (see e.g. Abu Zed et al., 2022). The model has been set
273 up for the Palma Bay with a 100 x 100 m spatial resolution (Fig. 4), and uses the bathymetry grid
274 obtained from GEBCO, the General Bathymetric Chart Of Oceans (Weatherall et al., 2015).

275 Once the nearshore wave set-up and the wave climate was obtained at the control points (points 1
276 to 20 in Fig. 4), hourly sea state parameters (H_s and T_p) were used to calculate the RU2%. The
277 estimation of RU2% depends on the coastal typology at each control point: where the coast is
278 protected by artificial structures such as dikes or seawalls (magenta dots in Fig. 4), RU2% is
279 estimated using an empirical formulations derived from laboratory experiments (Eurotop, 2018),
280 while on beaches (white dots in Fig. 4) it is estimated using the empirical equation developed by
281 Stockdon et al. (2006) and commonly used in coastal engineering studies (see e.g. Fiedler et al.,
282 2018; Vousdoukas et al., 2012). For the beaches, we use the slope values estimated by Agulles et
283 al. (2021) for the entire Balearic coastline, based on the equilibrium profiles.

284 In order to evaluate the impact of adding the wave contribution, we estimated the potentially
285 flood-prone extension along Palma Bay, considering a mean sea level rise (MSLR) of 0.67 m,
286 the regional value projected for the period 2080-2100 under the RCP8.5 scenario (Agulles et al.,
287 2021; Cherif et al., 2020). On top of this MSLR, we considered 3 extreme sea level scenarios: i)
288 the maximum sea level recorded by the Palma tide gauge (2010-2022), where wave effects are

289 minimal (ESC1); ii) the combination of the maximum recorded sea level (ESC1) with the wave
 290 set-up obtained at the control points (ESC2); iii) the combination of the maximum recorded sea
 291 level (ESC1) with the RU2% contribution obtained at the control points. The area flooded under
 292 each scenario was estimated by combining the “bathtub” approximation algorithm developed by
 293 Enríquez (2022) with the digital terrain elevation model developed by the Spanish National
 294 Geographic Institute, IGN
 295 (https://centrodedescargas.cnig.es/CentroDescargas/locale?request_locale=es). Although the
 296 “bathtub” approximation may be too simplistic to estimate the actual flooding caused by short
 297 events, it provides a useful first approximation to the impact of different definitions of extreme
 298 events.

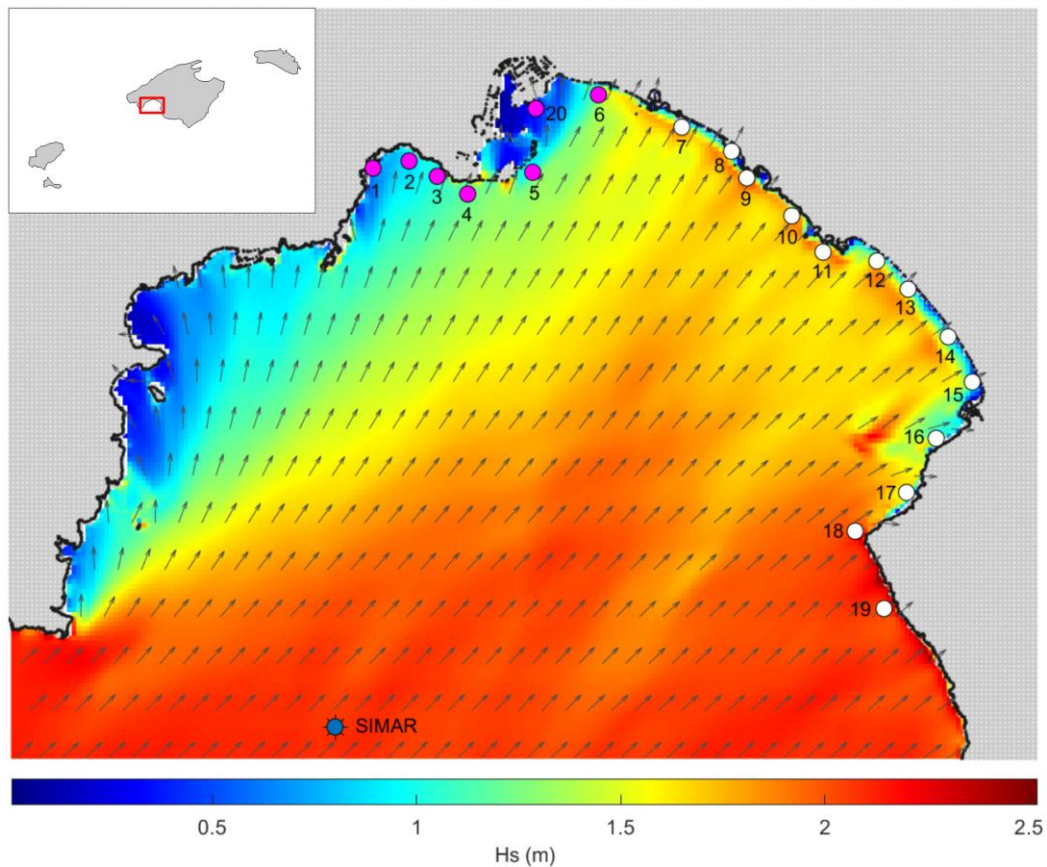


Figure 4: Example of the propagation of an offshore southwesterly sea state given at a SIMAR point (blue dot) towards the coasts of Palma Bay using the SWAN model. The control points where coastal waves are obtained are denoted by numbers from 1 to 20. The wave runup is calculated for artificial coastal protection (magenta dots) and on sandy beaches (white dots).

299 2.6 Spatial scales of the contributors to extreme events

300 To study the characteristic spatial scales of the different processes contributing to extreme sea
 301 level events, we calculated time correlations between the peak events identified at different
 302 stations for each component. But first, the time and intensity of the extreme values of each
 303 component had to be identified; we considered as independent events those separated by a
 304 minimum time lag that was set accordingly to the characteristic time scale of the component: 3
 305 days for the total SLA series, 15 days for the low-frequency atmospheric component, 6 hours for
 306 the storm surge and half an hour for the sub-hourly residuals. Then, time correlation between all
 307 pairs of tide gauges were computed for each component; in order to allow for a certain time lag
 308 (i.e. the expected lag due to a moving storm), we considered the maximum value within a 1-day
 309 window around the date of each event. The result of the process is a set of correlation values
 310 (one for each pair of tide gauges) which are expected to show some dependence with respect to
 311 the separation distance between the instruments. Hence, fitting a spatial correlation function
 312 depending only on the separation distance $\rho(d_{ij})$, a characteristic length-scale L_s can be
 313 estimated. As spatial correlation model we used a Gaussian function (Rasmussen & Williams,
 314 2008; Wilson & Adams, 2013):

$$315 \quad \rho(d_{ij}) = \exp(-0.5 d_{ij}^2 / L_s^2) \quad (3)$$

316 where d_{ij} is the distance between stations i, j .

317 3 Results

318 3.1 Overall characterization of extreme events

319 Figure 5 shows an overview of the peak values of the extreme events identified in the 17 tide
 320 gauge records covering the western sector of the Western Mediterranean and spanning the period
 321 2010-2022 (see Table 1). Most of the medians of the peak values are between 30 and 40 cm, but
 322 they progressively increase for stations close to the Strait of Gibraltar. The reason for this
 323 behaviour is that the tidal regime of the Western Mediterranean is dominated by the M2 tidal
 324 component, which strongly reduces its amplitude after entering the basin through Gibraltar
 325 (Ferrarin et al., 2018). Therefore, the location of the station is expected to play a key role in the
 326 contribution of the tidal component to extreme events.

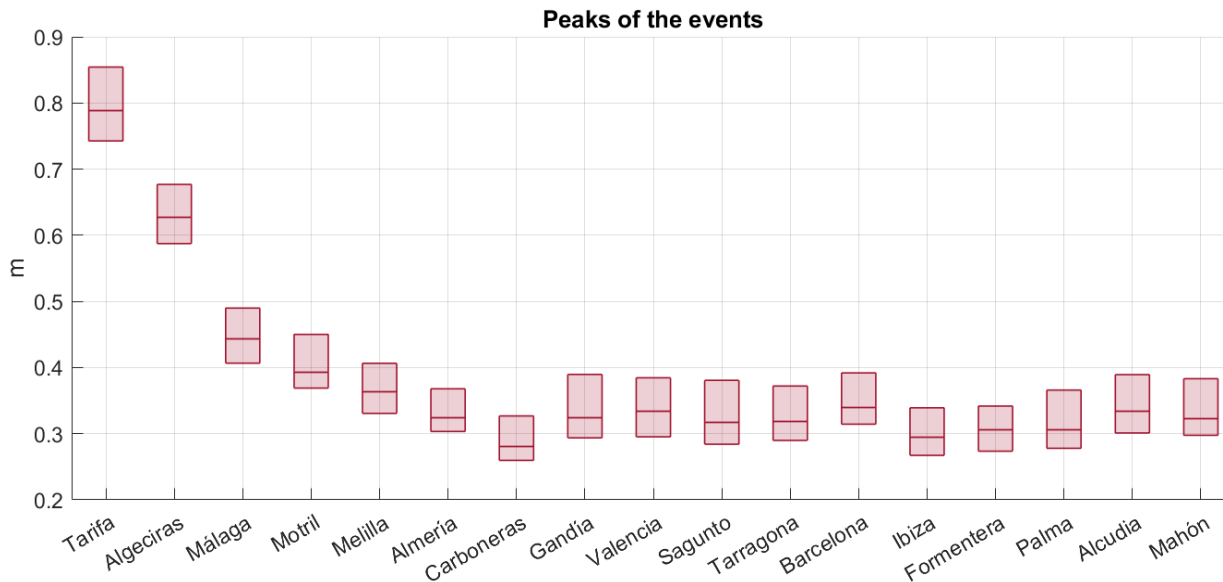


Figure 5: Peak values of the extreme events identified in the 17 tide gauge records spanning the period 2010-2022 (listed in Table 1). Boxplots report the median (inbox solid lines) and the 25th and 75th percentiles (bottom and top limit of the boxes).

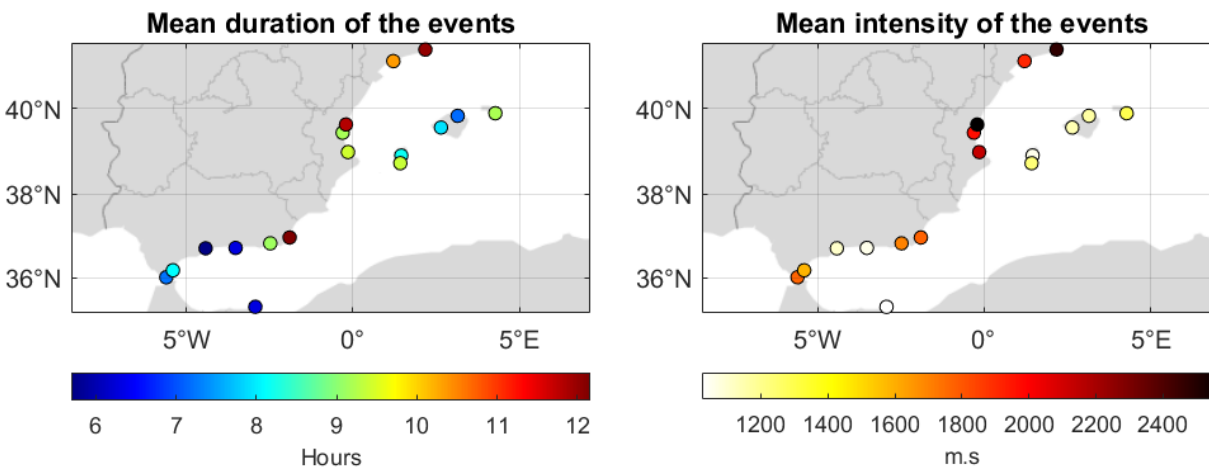


Figure 6: Mean duration (a) and mean intensity (b) of the extreme sea level events identified in the tide gauge records listed in Table 1.

Table 3: Additional information on the extreme sea level events identified in the tide gauge records of Table 1: maximum peak value, 99th percentile of the series, maximum duration, maximum intensity and 15-year return levels computed from hourly and minute series. The values in brackets of the last column are the % of increase with respect to the return levels computed from hourly series.

Station	99th percentile (m)	Maximum level (m)	Maximum duration (days)	Maximum intensity ($\cdot 10^3$ m·s)	Hourly 15-year return levels (m)	Minute 15-year return levels (m)
Tarifa	0.71	1.09	1.21	16.60	1.02	1.07 (5 %)
Algeciras	0.56	0.84	1.75	13.87	0.8	0.84 (5 %)
Málaga	0.39	0.71	3.22	25.59	0.63	0.75 (19 %)
Motril	0.35	0.62	3.12	18.99	0.55	0.66 (20 %)
Melilla	0.31	0.56	3.89	27.57	0.49	0.56 (14 %)
Almería	0.29	0.50	6.15	38.96	0.46	0.52 (13 %)
Carboneras	0.25	0.43	4.42	25.17	0.4	0.43 (8 %)
Gandía	0.27	0.44	6.36	56.78	0.4	0.44 (10 %)
Valencia	0.27	0.44	6.13	55.52	0.4	0.44 (10 %)
Sagunto	0.27	0.43	5.97	55.63	0.41	0.43 (5 %)
Tarragona	0.27	0.45	5.72	52.25	0.42	0.45 (7 %)
Barcelona	0.29	0.45	5.34	47.34	0.43	0.45 (5 %)
Ibiza	0.25	0.45	3.56	14.55	0.38	0.46 (21 %)
Formentera	0.26	0.47	7.33	30.77	0.4	0.46 (15 %)
Palma	0.26	0.46	4.69	18.22	0.41	0.48 (17 %)
Alcudia	0.28	0.49	5.30	24.59	0.43	0.49 (14 %)
Mahón	0.28	0.49	5.08	20.20	0.44	0.49 (11 %)

328 The duration and intensity of the identified extreme events is shown in Fig. 6. The mean duration
329 ranges between 5.7 and 12.2 hours, with the largest values obtained in the northern sector of the
330 Iberian peninsula coasts and the smallest values corresponding to stations near the Strait of
331 Gibraltar (Fig. 6a). The mean intensity shows a similar pattern regarding the largest values,
332 which exceed 2400 m·s for Barcelona and Sagunto stations; the smallest intensities correspond
333 to the stations of the Balearic archipelago and the Alborán Sea (Fig. 6b).

334 Table 3 provides further information on the identified extreme events: the maximum peak value,
335 the 99th percentile of the series, the maximum duration and intensity and the 15-year return
336 levels are reported for each station. As expected, the maximum peak values correspond to the
337 stations close to the Strait of Gibraltar; namely, the largest maximum for the considered period is

338 the 1.1 m obtained in Tarifa. The 99th percentiles, which are used as thresholds to identify
 339 extreme sea level levels, show a distribution similar to that of the maximum values, with a
 340 maximum of 0.71 m at Tarifa and a minimum of 0.25 m at Carboneras (southeast coast of the
 341 Iberian Peninsula). The maximum durations shows that sea level can be above the 99th
 342 percentile for more than 1 week (e.g. in Formentera). As it was the case for the mean duration,
 343 also the maximum durations are shorter close to the Strait of Gibraltar and larger at the northeast
 344 coast of the Iberian peninsula. The maximum intensities correspond to the east coast of the
 345 Iberian Peninsula, more precisely to the Gulf of Valencia, a region that is prone to the
 346 topographic blocking of storms coming from the East.

347 The computation of the monthly distribution of extreme events for each tide gauge of Table 1
 348 (Fig. 7) confirms that they mostly occur in autumn, with October and November accounting for
 349 the highest number of events in almost all stations. The lowest occurrence is observed in late

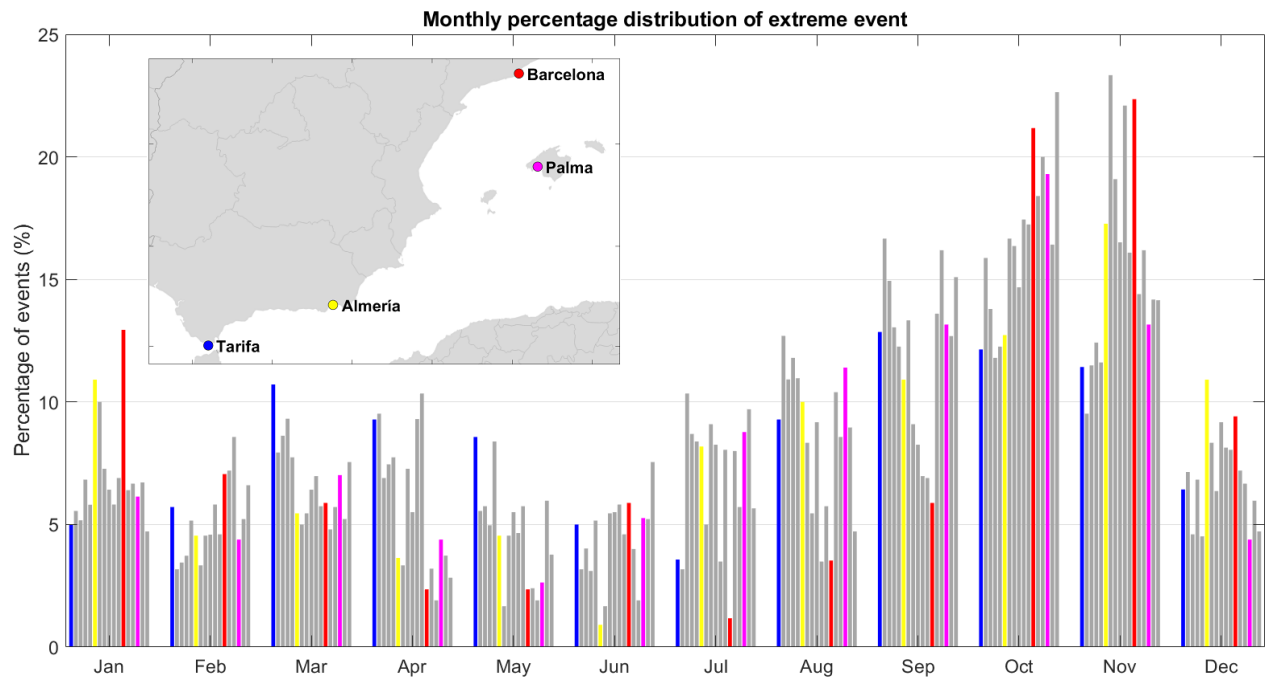


Figure 7: Monthly percentage distribution of extreme events in each tide gauge of Table 1. Four stations distributed throughout the basin (Tarifa, Almería, Barcelona and Palma) have been highlighted in colour.

350 spring and early summer. For the tide gauges located near the Strait of Gibraltar (Tarifa,
 351 Algeciras, Málaga, Motril, and Melilla), autumn is still the main season for extreme events, but
 352 the month with the highest occurrence is September. Moreover, the extreme events identified in
 353 these stations are more uniformly distributed throughout the year than for the stations located in
 354 the east coast of the Iberian Peninsula and the Balearic Islands.

355 A key feature revealed by Table 3 is the importance of using high frequency sea level series for
 356 studying extreme events. Comparing the return levels obtained from the minute and hourly
 357 series, the first exceed the second by an average of 6 cm. In relative terms, the increase in the
 358 return levels when using minute time series ranges between the ~5% of Tarifa, Algeciras,
 359 Sagunto and Barcelona to the ~20% of Málaga, Motril and Ibiza, the average increase being of
 360 about 11%.

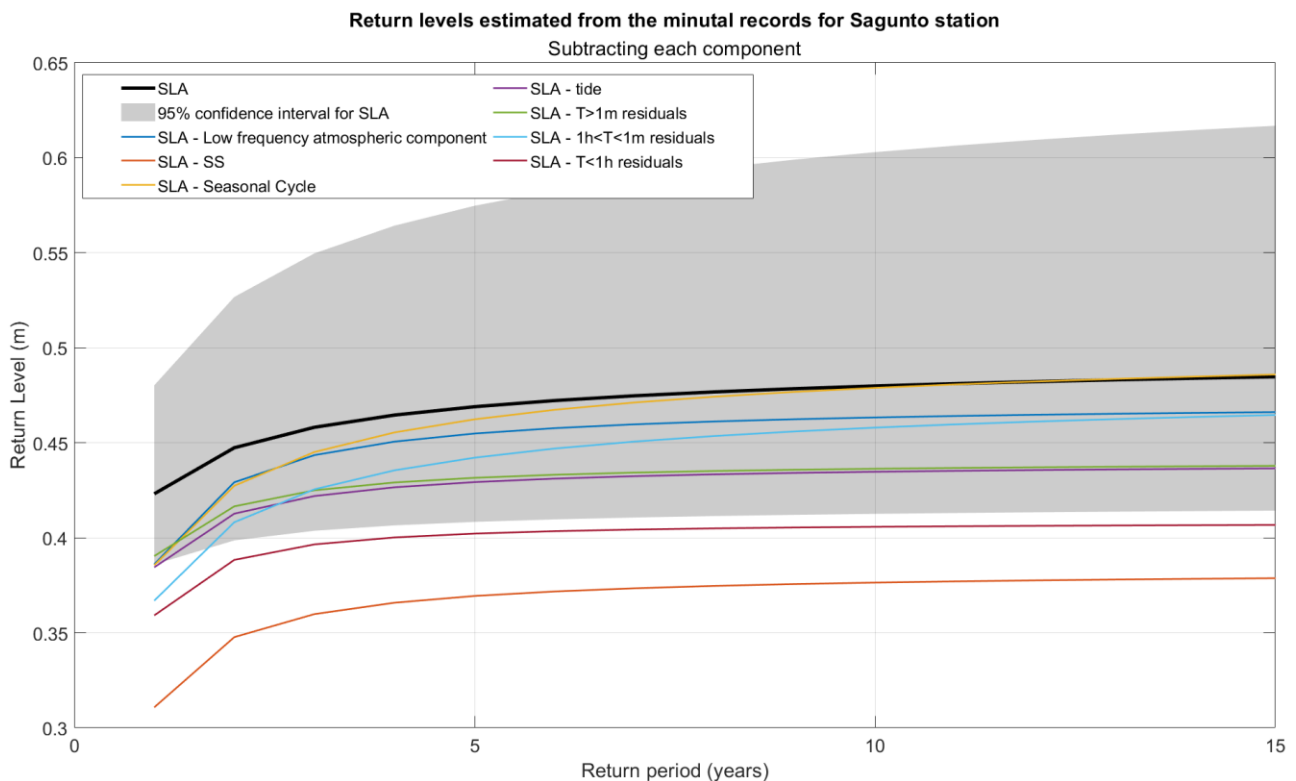


Figure 8: Estimated return levels for the Sagunto tide gauge. They are computed for the total SLA series and for the series resulting after the subtraction of each component. The grey area delimits the 95% confidence intervals of the original series return levels.

361 In order to highlight the importance of high-frequency processes, Fig. 8 shows the return levels
362 computed for Sagunto, a tide gauge reporting large duration and intensity values but with the
363 smallest difference between return levels computed from hourly series and minute series. The
364 figure shows the return levels for the total SLA series and those obtained after subtracting each
365 components from the total series. The decrease in the return levels observed after the subtraction
366 of a components gives an idea of the relevance of that component. The largest reduction, slightly
367 more than 10 cm, is obtained when subtracting the storm surge, and the second one, of the order
368 of 7-8 cm, when subtracting the sub-hourly residuals. Removing the atmospheric signal with $T > 1$
369 month reduces the return levels by about 5 cm, and subtracting the other components results is
370 less relevant reductions. That is, high frequency ($T < 1h$) processes are the second most relevant
371 contributor to return levels even at the station with the smallest difference between return levels
372 computed from hourly series and minute series. In general, the largest reductions in return levels
373 are obtained when subtracting storm surge and high-frequency residuals at stations with a
374 microtidal regime, whereas at those stations with a meso-tidal regime, the originally larger return
375 levels are considerably reduced when subtracting the tide.

376 3.2 Contributors to the extreme events

377 The contribution of the tidal component is obviously very different between the stations with a
378 meso-tidal regime (those located in the Alborán Sea) and the stations with a micro-tidal regime
379 (those located on the eastern Iberian coast and the Balearic Islands). Therefore, when quantifying
380 the different contributions of extreme sea levels the stations have been separated into two groups
381 according to their tidal regime (Fig. 9). For the stations with a microtidal regime the most
382 important contributions are atmospheric: the median values of the low frequency atmospheric
383 contribution account for 5-14% of the peak values, while the median values of the storm surge
384 account for 20-31% of the peak values. The contributions from sub-hourly periods also stands
385 out as a relevant component, accounting for 8-24% of the peak values. For stations with a meso-
386 tidal regime, the tide is by far the most important component, with a contribution that strongly
387 depends on location: from the 88% of Tarifa (located just at the Strait of Gibraltar) to the 38% of
388 Almería (located at the eastern boundary of the Alborán Sea). However, for an extreme event to
389 take place, it is usually necessary that during neap tides some other component has a high value.
390 The median contributions of the other components to peak values are: 1-5% from low frequency

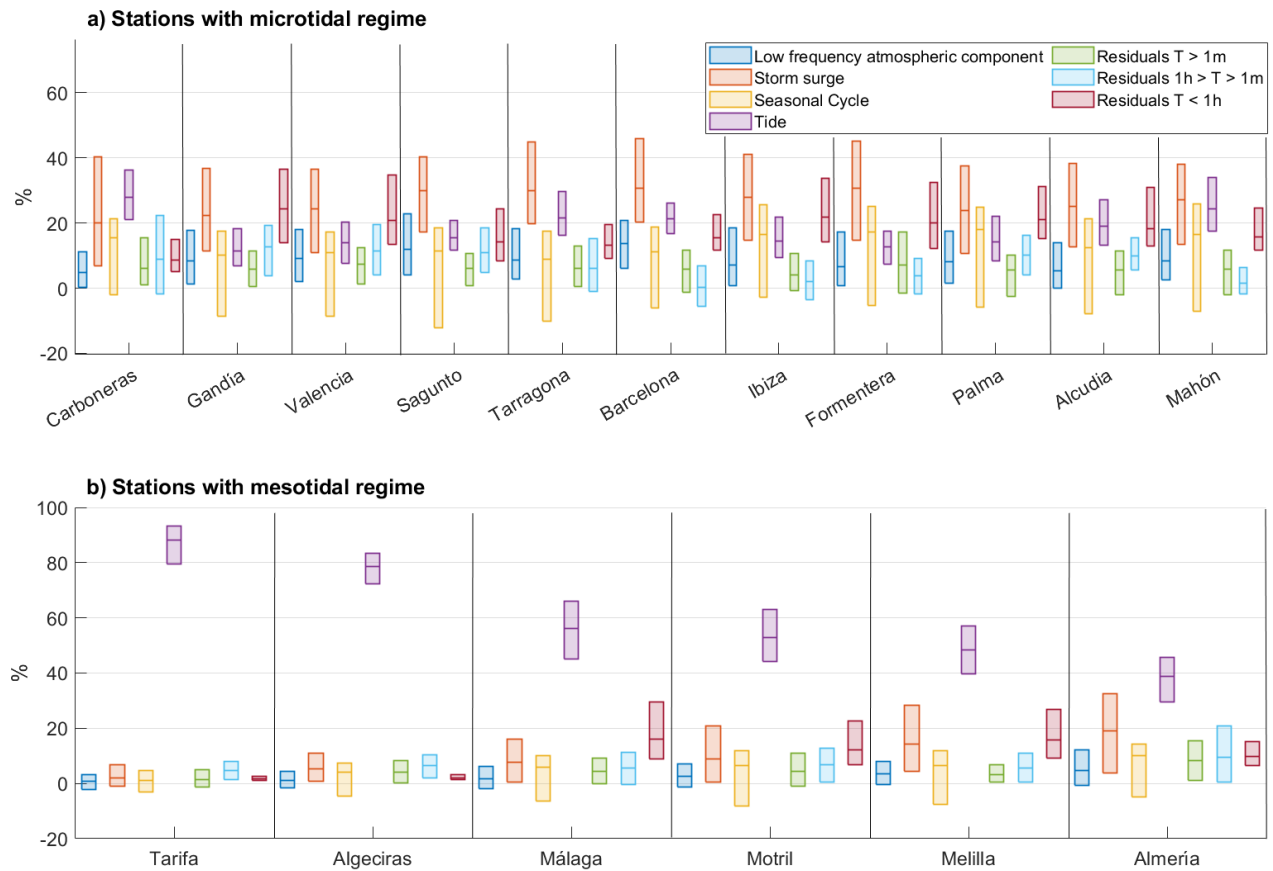


Figure 9: Percentage contributions of each sea level component to the peaks of extreme events identified in: a) tide gauges of Table 1 with a microtidal regime; b) tide gauges of Table 1 with a meso-tidal regime. Boxplots report the median (inbox solid lines) and the 25th and 75th percentiles (bottom and top limit of the boxes).

391 atmospheric processes, 2-19% from storm surges and 2-16% from high frequency (T<1h)
 392 processes.

393 The relevance of each contributor can also be inferred from the probability of extreme joint
 394 events distributions of total SLA and each component. As an example, Fig. 10 shows the pdfs
 395 obtained for Palma de Mallorca, with the 0 level of total SLA marked in black and the 99th
 396 percentile marked in red. For the case of Palma de Mallorca, the probability of having an
 397 extreme value in the total SLA series is larger (18%) when there is an extreme value in the storm
 398 surge component. However, the sub-hourly residuals (T<1h) are the second most important

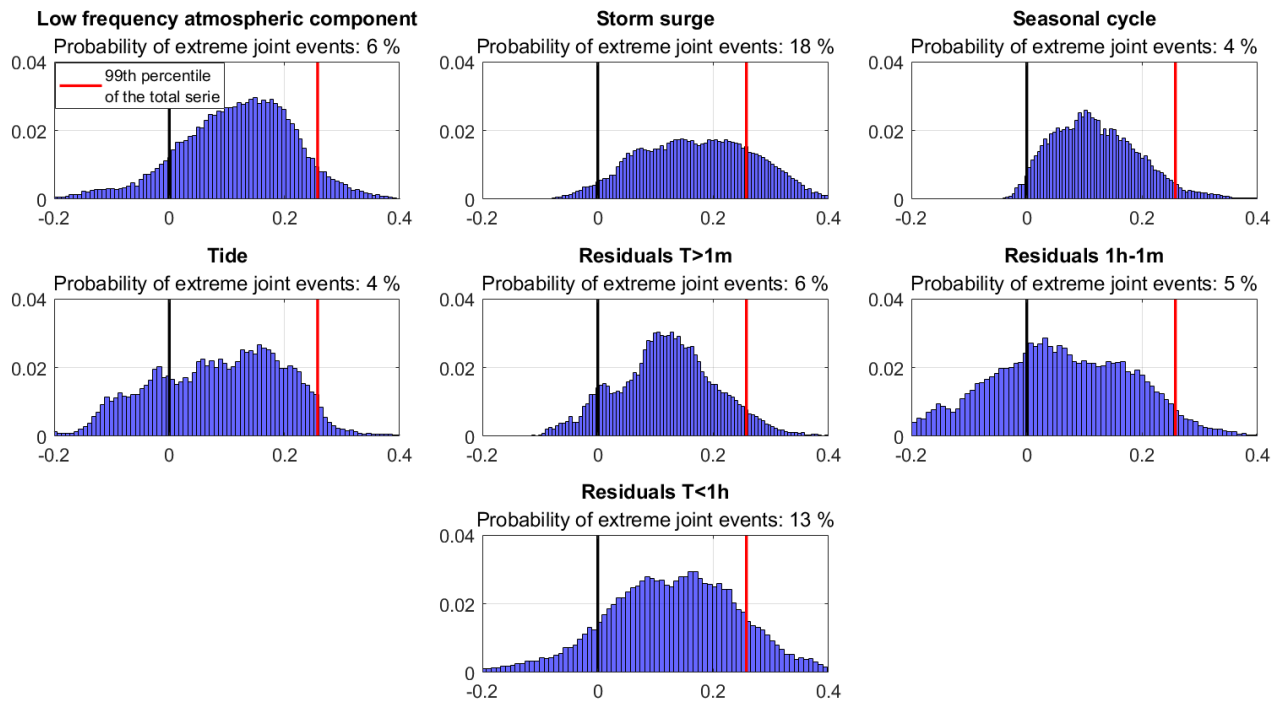


Figure 10: Probability of extreme joint events distributions of total SLA and each component for Palma de Mallorca tide gauge: a) Low-frequency atmospheric component; b) Storm surges; c) Tidal component; d) Seasonal cycle; e) Residuals with $T > 1m$; f) Residuals with $1m < T < 1h$; g) Residuals with $T < 1h$. The black line indicates the 0 level of total SLA marked and the red line indicates the 99th percentile.

399 component, with a probability of 13%. On the other hand, the probability that an extreme in the
 400 total SLA series coincides with an extreme in the tidal and seasonal cycle components is of only
 401 4% in both cases, indicating that these components have a limited impact in this station.
 402 Nevertheless, it is worth noting that the distributions of all components are centred on positive
 403 values, meaning that in general, the presence of extreme values in any component contributes
 404 more or less to having high values in total sea level.

405 Figure 11 shows the results of applying the same analysis to all tide gauges of Table 1. The tidal
 406 contribution is obviously crucial in the occurrence of extreme events near the Strait of Gibraltar.
 407 However, the probability of extreme joint events of this component is about 55% at Tarifa, less

408 than 40% at Algeciras, and smaller at the other stations, indicating that although tides are the
 409 main contributor, high values of other components are also required for an extreme value to
 410 occur. At stations with a microtidal regime, the extremes in the storm surge have the highest
 411 probability of yielding a SLA extreme, with values ranging between 11.2 and 20.2%. The
 412 probability is also significant for subourly residuals, ranging from 5.6 to 13.3% and being
 413 particularly relevant at Gandía, Valencia and the Balearic Islands. The probabilities of the lower
 414 frequency residuals ($T > 1m$ and $1m < T < 1h$) are smaller and have an heterogeneous spatial pattern.

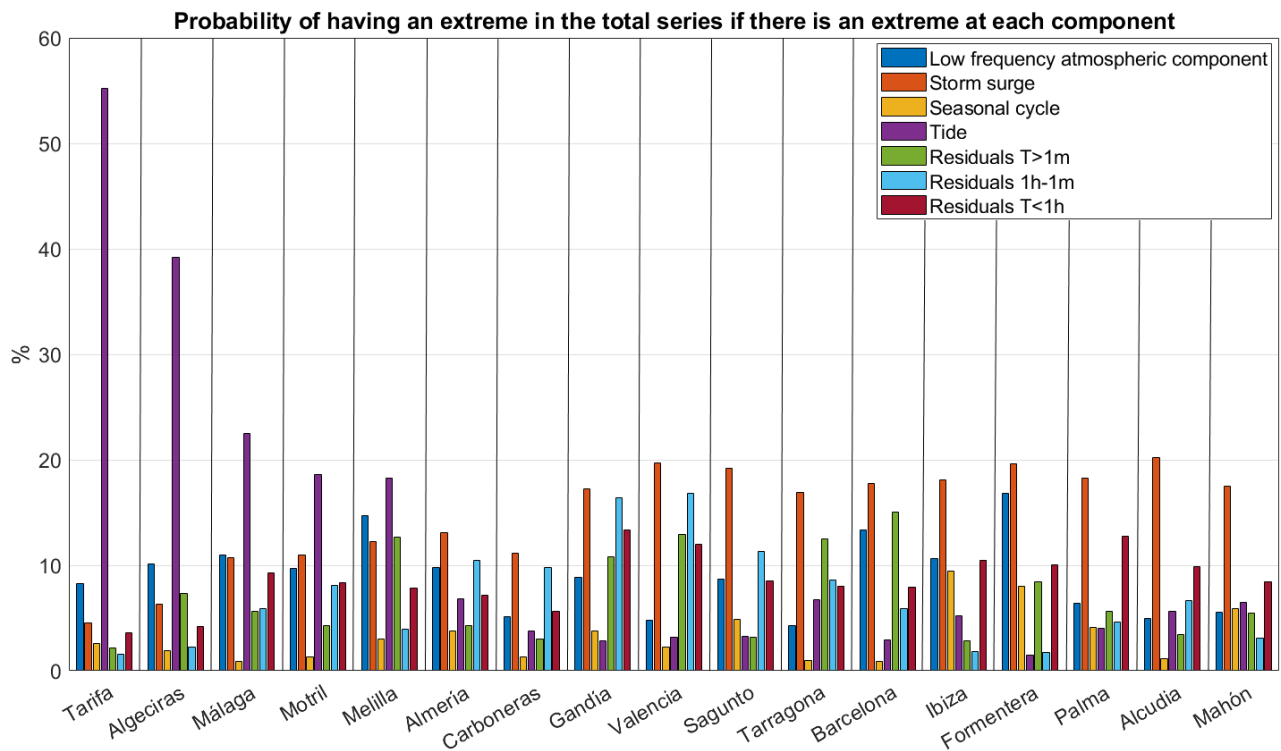


Figure 11: Probability of having an extreme event in the total SLA and simultaneously in one of the different contributors to sea level, estimated for each contributor and each tide gauge of Table 1.

415 3.3 Short-scale spatial variability of extreme events

416 As stated in Section 2, the recent availability of a tide gauge network with an unprecedented
 417 spatial resolution allows some insight into the short-scale spatial variability of extreme events.
 418 The analysis must however be taken with caution, as the short period spanned so far by the series

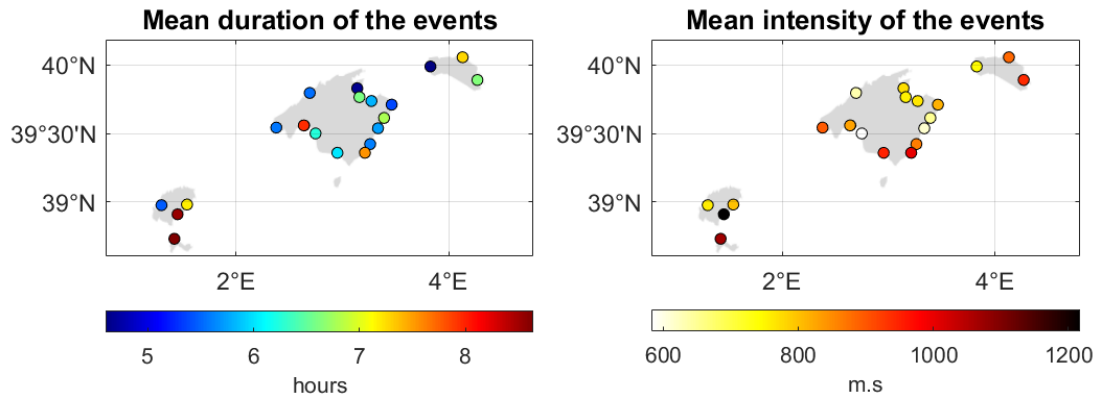


Figure 12: a) Average duration of extreme events in each station of the Balearic Islands, b) Average intensity of extreme events in each station of the Balearic Islands. Note that different colour maps have been used for each variable.

419 (2 years) does not allow a robust extreme value statistics. Figure 12 shows the mean duration
 420 (Fig. 12a) and mean intensity (Fig. 12b) of the extreme events identified for each tide gauge of
 421 Table 2. As a consequence of the short time period considered here, the five stations already used
 422 in Fig. 6 (in that case spanning more than 12 years) show similarities, but also some
 423 differences with respect to Fig. 12. Thus, the mean intensities of the events shown in Fig. 12 are
 424 considerably lower than those of Fig. 6, due to the smaller number of high level events in the
 425 series. Regarding the duration of the events (Fig. 12a), Palma, S'Arenal, Ibiza, and Formentera
 426 stand out, with a mean duration of more than 8 hours. The highest mean intensity corresponds to
 427 Ibiza, and amounts to ~ 1200 m.s. Table 4 shows additional information on the extreme events
 428 identified in each tide gauge record. The 99th percentiles are between 25 and 29 cm for all the
 429 stations, and the highest sea level value recorded in the region during the two-year period is the
 430 73 cm recorded at Ciutadella. That location is well known for the occurrence of large amplitude
 431 sea level oscillations resulting from the resonant response of the harbour to incoming
 432 meteotsunami waves (locally known as “rissaga”, see e.g. Monserrat et al., 2006). The maximum
 433 duration and intensities are very heterogeneous throughout the stations, with the longest event
 434 lasting 3.5 days (in Sa Ràpita) and the most intense event amounting almost $18.7 \cdot 10^3$ m.s (in
 435 Andratx). Since the results obtained so far indicate that the contribution of sub-hourly processes
 436 can be quite relevant, the focus will now be put on the variability of this high-frequency

437 component in the regional context of the Balearic Islands (the domain covered by the dense
438 network of tide gauges).

439 Figure 13 shows the percentage contribution of sub-hourly processes to the peak value of the
440 extreme events identified in each tide gauge. Results show a marked heterogeneity, even for
441 stations separated a few kilometres. The stations with the highest contribution from this

Table 4: Information on the extreme events identified in each series in the Balearic Islands: maximum value reached, 99th percentile of the series, duration of the longest event recorded, and maximum intensity recorded for an event.

Station	99th percentile (m)	Maximum (m)	Maximum duration (days)	Maximum intensity ($\cdot 10^3$ m·s)
Formentera	0.25	0.43	1.9	9.69
Sant Antoni	0.26	0.55	1.58	7.98
Ibiza	0.25	0.48	2	10.47
Santa Eulàlia	0.25	0.54	2.37	7.01
Sa Ràpita	0.26	0.58	3.53	18.46
S'Arenal	0.29	0.49	1.41	2.9
Palma	0.25	0.52	3.04	15.2
Palma	0.28	0.43	1.5	4.44
Andratx	0.26	0.5	3.35	18.67
Port de Sóller	0.28	0.52	1.15	5.19
Alcudia	0.28	0.54	2	12.35
Can Picafort	0.28	0.58	1.18	3.73
Colonia Sant Pere	0.26	0.45	1.89	5.46
Cala Rajada	0.26	0.5	2.05	11.45
Cala Bona	0.27	0.41	1.22	2.81
Porto Cristo	0.27	0.56	1.59	8.46
Portocolom	0.27	0.64	2.61	13.1
Portopetro	0.25	0.47	1.97	9.78
Mahón	0.27	0.51	2.39	11.64
Ciutadella	0.28	0.73	1.57	8.56
Fornells	0.26	0.4	1.55	6.8

442 component are Ciutadella, with a 53.5%, Portocolom with 47.3%, Port de Sóller, with 42.1%,
 443 and Sant Antoni, with 40.7%. All them have at least one event in which the contribution of this
 444 component is greater than 100%, indicating that it is the only responsible for these events (and
 445 that it compensates the negative levels associated with other components). These stations are all
 446 located in sheltered harbours where meteotsunami episodes are relatively frequent (Rabinovich,
 447 2020). On the other hand, there are stations where the contribution of this component is very
 448 small, such as Fornells, Port de Valldemossa or Sa Calobra; these stations are located in places
 449 where neither shelf nor harbour resonance have been reported.

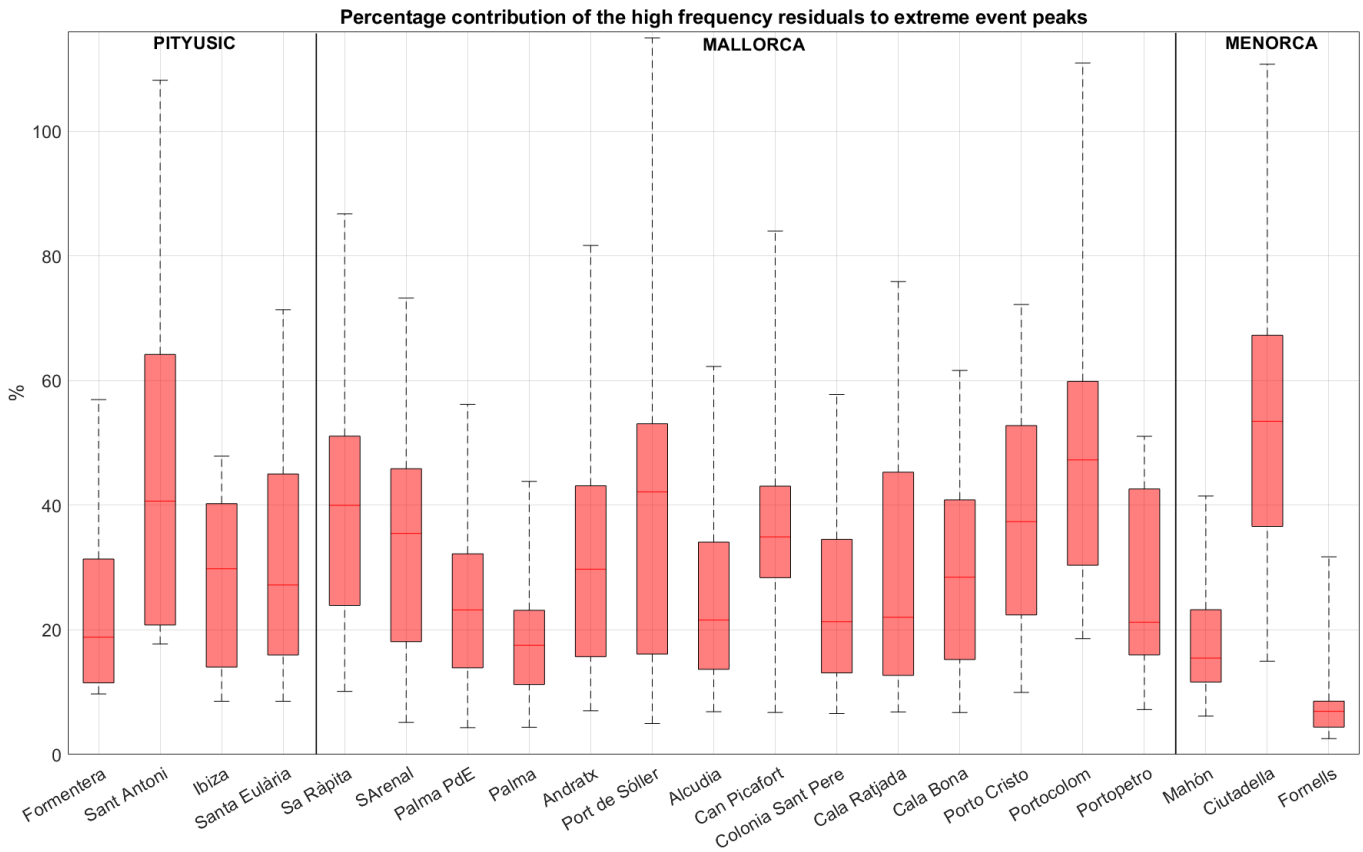


Figure 13: Percentage contributions of high-frequency residuals ($T < 1h$) to extreme sea levels in the Balearic Islands. The stations are separated by islands: Pityusic (Ibiza and Formentera), Mallorca and Menorca. Boxplots report the median (in box solid lines) and the 25th and 75th percentiles (bottom and top limit of the boxes). The whiskers represent the minimum and maximum values of the contribution of this component to the extremes of each series.

450 3.4 Wave contribution to extreme events

451 Here we present the results of the wave contribution to Total Water Level (TWL) at the 20
 452 control points shown in Fig. 4. The maximum value measured by the Palma station operating
 453 with 1-min resolution is 46 cm; the tide gauge is located in the vicinity of point 20 (see Fig. 4),
 454 and it can be considered representative of the sea level of the whole bay without considering the
 455 wave contribution. When the set-up contribution is added, then TWL reaches values between
 456 0.46 and 0.49 m over artificial coastal structures (points 1-6 and 20), and between 0.46 and 0.78
 457 m on the beach (see Table 5). When the RU2% contribution is considered, then TWL reaches

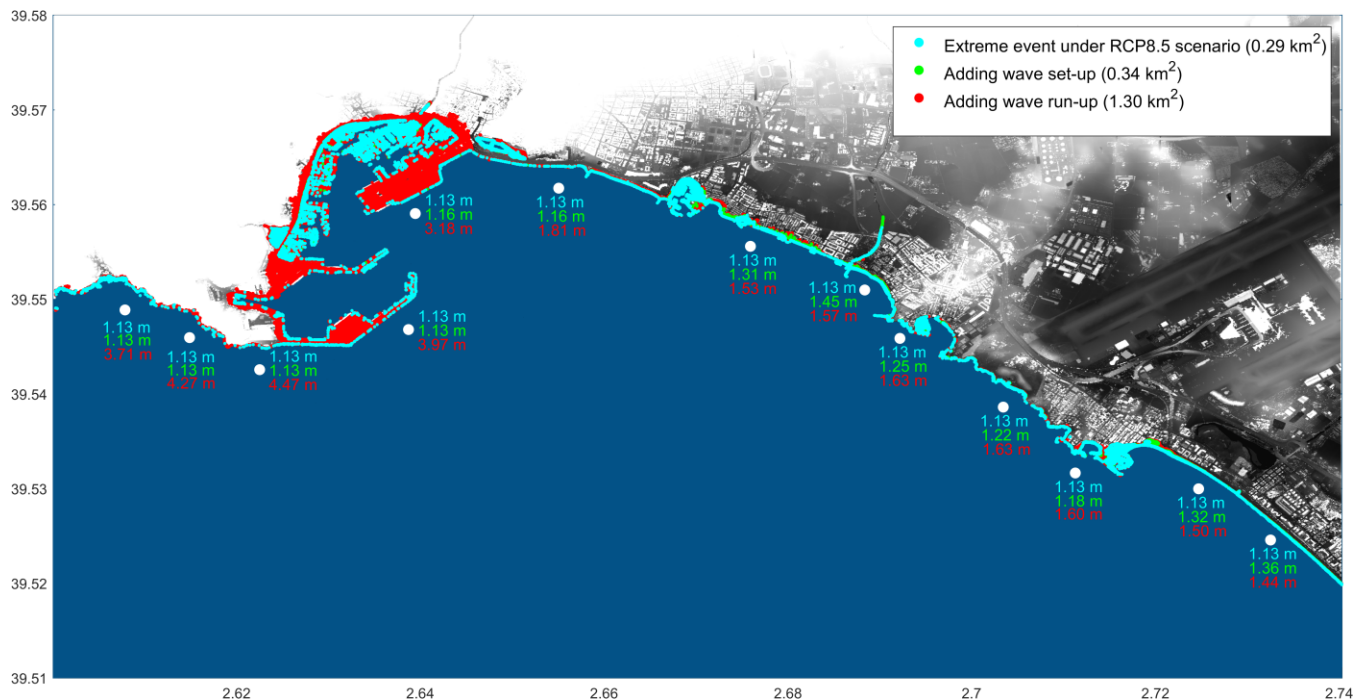


Figure 14: Potentially flood-prone areas of Palma Bay during an intense extreme event occurring under the RCP8.5 scenario projected for the end of the century (2080-2100). Cyan areas are those flooded without considering the wave contribution, green areas are those flooded when considering the wave set-up contribution, and red areas are those impacted when adding the RU2% contribution. The vertical values of sea level at each control point (TWL) are also given with and without the wave contribution.

Table 5: Total Water Level (TWL) at the 20 shore points of Palma Bay shown in Fig. 4. It includes the TWL when adding the wave set-up, provided by the SWAN model, and the TWL calculated when adding the estimated wave run-up contribution, both considering the maximum level recorded at Palma tide gauge (0.46 m); the type of coastal protection and the parameterisation used in the calculation of the RU2% are indicated for each point. Future TWLs would be obtained by adding a mean sea level rise of 0.67m (the regional value projected for 2100 under the RCP8.5 scenario) to present TWLs.

Control point	Coastal typology	TWL when adding set-up (m)	TWL when adding RU2%	
			Source	Value (m)
1	Dike	0.46	Eurotop	3.29
2	Dike	0.46	Eurotop	3.04
3	Dike	0.46	Eurotop	3.60
4	Dike	0.46	Eurotop	3.80
5	Dike	0.46	Eurotop	3.30
6	Dike	0.49	Eurotop	2.51
7	Beach	0.64	ST2006	0.86
8	Beach	0.78	ST2006	0.90
9	Beach	0.58	ST2006	0.96
10	Beach	0.55	ST2006	0.96
11	Beach	0.51	ST2006	0.93
12	Beach	0.65	ST2006	0.83
13	Beach	0.69	ST2006	0.77
14	Beach	0.67	ST2006	0.75
15	Beach	0.63	ST2006	0.73
16	Beach	0.48	ST2006	0.79
17	Beach	0.48	ST2006	0.90
18	Beach	0.46	ST2006	1.00
19	Beach	0.46	ST2006	1.00
20	Vertical	0.49	Eurotop	1.14

458 values between 1.14 and 3.80 m over artificial coastal structures (points 1-6 and 20), and
459 between 0.73 and 1.00 m on the beach. The contribution of waves is therefore very relevant,
460 specially in the artificial parts of the shore, where TWL can exceed the maximum tide gauge
461 value by more than 3 m. It is worth noting that set-up contribution typically lasts as long as the

462 storm duration is (~hours), while the maximum values associated with the RU2% have a
463 duration determined by the wave period (~10 secs).

464 The contributions of the wave set-up and the RU2% have been considered separately, as their
465 durations are different: whereas set-up leads to a more persistent total level rise over the duration
466 of the storm, the RU2% generates a periodic vertical elevation with the period of incoming
467 waves. This makes that the coastal areas reached by the set-up can be effectively flooded;
468 conversely, the flow associated with the RU2% is too small as to flood all the area predicted by
469 the bathtub approximation, even if the effect of the swash in storms can be a major hazard in
470 coastal regions. Under the RCP8.5 scenario, future TWL would be equal to present values plus
471 0.67 m, the mean sea level rise projected for the end of this century. Under that scenario, the
472 potentially floodable areas of Palma Bay during an intense extreme event are shown in Fig. 14.
473 When the contribution of waves is not considered, the floodable area along the bay coast is 0.29
474 km². When adding the estimated wave set-up, the potentially floodable area increases up to 0.34
475 km², that is, an additional 17%. The impacted area when considering the runup is 1.30 km²,
476 which is an increase of almost 350% over the area covered by the still water level.

477 3.5. Spatial scale of main contributors

478 The spatial scales of the extreme sea level events identified in the total series, and of the extreme
479 values of the main contributors to these events are inferred from Fig. 15. This Figure shows, for
480 all station pairs, the correlation between the time sequence of peaks identified at each station.

481 The correlations between station pairs have been computed for the total series (Fig. 15a), the low
482 frequency atmospheric component (Fig. 15b) and the storm surge component (Fig. 15c), and are
483 represented in all cases as a function of the distance between the two stations. The stations
484 considered for the referred components are the 17 tide gauges listed in Table 1, which result in a
485 total of 136 station pairs. For the sub-hourly residuals ($T < 1h$), which are expected to have a
486 shorter spatial scale, the stations considered are the 21 tide gauges located in the Balearic
487 archipelago (listed in Table 2); in this case the number of correlation values between station pairs
488 is 210 (Fig. 15d).

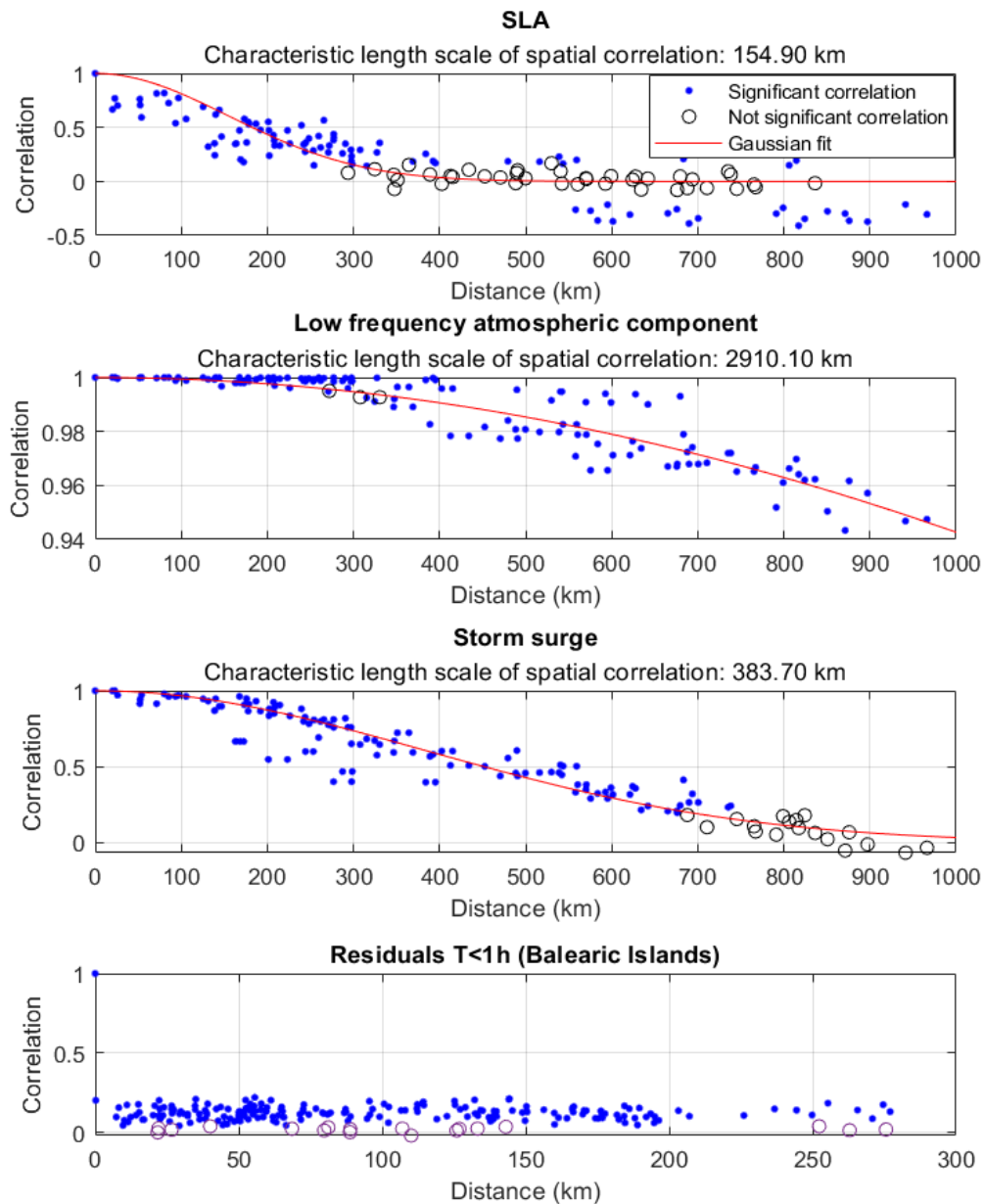


Figure 15: Correlation between the time sequences of peak values identified at each station pair. The correlation value obtained for each station pair is plotted as a function of the distance between the two stations in the form of a blue square (when the correlation is statistically significant) or an empty circle (when the correlation is not statistically significant). The procedure has been applied to the Western Mediterranean tide gauges of Table 1 (spanning the period 2010-2022) for: a) the total SLA series; b) the low frequency atmospheric component; c) the storm surge component; and to the Balearic Island tide gauges of Table 2 (spanning the period 2020-2022) for: d) the subhourly component. Note that the x-axis (distances) of panel d) are different from the other three panels.

489 For the extreme events of the low frequency atmospheric component and of the storm surge
490 component, the fit of Eq. (3) to the significant correlations resulted in characteristic scale values
491 of about 2900 km and 380 km, respectively. These values are consistent with the typical scales of
492 the perturbations generating the extreme sea levels associated with these components. The
493 characteristic scale obtained for total SLA is about 150 km; in this case, extreme values result
494 from the overlapping of different processes with different scales, so that the value of 150 km
495 must be considered a sort of average scale. The correlations obtained for the sub-hourly
496 component are in general very low, regardless of the distance between stations, which prevents
497 the estimation of a meaningful characteristic length scale for this component.

498 **4. Discussion**

499 A major objective of this work was to revisit the characteristics of extreme sea level events in the
500 Western Mediterranean in the light of tide gauge data with a high spatio-temporal resolution. The
501 importance of extreme events in that region is demonstrated by their duration (the time during
502 which sea level remains above the 99th percentile during the event), which can be of more than
503 one week during intense events.

504 The sampling rate of tide gauges has often been a limiting factor for the identification of the
505 actual magnitude of the peaks, since relevant high-frequency processes remain undersampled
506 when using hourly records, for instance. Thus, previous works had already anticipated that the
507 estimated return levels would increase if working with sea level series with a sampling period
508 smaller than 1 hour (Tsimplis et al., 2009). Here we have shown that 15-yr return levels do
509 indeed increase, namely between 5% to 20%, when working with minute series instead of hourly
510 series. In terms of physical processes, missing the contribution of high frequencies to extreme
511 sea levels leads to an overestimation of the importance of other contributions such as storm
512 surges, to the point that the latter are often considered the only process responsible for extreme
513 values.

514 A second, related objective of the work was the quantification of the contribution of different
515 physical processes to extreme events. In many works, the residuals of de-trended and de-tided
516 hourly series are directly considered as storm surges (see e.g. Enríquez et al., 2020; Haigh et al.,
517 2016; Marcos & Woodworth, 2017). Here, we have split the total SLA series into different

518 contributions beyond tides and storm surges, finding that the de-tided residuals of the series after
519 removing the steric and the atmospheric component can significantly contribute to the extreme
520 levels, at least in some cases and at some stations. In fact, at many coastal sites with a micro-tidal
521 regime (the whole Western Mediterranean except the Alborán Sea), sub-hourly processes (which
522 include for instance meteotsunamis and shelf waves) are the second most important contributor
523 to extreme levels, storm surges being always the main contributor. It is also worth noting, that
524 even if storm surges are the main contributor, they contribute to 20-30 % of the peak level,
525 which enforces the idea that extreme events require multiple contributions from different
526 mechanisms.

527 The deployment in the Balearic Islands of a tide gauge network with an unprecedented spatio-
528 temporal resolution has allowed a further insight into the contribution of sub-hourly residuals to
529 extreme levels. It has been shown that high frequency processes ($T < 1$ h) are a key factor in the
530 occurrence of extreme events in some ports, and that they are often absolutely local processes. In
531 this sense it is worth noting that the conventional tide gauge networks (i.e. with less spatial
532 resolution), may be unadequate to assess the importance of those events.

533 A third key feature of the study has been the evaluation of the impact that waves can have on
534 total sea levels measured at the coast. The contribution of waves is highly dependent on the
535 morphology of the coast (e.g., the estimated wave runup is considerably higher in the presence of
536 rigid structures than on beaches) and on the orientation of the coastline with respect to the
537 direction of the waves. Namely, our case study for the Bay of Palma has shown that during an
538 intense event, sea level at coastal sites with artificial structures can be up to 2.5 m higher than in
539 neighbouring sites with a beach-type morphology. Therefore, the approach followed in some
540 works in which the wave runup is quantified without a detailed consideration of the coastline or
541 coastal structure (see e.g. Melet et al., 2018; Sayol & Marcos, 2018) may be too simplistic. On
542 the other hand, it should also be noted that those extreme values would occur over short periods
543 (~secs), as they are associated to the swash part of the wave runup. Thus, the flood-prone areas
544 shown in Fig. 14 constitute only a first illustrative approximation, as the bathtub approach tends
545 to overestimate the extent of the flooded area.

546 Finally, regarding the characteristic spatial scale of the main contributors to extreme levels, it
547 seems clear that the atmospheric contribution operates over a wide range of spatial scales: from

548 ~3000 km in the case of the low frequency atmospheric component to a few km in the case of the
549 resonant response of shelves and harbours. In fact, the inference of a characteristic scale for the
550 subhourly residuals has not been possible, even using a tide gauge network with a mean
551 separation distance of ~10 km in large parts of the domain. The characteristic scale of storm
552 surges has been quantified in 380 km, a value that differs significantly from the results given in
553 other studies. Thus, Enríquez et al. (2020), who also estimated the spatial footprints of storm
554 surges in the Western Mediterranean, obtained a coastal correlation length of 830 km (using a
555 clustering analysis technique) and cluster lengths between 2000 and 3500 km (using the match
556 level analysis and copula analysis methods). The differences are likely due to the fact that
557 Enríquez et al. (2020) considered as storm surge all non-tidal residuals; this includes the low-
558 frequency atmospheric component, which has been analysed separately in our work and for
559 which we have obtained a characteristic scale of a few thousand km.

560 **5. Conclusions**

561 In this work we have provided a detailed description of the extreme events observed by tide
562 gauges deployed on the coasts of the Western Mediterranean basin. We have analysed different
563 time scales separately, in order to characterise and quantify the different processes that contribute
564 to the occurrence of extreme sea levels on the coast. The different tidal regimes of the analysed
565 domain condition the magnitude of extreme levels and determine at least in part the relative
566 importance of the different components of extreme events. A feature common to the whole
567 domain is that Autumn is clearly the season with the highest occurrence of extreme events.

568 A main conclusion of this work is that the availability of sea level records with a high sampling
569 rate is of paramount importance for the study of extreme levels. Records with a 1-minute
570 sampling interval allow a better identification of the contributors to coastal extreme sea level and
571 a more accurate estimation of the maximum value of the peaks. In fact, they allow taking into
572 account processes that are usually not considered in previous works using hourly time series.

573 For the stations of the Western Mediterranean with a microtidal regime, the main contributors to
574 the extreme values are the storm surge, the low frequency component of the atmospheric
575 contribution, and the sub-hourly processes. The tidal contribution is more important close to the
576 Strait of Gibraltar, but still requires peaks in other components for an extreme to occur. The high

577 spatio-temporal resolution resulting from the deployment of the VENOM tide gauges (altogether
578 with the tide gauges operated by other institutions in the Balearic Islands) has allowed a further
579 insight into the contributions of sub-hourly processes to extreme sea levels. We have shown that
580 these processes have a very small spatial scale, but they can nevertheless be very important at
581 certain locations, becoming eventually the main contribution. The ports where this contribution
582 is most important coincide with those places where meteotsunamis are usually reported,
583 indicating that these phenomena are the dominant processes of the sub-hourly domain.

584 Finally, we have shown that waves can play a key role in the total water level reached during
585 extreme events, as they can lead to a rise of several meters. The contribution of waves to coastal
586 sea level is highly dependent on the type of coastal structure, reaching considerably higher
587 values when they imping on rigid protections. As an application, we have obtained a first
588 approximation to potentially flood-prone areas of the Bay of Palma during extreme events. The
589 methodology applied to propagate the waves and obtain the flooding areas could be extrapolated
590 to other regions. By adding the mean sea level rise projected under future climate scenarios, they
591 constitutes a useful tool for stakeholders dealing with the coastal adaptation to climate change.

592 **Acknowledgments**

593 This work is part of the R+D+I coordinated project VENOM (PGC2018-099285-B-C21,
594 PGC2018-099285-B-C22) and the project UNCHAIN (PCI2019-103680), both funded by
595 MCIN/AEI/10.13039/501100011033 and by the ERDF (A way of making Europe). This research
596 has been supported by the Ministerio de Ciencia e Innovación and the European Regional
597 Development Fund, Interreg. We thank the data providers (Puertos del Estado, SOCIB and Ports-
598 IB) for making their datasets freely available. We also want to thank the support of the Balearic
599 Holding of Harbours (Ports-IB) to the deployment of the VENOM tide gauge network and all the
600 members of the Sea Level and Climate group that have participated in the design, installation and
601 maintenance of the network, particularly Joan Puigdefabregas, Aida Frank-Comas, Joan
602 Villalonga, Joaquim Tomàs-Ferrer, Albert Font and Javier Soto-Navarro.

603

604 **Open Research**

605 The data of the REDMAR tide gauges network of Puertos del Estado are accessible through its
 606 web catalogue (<https://opendap.puertos.es/thredds/catalog.html>, last accessed 9 february 2023,
 607 Pérez et al., 2013). In the same catalogue the outputs of the NIVMAR forecasting system
 608 (https://opendap.puertos.es/thredds/catalog/nivmar_large_nivmar/catalog.html, last accessed 9
 609 february 2023, Álvarez Fanjul et al., 2001) are also available. The wave parameters of the
 610 SIMAR wave hindcast can be consulted on the web page of Puertos del Estado
 611 (<https://www.puertos.es/es-es/oceanografia/Paginas/portus.aspx>, last accessed 9 february 2023,
 612 Pilar et al., 2008). The bathymetric grid used for the shoreward wave propagation was obtained
 613 from the GEBCO website (<https://www.gebco.net/>, last accessed 9 february 2023, Weatherall et
 614 al., 2015). The code developed to identify and analyse the extreme events of the tide gauge series
 615 can be accessed at <https://doi.org/10.5281/zenodo.7848818> (Ramos-Alcántara et al., 2023).

616 **References**

- 617 Abu Zed, A. A., Kansoh, R. M., Iskander, M. M., & Elkholy, M. (2022). Wind and wave climate
 618 southeastern of the Mediterranean Sea based on a high-resolution SWAN model.
 619 *Dynamics of Atmospheres and Oceans*, 99, 101311.
 620 <https://doi.org/10.1016/j.dynatmoce.2022.101311>
- 621 Agulles, M., Jordà, G., & Lionello, P. (2021). Flooding of Sandy Beaches in a Changing
 622 Climate. The Case of the Balearic Islands (NW Mediterranean). *Frontiers in Marine
 623 Science*, 8, 760725. <https://doi.org/10.3389/fmars.2021.760725>
- 624 Álvarez Fanjul, E., Pérez Gómez, B., & Rodríguez Sánchez Arévalo, I. (2001). Nivmar: A storm
 625 surge forecasting system for Spanish waters. *Scientia Marina*, 65(S1), 145–154.
 626 <https://doi.org/10.3989/scimar.2001.65s1145>
- 627 Amores, A., Marcos, M., Carrió, D. S., & Gómez-Pujol, L. (2020). Coastal impacts of Storm
 628 Gloria (January 2020) over the north-western Mediterranean. *Natural Hazards and Earth
 629 System Sciences*, 20(7), 1955–1968. <https://doi.org/10.5194/nhess-20-1955-2020>
- 630 Backhaus, J. O. (1985). A three-dimensional model for the simulation of shelf sea dynamics.
 631 *Deutsche Hydrographische Zeitschrift*, 38(4), 165–187.
 632 <https://doi.org/10.1007/BF02328975>

- 633 Booij, N., & Holthuijsen, L. H. (1987). Propagation of ocean waves in discrete spectral wave
634 models. *Journal of Computational Physics*, *68*(2), 307–326.
635 [https://doi.org/10.1016/0021-9991\(87\)90060-X](https://doi.org/10.1016/0021-9991(87)90060-X)
- 636 Calafat, F. M., Avgoustoglou, E., Jordà, G., Flocas, H., Zodiatis, G., Tsimplis, M. N., &
637 Kouroutzoglou, J. (2014). The ability of a barotropic model to simulate sea level
638 extremes of meteorological origin in the Mediterranean Sea, including those caused by
639 explosive cyclones. *Journal of Geophysical Research: Oceans*, *119*(11), 7840–7853.
640 <https://doi.org/10.1002/2014JC010360>
- 641 Calafat, F. M., Gomis, D., & Marcos, M. (2009). Comparison of Mediterranean sea level fields
642 for the period 1961–2000 as given by a data reconstruction and a 3D model. *Global and
643 Planetary Change*, *68*(3), 175–184. <https://doi.org/10.1016/j.gloplacha.2009.04.003>
- 644 Callahan, J. A., & Leathers, D. J. (2021). Estimation of Return Levels for Extreme Skew Surge
645 Coastal Flooding Events in the Delaware and Chesapeake Bays for 1980–2019. *Frontiers
646 in Climate*, *3*, 684834. <https://doi.org/10.3389/fclim.2021.684834>
- 647 Cherif, S., Doblus-Miranda, E., Lionello, P., Borrego, C., Giorgi, F., Iglesias, A., Jebari, S.,
648 Mahmoudi, E., Moriondo, M., Pringault, O., Rilov, G., Somot, S., Tsikliras, A., Vila, M.,
649 & Zittis, G. (2020). Drivers of Change. In W. Cramer, J. Guiot, & K. Marini (Eds.),
650 *Climate and Environmental Change in the Mediterranean Basin – Current Situation and
651 Risks for the Future. First Mediterranean Assessment Report* (pp. 59–180). Union for the
652 Mediterranean, Plan Bleu, UNEP/MAP. 10.5281/zenodo.7100601
- 653 Cid, A., Menéndez, M., Castanedo, S., Abascal, A. J., Méndez, F. J., & Medina, R. (2016).
654 Long-term changes in the frequency, intensity and duration of extreme storm surge
655 events in southern Europe. *Climate Dynamics*, *46*(5–6), 1503–1516.
656 <https://doi.org/10.1007/s00382-015-2659-1>
- 657 Codiga, D. (2023). UTide Unified Tidal Analysis and Prediction Functions. [Software].
658 Mathworks. [https://www.mathworks.com/matlabcentral/fileexchange/46523-utide-
659 unified-tidal-analysis-and-prediction-functions](https://www.mathworks.com/matlabcentral/fileexchange/46523-utide-unified-tidal-analysis-and-prediction-functions)
- 660 de Alfonso, M., Lin-Ye, J., García-Valdecasas, J. M., Pérez-Rubio, S., Luna, M. Y., Santos-
661 Muñoz, D., Ruiz, M. I., Pérez-Gómez, B., & Álvarez-Fanjul, E. (2021). Storm Gloria:
662 Sea State Evolution Based on in situ Measurements and Modeled Data and Its Impact on

- 663 Extreme Values. *Frontiers in Marine Science*, 8, 646873.
664 <https://doi.org/10.3389/fmars.2021.646873>
- 665 Del-Rosal-Salido, J., Folgueras, P., Bermúdez, M., Ortega-Sánchez, M., & Losada, M. Á.
666 (2021). Flood management challenges in transitional environments: Assessing the effects
667 of sea-level rise on compound flooding in the 21st century. *Coastal Engineering*, 167,
668 103872. <https://doi.org/10.1016/j.coastaleng.2021.103872>
- 669 Dey, A. K., & Das, K. P. (2016). Modeling Extreme Hurricane Damage Using the Generalized
670 Pareto Distribution. *American Journal of Mathematical and Management Sciences*,
671 35(1), 55–66. <https://doi.org/10.1080/01966324.2015.1075926>
- 672 Dodet, G., Melet, A., Ardhuin, F., Bertin, X., Idier, D., & Almar, R. (2019). The Contribution of
673 Wind-Generated Waves to Coastal Sea-Level Changes. *Surveys in Geophysics*, 40(6),
674 1563–1601. <https://doi.org/10.1007/s10712-019-09557-5>
- 675 Dupuis, D. J. (1999). Exceedances over High Thresholds: A Guide to Threshold Selection.
676 *Extremes*, 1, 251–261. <https://doi.org/10.1023/A:1009914915709>
- 677 Enríquez, A. R. (2022). MatFlood. [Software]. Zenodo. <https://doi.org/10.5281/zenodo.7448967>
- 678 Enríquez, A. R., Wahl, T., Marcos, M., & Haigh, I. D. (2020). Spatial Footprints of Storm Surges
679 Along the Global Coastlines. *Journal of Geophysical Research: Oceans*, 125(9).
680 <https://doi.org/10.1029/2020JC016367>
- 681 Eurotop, Van der Meer, J. W., Allsop, N. W. H., Bruce, T., De Rouck, J., Kortenhaus, A., Pullen,
682 T., Schüttrumpf, H., Troch, P., & Zanuttigh, B. (2018). *Manual on wave overtopping of*
683 *sea defences and related structures. An overtopping manual largely based on European*
684 *research, but for worldwide application.* www.overtopping-manual.com
- 685 Ferrarin, C., Bellafiore, D., Sannino, G., Bajo, M., & Umgiesser, G. (2018). Tidal dynamics in
686 the inter-connected Mediterranean, Marmara, Black and Azov seas. *Progress in*
687 *Oceanography*, 161, 102–115. <https://doi.org/10.1016/j.pocean.2018.02.006>
- 688 Fiedler, J. W., Smit, P. B., Brodie, K. L., McNinch, J., & Guza, R. T. (2018). Numerical
689 modeling of wave runup on steep and mildly sloping natural beaches. *Coastal*
690 *Engineering*, 131, 106–113. <https://doi.org/10.1016/j.coastaleng.2017.09.004>
- 691 García-Valdecasas, J., Pérez Gómez, B., Molina, R., Rodríguez, A., Rodríguez, D., Pérez, S.,
692 Campos, Á., Rodríguez Rubio, P., Gracia, S., Ripollés, L., Terrés Nicoli, J. M., de los
693 Santos, F. J., & Álvarez Fanjul, E. (2021). *Operational tool for characterizing high*

- 694 *frequency sea level oscillations*. *106*, 1149–1167.
695 <https://doi.org/10.3989/scimar.2001.65s1145>
- 696 Gomis, D., Tsimplis, M., Marcos, M., Fenoglio-Marc, L., Pérez, B., Raicich, F., Vilibić, I.,
697 Wöppelmann, G., & Monserrat, S. (2012). Mediterranean Sea-Level Variability and
698 Trends. In P. Lionello (Ed.), *The Climate of the Mediterranean Region* (pp. 257–299).
699 Elsevier. <https://doi.org/10.1016/B978-0-12-416042-2.00004-5>
- 700 Haigh, I. D., Wadey, M. P., Wahl, T., Ozsoy, O., Nicholls, R. J., Brown, J. M., Horsburgh, K., &
701 Gouldby, B. (2016). Spatial and temporal analysis of extreme sea level and storm surge
702 events around the coastline of the UK. *Scientific Data*, *3*(1), 160107.
703 <https://doi.org/10.1038/sdata.2016.107>
- 704 Hasselmann, S., Hasselmann, K., Bauer, E., Janssen, P. A. E., Komen, G. J., Bertotti, L.,
705 Lionello, P., Guillaume, A., Cardone, V. C., Greenwood, J. A., Reistad, M., Zambresky,
706 L., & Ewing, J. A. (1988). The WAM Model—A Third Generation Ocean Wave
707 Prediction Model. *Journal of Physical Oceanography*, *18*(12), 1775–1810.
- 708 Holthuijsen, L. H. (2007). *Waves in Oceanic and Coastal Waters*.
- 709 Horsburgh, K. J., & Wilson, C. (2007). Tide-surge interaction and its role in the distribution of
710 surge residuals in the North Sea. *Journal of Geophysical Research*, *112*(C8), C08003.
711 <https://doi.org/10.1029/2006JC004033>
- 712 Huthnance, J. M., Mysak, L. A., & Wang, D.-P. (1986). Coastal trapped waves. In C. N. K.
713 Mooers (Ed.), *Coastal and Estuarine Sciences* (Vol. 3, pp. 1–18). American Geophysical
714 Union. <https://doi.org/10.1029/CO003p0001>
- 715 Lambert, E., Rohmer, J., Le Cozannet, G., & van de Wal, R. S. W. (2020). Adaptation time to
716 magnified flood hazards underestimated when derived from tide gauge records.
717 *Environmental Research Letters*, *15*(7), 074015. [https://doi.org/10.1088/1748-](https://doi.org/10.1088/1748-9326/ab8336)
718 [9326/ab8336](https://doi.org/10.1088/1748-9326/ab8336)
- 719 Larnicol, G., Ayoub, N., & Le Traon, P. Y. (2002). Major changes in Mediterranean Sea level
720 variability from 7 years of TOPEX/Poseidon and ERS-1/2 data. *Journal of Marine*
721 *Systems*, *33–34*, 63–89. [https://doi.org/10.1016/S0924-7963\(02\)00053-2](https://doi.org/10.1016/S0924-7963(02)00053-2)
- 722 Marcos, M., Tsimplis, M. N., & Shaw, A. G. P. (2009). Sea level extremes in southern Europe.
723 *Journal of Geophysical Research*, *114*(C1), C01007.
724 <https://doi.org/10.1029/2008JC004912>

- 725 Marcos, M., & Woodworth, P. L. (2017). Spatiotemporal changes in extreme sea levels along the
726 coasts of the North Atlantic and the Gulf of Mexico. *Journal of Geophysical Research:
727 Oceans*, 122(9), 7031–7048. <https://doi.org/10.1002/2017JC013065>
- 728 Melet, A., Meyssignac, B., Almar, R., & Le Cozannet, G. (2018). Under-estimated wave
729 contribution to coastal sea-level rise. *Nature Climate Change*, 8(3), 234–239.
730 <https://doi.org/10.1038/s41558-018-0088-y>
- 731 Menéndez, M., & Woodworth, P. L. (2010). Changes in extreme high water levels based on a
732 quasi-global tide-gauge data set. *Journal of Geophysical Research: Oceans*, 115(C10),
733 2009JC005997. <https://doi.org/10.1029/2009JC005997>
- 734 Middleton, J. F., & Thompson, K. R. (1986). Return periods of extreme sea levels from short
735 records. *Journal of Geophysical Research*, 91(C10), 11707.
736 <https://doi.org/10.1029/JC091iC10p11707>
- 737 Monserrat, S., Vilibić, I., & Rabinovich, A. B. (2006). Meteotsunamis: Atmospherically induced
738 destructive ocean waves in the tsunami frequency band. *Natural Hazards and Earth
739 System Sciences*, 6(6), 1035–1051. <https://doi.org/10.5194/nhess-6-1035-2006>
- 740 Muis, S., Verlaan, M., Winsemius, H. C., Aerts, J. C. J. H., & Ward, P. J. (2016). A global
741 reanalysis of storm surges and extreme sea levels. *Nature Communications*, 7(1), 11969.
742 <https://doi.org/10.1038/ncomms11969>
- 743 Nicholls, R. J., Hanson, S. E., Lowe, J. A., Warrick, R. A., Lu, X., & Long, A. J. (2014).
744 Sea-level scenarios for evaluating coastal impacts. *WIREs Climate Change*, 5(1), 129–
745 150. <https://doi.org/10.1002/wcc.253>
- 746 Noji, E. K. (1991). Natural Disasters. *Critical Care Clinics*, 7(2), 271–292.
747 [https://doi.org/10.1016/S0749-0704\(18\)30306-3](https://doi.org/10.1016/S0749-0704(18)30306-3)
- 748 Pérez, B., Álvarez Fanjul, E., Pérez, S., de Alfonso, M., & Vela, J. (2013). Use of tide gauge data
749 in operational oceanography and sea level hazard warning systems. *Journal of
750 Operational Oceanography*, 6(2), 1–18.
751 <https://doi.org/10.1080/1755876X.2013.11020147>
- 752 Pérez Gómez, B., Vilibić, I., Šepić, J., Međugorac, I., Ličer, M., Testut, L., Fraboul, C., Marcos,
753 M., Abdellaoui, H., Álvarez Fanjul, E., Barbalić, D., Casas, B., Castaño-Tierno, A.,
754 Čupić, S., Drago, A., Fraile, M. A., Galliano, D. A., Gauci, A., Gloginja, B., ... Zodiatis,

- 755 G. (2022). Coastal sea level monitoring in the Mediterranean and Black seas. *Ocean*
756 *Science*, 18(4), 997–1053. <https://doi.org/10.5194/os-18-997-2022>
- 757 Pilar, P., Soares, C. G., & Carretero, J. C. (2008). 44-year wave hindcast for the North East
758 Atlantic European coast. *Coastal Engineering*, 55(11), 861–871.
759 <https://doi.org/10.1016/j.coastaleng.2008.02.027>
- 760 Rabinovich, A. B. (2020). Twenty-Seven Years of Progress in the Science of Meteorological
761 Tsunamis Following the 1992 Daytona Beach Event. *Pure and Applied Geophysics*,
762 177(3), 1193–1230. <https://doi.org/10.1007/s00024-019-02349-3>
- 763 Raby, A. (2003). *Extreme Waves, Overtopping and Flooding at Sea Defences* [University of
764 Oxford]. <https://ora.ox.ac.uk/objects/uuid:82fcc770-8838-4f9b-9abe-32eecd05f9a>
- 765 Ramos-Alcántara, J., Agulles, M., Villalonga, J., Gomis, D., & Jordà, G. (2023). Sea Level
766 Extremes Analysis [Software]. Zenodo. <https://doi.org/10.5281/zenodo.7848818>
- 767 Rasmussen, C. E., & Williams, C. K. I. (2008). *Gaussian processes for machine learning* (3.
768 print). MIT Press.
- 769 Reek, T., Doty, S. R., & Owen, T. W. (1992). A Deterministic Approach to the Validation of
770 Historical Daily Temperature and Precipitation Data from the Cooperative Network.
771 *Bulletin of the American Meteorological Society*, 73(6), 753–762.
772 [https://doi.org/10.1175/1520-0477\(1992\)073<0753:ADATTV>2.0.CO;2](https://doi.org/10.1175/1520-0477(1992)073<0753:ADATTV>2.0.CO;2)
- 773 Ruggiero, P., Komar, P. D., McDougal, W. G., Marra, J. J., & Beach, R. A. (2001). Wave
774 Runup, Extreme Water Levels and the Erosion of Properties Backing Beaches. *Journal of*
775 *Coastal Research*, 17(2), 407–419.
- 776 Sayol, J. M., & Marcos, M. (2018). Assessing Flood Risk Under Sea Level Rise and Extreme
777 Sea Levels Scenarios: Application to the Ebro Delta (Spain). *Journal of Geophysical*
778 *Research: Oceans*, 123(2), 794–811. <https://doi.org/10.1002/2017JC013355>
- 779 Smyth, G. K. (2005). Numerical Integration. In P. Armitage & T. Colton (Eds.), *Encyclopedia of*
780 *Biostatistics* (p. b2a14026). John Wiley & Sons, Ltd.
781 <https://doi.org/10.1002/0470011815.b2a14026>
- 782 Soto-Navarro, J., Criado-Aldeanueva, F., García-Lafuente, J., & Sánchez-Román, A. (2010).
783 Estimation of the Atlantic inflow through the Strait of Gibraltar from climatological and
784 in situ data. *Journal of Geophysical Research: Oceans*, 115(C10), 2010JC006302.
785 <https://doi.org/10.1029/2010JC006302>

- 786 Stockdon, H. F., Holman, R. A., Howd, P. A., & Sallenger, A. H. (2006). Empirical
787 parameterization of setup, swash, and runup. *Coastal Engineering*, *53*(7), 573–588.
788 <https://doi.org/10.1016/j.coastaleng.2005.12.005>
- 789 Tintoré, J., Vizoso, G., Casas, B., Heslop, E., Pascual, A., Orfila, A., Ruiz, S., Martínez-
790 Ledesma, M., Torner, M., Cusí, S., Diedrich, A., Balaguer, P., Gómez-Pujol, L., Álvarez-
791 Ellacuria, A., Gómara, S., Sebastian, K., Lora, S., Beltrán, J. P., Renault, L., ...
792 Manriquez, M. (2013). SOCIB: The Balearic Islands Coastal Ocean Observing and
793 Forecasting System Responding to Science, Technology and Society Needs. *Marine*
794 *Technology Society Journal*, *47*(1), 101–117. <https://doi.org/10.4031/MTSJ.47.1.10>
- 795 Tolman, H. L. (1991). A third-generation model for wind waves on slowly varying, unsteady,
796 and inhomogeneous depths and currents. *Journal of Physical Oceanography*, *21*(6), 782–
797 797. [https://doi.org/10.1175/1520-0485\(1991\)021<0782:ATGMFW>2.0.CO;2](https://doi.org/10.1175/1520-0485(1991)021<0782:ATGMFW>2.0.CO;2)
- 798 Tsimplis, M. N., Calafat, F. M., Marcos, M., Jordà, G., Gomis, D., Fenoglio-Marc, L., Struglia,
799 M. V., Josey, S. A., & Chambers, D. P. (2013). The effect of the NAO on sea level and
800 on mass changes in the Mediterranean Sea: NAO effects on Mediterranean Sea level.
801 *Journal of Geophysical Research: Oceans*, *118*(2), 944–952.
802 <https://doi.org/10.1002/jgrc.20078>
- 803 Tsimplis, M. N., Marcos, M., Pérez, B., Challenor, P., Garcia-Fernandez, M. J., & Raicich, F.
804 (2009). On the effect of the sampling frequency of sea level measurements on return
805 period estimate of extremes—Southern European examples. *Continental Shelf Research*,
806 *29*(18), 2214–2221. <https://doi.org/10.1016/j.csr.2009.08.015>
- 807 Tsimplis, M. N., & Shaw, A. G. P. (2010). Seasonal sea level extremes in the Mediterranean Sea
808 and at the Atlantic European coasts. *Natural Hazards and Earth System Sciences*, *10*(7),
809 1457–1475. <https://doi.org/10.5194/nhess-10-1457-2010>
- 810 Tsimplis, M. N., & Woodworth, P. L. (1994). The global distribution of the seasonal sea level
811 cycle calculated from coastal tide gauge data. *Journal of Geophysical Research*, *99*(C8),
812 16031. <https://doi.org/10.1029/94JC01115>
- 813 Vilibić, I., & Šepić, J. (2017). Global mapping of nonseismic sea level oscillations at tsunami
814 timescales. *Scientific Reports*, *7*(1), 40818. <https://doi.org/10.1038/srep40818>

- 815 Vousdoukas, M. I., Wziatek, D., & Almeida, L. P. (2012). Coastal vulnerability assessment
816 based on video wave run-up observations at a mesotidal, steep-sloped beach. *Ocean
817 Dynamics*, 62(1), 123–137. <https://doi.org/10.1007/s10236-011-0480-x>
- 818 Wahl, T., Haigh, I. D., Nicholls, R. J., Arns, A., Dangendorf, S., Hinkel, J., & Slangen, A. B. A.
819 (2017). Understanding extreme sea levels for broad-scale coastal impact and adaptation
820 analysis. *Nature Communications*, 8(1), 16075. <https://doi.org/10.1038/ncomms16075>
- 821 Weatherall, P., Marks, K. M., Jakobsson, M., Schmitt, T., Tani, S., Arndt, J. E., Rovere, M.,
822 Chayes, D., Ferrini, V., & Wigley, R. (2015). A new digital bathymetric model of the
823 world's oceans. *Earth and Space Science*, 2(8), 331–345.
824 <https://doi.org/10.1002/2015EA000107>
- 825 Williams, J., Matthews, A., & Jevrejeva, S. (2019). Development of an automatic tide gauge
826 processing system. *National Oceanography Centre Research and Consultancy Report*,
827 64, 26.
- 828 Wilson, A. G., & Adams, R. P. (2013). Gaussian Process Kernels for Pattern Discovery and
829 Extrapolation. *Proceedings of the 30th International Conference on Machine Learning*,
830 28(3), 1067–1075.
- 831 Wolf, J. (2009). Coastal flooding: Impacts of coupled wave–surge–tide models. *Natural
832 Hazards*, 49(2), 241–260. <https://doi.org/10.1007/s11069-008-9316-5>
- 833 Woodworth, P. L., Melet, A., Marcos, M., Ray, R. D., Wöppelmann, G., Sasaki, Y. N., Cirano,
834 M., Hibbert, A., Huthnance, J. M., Monserrat, S., & Merrifield, M. A. (2019). Forcing
835 Factors Affecting Sea Level Changes at the Coast. *Surveys in Geophysics*, 40(6), 1351–
836 1397. <https://doi.org/10.1007/s10712-019-09531-1>
- 837

1 **Quantifying the Contributors to Extreme Sea Level Events in the Western**
2 **Mediterranean at High Spatio-temporal Resolution**

3
4 **J. Ramos-Alcántara^{1,2}, M. Agulles², D. Gomis² and G. Jordà¹**

5
6 ¹ Centre Oceanogràfic de Balears, C.N. Instituto Español de Oceanografía (CSIC), Palma de
7 Mallorca, 07015, Spain.

8 ² Institut Mediterrani d'Estudis Avançats, IMEDEA (UIB-CSIC), Esporles (Mallorca), 07190,
9 Spain.

10 Corresponding author: Jorge Ramos Alcántara (jorge.ramos@ieo.csic.es), Gabriel Jordà
11 (gabriel.jorda@ieo.csic.es)

12
13 **Key Points:**

- 14 • High frequency sea level records are needed to get a complete view of the processes
15 contributing to extreme sea levels.
- 16 • Sub-hourly processes can be a major contributor to extreme levels in some locations,
17 although they usually have a local scale.
- 18 • The contribution of waves to total sea level is highly dependent on the coastal
19 morphology, and can lead to a rise of several meters.

20 **Abstract**

21 A comprehensive characterisation of extreme sea levels at different spatio-temporal scales is
22 presented for the Western Mediterranean. The classical view of extreme sea levels as a
23 consequence of the concurrence of storm events and high tides may lead to an incomplete picture
24 for the Mediterranean coasts, where the tidal regime is small and processes operating at high
25 frequencies can contribute significantly to extreme levels. Our approach bases on the analysis of
26 tide gauge records with a high sampling frequency (1 minute), in order to consider other
27 contributors beyond storm surges and tides. To have a basin-scale view, we first analyse the tide
28 gauges operated by Puertos del Estado, which are distributed over all the Spanish Mediterranean
29 coasts and cover at least from 2010 to 2022. Next, we focus on a more reduced domain to take
30 advantage of the unprecedented spatio-temporal resolution of the VENOM tide gauge network,
31 opening since 2020 in the Balearic archipelago. Last, we analyse the role of waves in local
32 extreme sea level events by propagating waves towards the coast in the Bay of Palma. The wave
33 run-up estimates are calculated considering the type of coastal protection and are used to
34 simulate the potential flooding that could occur in the future under an unfavourable climate
35 change scenario. Our results highlight the importance of high-frequency sea level records to
36 study extreme events, and the key role of processes such as meteotsunamis and waves in the
37 occurrence of extreme sea levels.

38 **Plain Language Summary**

39 Sea level extremes can cause significant environmental damage and affect the well-being of
40 populations living in coastal regions. It is therefore essential to understand and quantify the
41 mechanisms behind these extreme events. Storms are often considered to be the only cause of
42 extreme sea levels; however, in this work we show that in some Mediterranean harbours there
43 are other processes taking place at local scale and over short periods of time than can contribute
44 to sea level extremes. We also show that the contribution of waves to coastal sea extreme
45 elevations can be very significant, though it largely depends on the type of coastline. In
46 particular, we show an example of the areas that could be flooded due to the wave contribution
47 under an unfavourable scenario of sea level rise due to global warming. Overall, we show that
48 for the study of extreme sea levels in the Mediterranean, using tide gauge series reporting at least

49 one datum per minute is essential, in order to consider the contribution of processes that are not
50 usually taken into account.

51 **1 Introduction**

52 Extreme sea level events in coastal regions occur as a consequence of the overlapping of
53 different processes that can act at different spatial and temporal scales. Extreme high waters can
54 cause significant environmental damage and affect the well-being of populations living in coastal
55 regions. Coastal flooding is one of the most common natural disasters (Noji, 1991) and can lead
56 to erosion, damage to infrastructures and even loss of lifes (Ruggiero et al., 2001; Wolf, 2009).
57 Moreover, in a context of global warming and projected sea level rise, the intensity of coastal
58 impacts associated with extreme sea level events is expected to increase significantly (Nicholls et
59 al., 2014; Wahl et al., 2017). In order to make proper assessments of the associated risks and
60 hazards, it is necessary to characterise extreme sea level events, analysing in detail their spatio-
61 temporal variability and quantifying the different processes contributing to extreme values (Del-
62 Rosal-Salido et al., 2021).

63 In the Mediterranean coastal zone, the absolute magnitude of extreme events is small compared
64 to other coastal regions, in part due to the microtidal regime of the basin (Muis et al., 2016).
65 However, the microtidal regime also makes that coastal infrastructures are not as well adapted to
66 large sea level anomalies as in other regions with larger tidal ranges. Furthermore, an important
67 part of the economy of Mediterranean regions depends on coastal activities (e.g. tourism, trading
68 and transport, ...), making this region particularly vulnerable to the consequences of extreme sea
69 levels (Agulles et al., 2021; Gomis et al., 2012).

70 Coastal sea level variability results from the overlapping of many physical processes operating
71 over a wide range of frequencies and spatial scales. Those taking place on long time scales (e.g.
72 seasonal to multidecadal) are assumed to behave similarly in the coastal zone and in the open
73 ocean. On the other hand, coastal areas are also affected by other contributions with shorter
74 temporal and spatial scales, such as storm surges, seiches and wave runup (Woodworth et al.,
75 2019). In practice, extreme sea level events are often quantified as the result of just two
76 processes: tides and storm surges (Menéndez & Woodworth, 2010; Middleton & Thompson,
77 1986; Muis et al., 2016). However, up to our knowledge the accuracy of this approach has not

78 been assessed in the Mediterranean Sea, where there are clues suggesting the significant
79 contribution of other processes.

80 One of the coastal phenomena that may contribute to Mediterranean extreme events are
81 meteotsunamis, atmospherically-induced waves in the tsunami frequency band (2-120 min) that
82 can cause considerable damage to infrastructure and ships (see e.g. Monserrat et al., 2006;
83 Rabinovich, 2020). Vilibić & Šepić (2017) suggested that the contribution of such high
84 frequency phenomena to extreme coastal sea level events could be of up to 50%. Another
85 important driver of coastal sea level is the effect of waves reaching the coast, which can lead to
86 an elevation of sea level over the still water level (referred to as wave runup). The wave runup is
87 in fact the sum of the wave setup elevation onshore and the effect of swash fluctuations (Melet et
88 al., 2018; Ruggiero et al., 2001). This phenomenon can be a dominant contributor in coastal
89 extreme events causing overtopping of coastal infrastructures (Raby, 2003). Although
90 Mediterranean wave heights are usually smaller than in the large oceans, their role can be
91 important in extreme events such as the storm Gloria, in 2020, when the main impacts on the
92 coast were caused by the large waves associated with strong winds (Amores et al., 2020; de
93 Alfonso et al., 2021).

94 When high frequency processes play an important role, the characterization of extreme sea level
95 contributors requires an adequate temporal sampling. Most of the studies undertaken so far have
96 used hourly time series from tide gauges (see e.g. Calafat et al., 2009; Callahan & Leathers,
97 2021; Tsimplis & Shaw, 2010), mainly because few long records with a higher frequency
98 sampling were available. However, the situation has changed in the recent years, and nowadays
99 it is possible to find tide gauge datasets covering several years with a 1-min resolution (e.g.
100 García-Valdecasas et al., 2021; Pérez Gómez et al., 2022). Another feature to be considered is
101 that most tide gauges are located in sheltered harbours, where the wave set-up signal is
102 diminished or practically not present; as a consequence, many of the operational tide gauges only
103 record what is known as Still Water Level (SWLs) (Lambert et al., 2020; Melet et al., 2018).
104 This makes that the only way to obtain a proper regional characterization of the wave effect on
105 sea level is using numerical models (Holthuijsen, 2007).

106 The main objective of this paper is to understand and quantify the different mechanisms
107 contributing to coastal extreme sea level events in the western Mediterranean. For this purpose,

108 we use 1-min tide gauge records altogether with outputs from storm surge and wave numerical
109 models. The paper is organised as follows: in section 2, we describe the datasets and the
110 methodology used to characterize the different contributors to extreme sea levels. Results are
111 presented in section 3, and consist of a first general characterisation of Western Mediterranean
112 extremes (Sect. 3.1) followed by the quantification of the different contributors (Sect. 3.2).
113 Particular attention is paid to the quantification of sub-hourly processes (sampled by an ultra-
114 dense network of tide gauges operating in the Balearic archipelago, Sect. 3.3) and to the
115 contribution of waves to coastal flooding (for the particular case of the Bay of Palma, Sect. 3.4).
116 Results also include an analysis of the spatial scale of each of the main contributors to extreme
117 sea levels (Sect 3.5). Results are discussed in section 4 and the final remarks given in section 5.

118 **2 Data and Methodology**

119 **2.1 Tide gauges records**

120 Several sets of tide gauges with different time coverages have been used; in a first step we used
121 data from tide gauges operated by Puertos del Estado, the Spanish holding of State Harbours
122 (<https://opendap.puertos.es/thredds/catalog.html>). The REDMAR sea level network of Puertos
123 del Estado operates 40 tide gauge stations and the network has been recently improved with the
124 incorporation of new radar sensors that measure sea level at a frequency of 2 Hz (Pérez et al.,
125 2013). From this dataset, the 17 stations located in the Mediterranean Sea (Fig. 1a) were selected
126 and a minute time vector covering the period from 2010 to 2022 was defined (Table 1). In the
127 framework of the VENOM project (acronym in Spanish of “Spatial Variability of Sea Level in
128 the Western Mediterranean”), a low-cost ultra-dense and self-built tide gauge network has been
129 recently deployed along the coasts of the Balearic Islands. The 20 VENOM tide gauges record
130 sea level variations with a 1-min sampling rate, and add to other 12 tide gauges operated by other
131 institutions and recording at the same frequency rate. Basing on the location, sampling rate and
132 record length, we selected 21 tide gauges (listed in Table 2, Fig. 1b): 10 from the VENOM
133 network, 5 operated by Puertos del Estado, 5 operated by the Balearic Islands Coastal Observing
134 and Forecasting System (SOCIB: <https://www.socib.es/>, Tintoré et al (2013)) and 1 operated by
135 Ports IB (<http://webtrans.geonica.com>). Altogether they constitute a network with an
136 unprecedented high spatial density, which allows to investigate the small scale spatial variability
137 of the different contributors to extreme sea level events. The resulting dataset has an average

Table 1: Mediterranean tide gauges operated by Puertos del Estado, with their Location, Date of the first and last data of the considered series, and the Percentage of Missing Data.

Station	Latitude(°)	Longitude(°)	First data	Last data	Missing values (%)
Tarifa	36.01	-5.60	01 January 2010	09 May 2022	6.47
Algeciras	36.18	-5.40	01 January 2010	09 May 2022	5.53
Málaga	36.71	-4.42	01 January 2010	09 May 2022	8.48
Motril	36.72	-3.52	01 January 2010	09 May 2022	6.58
Melilla	35.29	-2.93	01 January 2010	09 May 2022	9.83
Almería	36.83	-2.48	01 January 2010	09 May 2022	7.41
Carboneras	36.97	-1.90	25 April 2013	09 May 2022	7.89
Gandía	38.99	-0.15	01 January 2010	09 May 2022	4.36
Valencia	39.44	-0.31	01 January 2010	09 May 2022	7.77
Sagunto	39.63	-0.21	01 January 2010	09 May 2022	6.07
Tarragona	41.08	1.21	27 May 2011	09 May 2022	6.09
Barcelona	41.34	2.17	01 January 2010	06 May 2022	5.51
Ibiza	38.91	1.45	01 January 2010	09 May 2022	5.57
Formentera	38.73	1.42	22 January 2010	09 May 2022	8.59
Palma	39.56	2.64	01 January 2010	09 May 2022	16.45
Alcudia	39.83	3.14	01 January 2010	09 May 2022	11.30
Mahón	39.89	4.27	01 January 2010	09 May 2022	10.10

138 separation between stations of 8.7 km, in contrast with the average separation of the REDMAR
 139 tide gauge network in the Western Mediterranean, which is of 58.7 km. The first instruments of
 140 the VENOM network were installed at the beginning of 2020; the period used for the analysis
 141 performed in this work covers two years, from July 2020 to July 2022.

142 Tide gauge measurements are subject to errors of different nature that can affect the consistency
 143 and reliability of the series. Thus, a manual control was first applied to the series in order to
 144 detect and correct eventual discontinuities in the datum, and to discard out-of-range and other
 145 clearly anomalous values. An automatic quality control based on well-established procedures
 146 (see e.g. Reek et al., 1992; Williams et al., 2019) was subsequently applied. That second step
 147 included: (i) the elimination of values outside the interval defined by the average of each series \pm
 148 4 times the standard deviation; (ii) the identification of spikes through the analysis of the
 149 differences between groups of 3 consecutive measurements. Finally, the measurements that

150 passed this quality control were converted into sea level anomalies (SLA) by subtracting the
 151 temporal average of the corresponding series.

Table 2: Selected tide gauges in the Balearic Islands, specifying the Institutions operating them, their Locations, the start and end Dates of the series and the Percentage of missing data.

Station	Institution	Latitude (°)	Longitude (°)	First data	Last data	Missing values (%)
Formentera	Puertos del Estado	38.73	1.42	19 July 2020	19 July 2022	1.41
Sant Antoni	SOCIB	38.98	1.30	19 July 2020	19 July 2022	1.26
Ibiza	Puertos del Estado	38.91	1.45	19 July 2020	19 July 2022	2.55
Santa Eulàlia	VENOM	38.98	1.54	10 March 2021	06 July 2022	34.44
Sa Ràpita	SOCIB	39.54	2.38	19 July 2020	19 July 2022	4.49
S'Arenal	VENOM	39.50	2.75	22 January 2021	17 June 2022	39.38
Palma	Puertos del Estado	39.56	2.64	19 July 2020	19 July 2022	0.29
Palma	VENOM	39.56	2.64	21 January 2021	02 June 2022	31.97
Andratx	SOCIB	39.36	2.95	19 July 2020	19 July 2022	7.18
Port de Sóller	VENOM	39.80	2.69	19 July 2020	15 July 2022	11.50
Alcudia	Puertos del Estado	39.83	3.14	19 July 2020	19 July 2022	1.58
Can Picafort	VENOM	39.77	3.16	03 March 2021	13 July 2022	32.23
Colonia Sant Pere	SOCIB	39.54	3.34	19 July 2020	19 July 2022	34.56
Cala Rajada	VENOM	39.71	3.46	19 July 2020	17 March 2022	23.11
Cala Bona	VENOM	39.61	3.39	24 February 2021	19 July 2022	30.23
Porto Cristo	SOCIB	39.74	3.27	19 July 2020	19 July 2022	0.40
Portocolom	VENOM	39.42	3.26	19 July 2020	19 July 2022	0.87
Portopetro	VENOM	39.36	3.21	19 July 2020	19 July 2022	0.97
Mahón	Puertos del Estado	39.89	4.27	19 July 2020	19 July 2022	1.74
Ciutadella	Ports IB	39.99	3.83	19 July 2020	19 July 2022	0.19
Fornells	VENOM	40.05	4.13	19 August 2020	30 December 2021	33.58

152

153 2.2 Decomposition of sea level records

154 In order to assess the role of the different processes contributing to sea level extremes, the tide
 155 gauge time series were split into several components (Fig. 2):



Figure 1: a) Location of the tide gauges from Puertos del Estado available in the Western Mediterranean, b) Location of the selected tide gauges in the Balearic archipelago, with the color indicating the institution operating them.

156 - **Atmospheric component:** Hourly sea level variations caused by changes in the atmospheric
 157 pressure and wind were obtained from the outputs of the NIVMAR forecasting system
 158 (Álvarez Fanjul et al., 2001), which are available from the website of Puertos del Estado
 159 (<http://opendap.puertos.es/thredds/catalog.html>). The NIVMAR system is based on the model
 160 HAMSON (Backhaus, 1985) forced by with wind and sea level pressure data provided by the

161 European Centre for Medium-Range Weather Forecasts (ECMWF, <https://www.ecmwf.int/>).
162 The hourly time series were first converted into 1-min time series using a linear interpolation
163 and then they were split into two frequency bands: $T > 1\text{month}$ and $T < 1\text{month}$, which will
164 hereafter be referred to as the low-frequency atmospheric contribution ($T > 1\text{month}$) and the
165 Storm Surge contribution ($T < 1\text{month}$). It is important to note that this approach differs from
166 other studies where the surge component is simply defined as the non-tidal residual of the
167 original series, without further considerations on the forcing mechanisms of the observed sea
168 level variability (Horsburgh & Wilson, 2007; Menéndez & Woodworth, 2010).

169 - **Seasonal cycle:** Seasonal sea level changes in the Mediterranean are mainly due to steric
170 effects in the upper ocean (Gomis et al., 2012; Tsimplis & Woodworth, 1994) and to seasonal
171 mass transports through the Strait of Gibraltar (Soto-Navarro et al., 2010). The seasonal cycle
172 was obtained by interpolating to 1-min the monthly averages of the tide gauge records once
173 the atmospheric component was removed.

174 - **Astronomical tide:** Once the atmospheric component and seasonal cycle were subtracted
175 from the original series, the remaining sea level signal was adjusted by using the Matlab
176 UTIDE functions (Codiga, 2023).

177 - **Residuals:** the residuals remaining after removing the previous components were separated
178 into three frequency bands: $T > 1\text{month}$, $1\text{hour} < T < 1\text{month}$, $T < 1\text{hour}$. Although these bands do
179 not correspond to specific physical processes, the main drivers of the variability of each band
180 are known. The lower frequency band ($T > 1\text{m}$) is mainly driven by the hydrodynamic
181 structure of the Mediterranean basin (Larnicol et al., 2002) and by changes in the
182 characteristics of the incoming Atlantic waters (Tsimplis et al., 2013). The high frequency
183 band ($T < 1\text{h}$) includes phenomena such as shelf waves or meteotsunamis, which can lead to
184 resonant responses of remarkable magnitude in different inlets and bays of the Western
185 Mediterranean (Monserrat et al., 2006). Finally, the intermediate frequency band ($1\text{h} < T < 1\text{m}$)
186 is the domain of other processes such as wave-induced variability or runoff from rivers
187 (Huthnance et al., 1986; Melet et al., 2018; Woodworth et al., 2019).

188 An example of the splitting of a tide gauge record (Mahón) into the described components is
189 shown in Fig. 2.

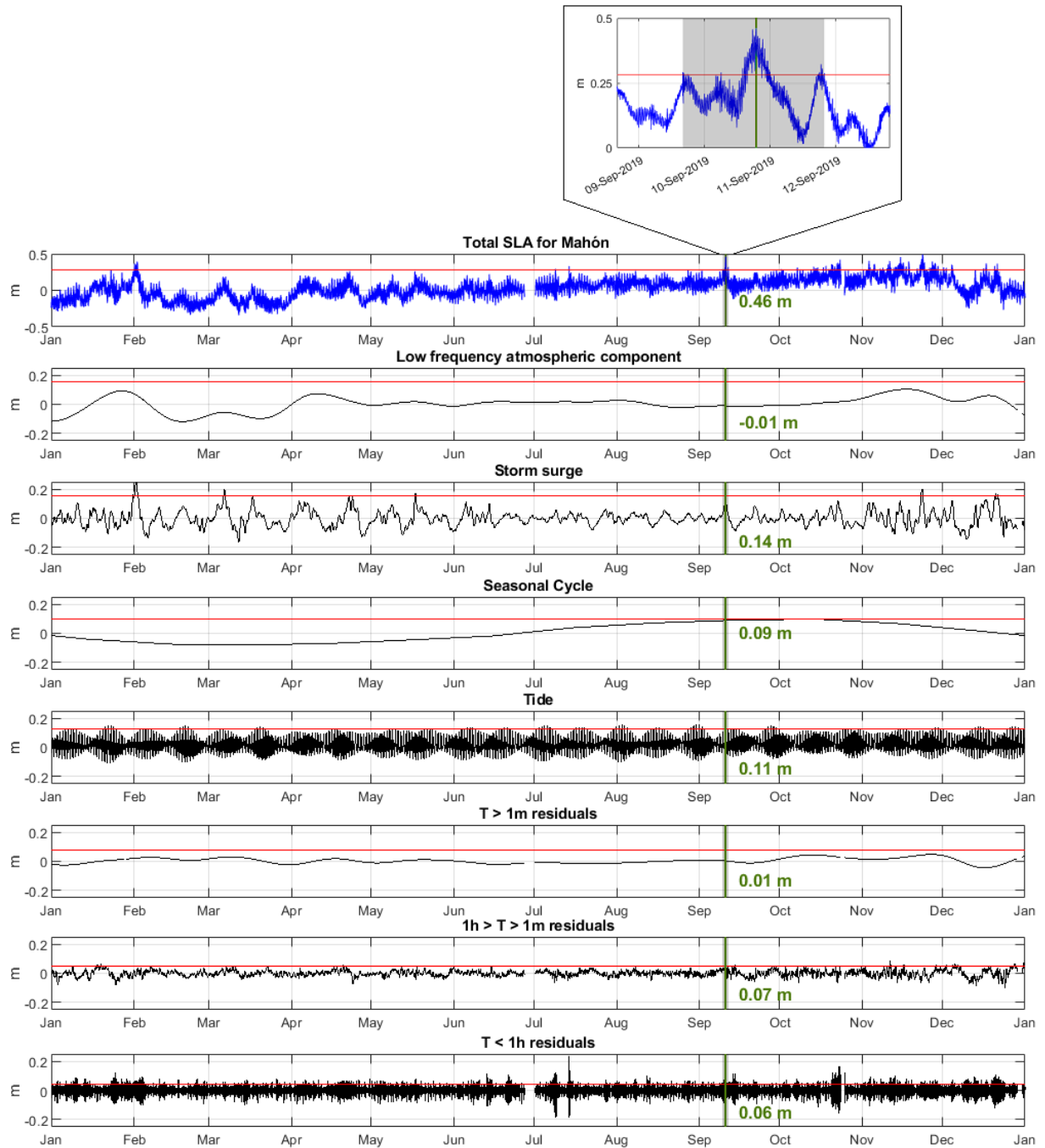


Figure 2: Component decomposition of the Mahón tide gauge record of 2019. For the total series and for each component, the 99th percentile has been marked with a red line. A particular extreme event is selected as example, indicating the time of its peak with a green line. The total sea level anomaly and the value of each component at the time of the peak is shown as green text. A zoom of this event is highlighted at the top of the figure.

190 2.3 Processing of extreme sea level events

191 Extreme sea level events were identified in the tide gauge series on the basis of their 99th
 192 percentile. Following the criteria of other authors (Calafat et al., 2014; Cid et al., 2016; Marcos
 193 & Woodworth, 2017), measurements over this threshold separated by less than 3 days were
 194 considered as a single event, in order to ensure the independence between events. After the
 195 identification, the main characteristics of the event (starting time, ending time, peak value,
 196 instant of maximum height and average value during the event) were determined. The duration
 197 of the event was determined as the time during which sea level was above the 99th percentile,
 198 between the starting and ending times of the event. Another interesting parameter is the intensity
 199 of the event, defined as the area between the series and the 99th percentile, integrated over the
 200 duration of the event. For this calculation we used the numerical integration method of the
 201 trapezoid rule (see e.g. Smyth, 2005).

202 To estimate return levels, we used the classical method of modelling exceedances over a
 203 threshold, through an Extreme-value distribution (Dupuis, 1999). The use of the extremes over a
 204 threshold is an appropriate alternative to modelling from the yearly maximum extremes, which
 205 can lead to a loss of information in the case that the extremes of any year are exceptionally low
 206 (Dey & Das, 2016; Marcos et al., 2009). Thus, if μ is the considered high threshold of a series
 207 (the 99.5th percentile in our case), the cumulative distribution function of the series of excesses
 208 $y = x - \mu$ can be approximated by the generalized Pareto distribution (GPD):

$$209 \quad H(y) = 1 - \left(1 - \frac{\xi y}{\sigma}\right)^{-\frac{1}{\xi}} \quad (1)$$

210 where ξ is the shape parameter and $\sigma (>0)$ is the scale parameter, both being estimated by
 211 maximum likelihood. In our case the shape parameter must be $\xi \leq 0$, otherwise the distribution
 212 would have no upper limit and the existence of values over the threshold would not be possible.
 213 Fitting the extreme values to a GPD allows the estimation of the 95% confidence intervals for the
 214 parameters of the distribution, which in turn enables to establish confidence intervals for the
 215 calculated return levels.

216 Return levels can be directly calculated from the parameters of the GPD distribution by means of
 217 the following expression:

218

$$R.L.(m) = \mu + \frac{\sigma}{\xi} (m^\xi - 1) \quad (2)$$

219 where $R.L.(m)$ is the level expected to be exceeded once every m years. For each tide gauge,
 220 return levels were calculated both for the original series and for the separate components.
 221 Namely, for each component we analysed the reduction in return levels resulting from fitting the
 222 GPD distribution to the levels corresponding to the instants of the exceedances above the same
 223 threshold used for the original series, but after each component had been subtracted.

224 2.4 Quantification of the component contributions

225 The contribution of each of the identified components to the sea level anomaly series was
 226 quantified through the percentage contribution of each of them to the magnitude of the event
 227 peaks. If we consider for instance the event in the Mahón series highlighted in Fig. 2, the
 228 magnitude of the peak is 46 cm, and the component that contributes the most to it is the Storm
 229 Surge, whose series has a value of 14 cm at the instant of the peak. The contribution of that

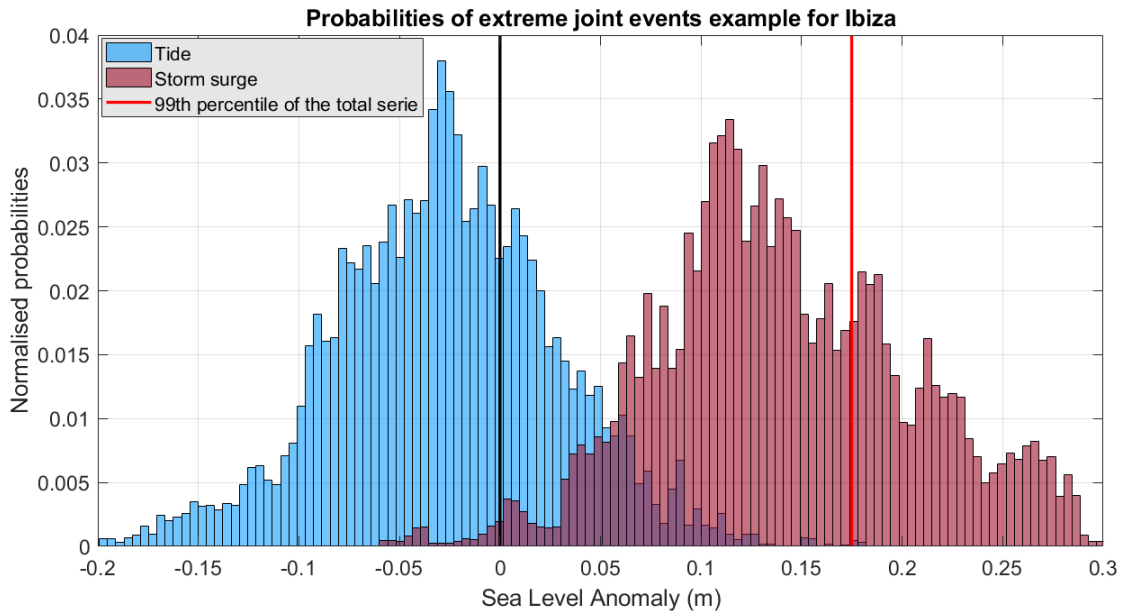


Figure 3: Probability distributions of extreme joint events derived from a synthetic series containing only the tidal and storm surge components. The black line marks the zero level of the total series, while the red line represents its 99th percentile.

230 component would then be evaluated in about 31%. The same procedure was applied to all the
231 events.

232 The probability of extreme joint events was also estimated, as a measure of the dependence of
233 extreme values with respect to each component (i.e., the probability of having an extreme value
234 in a component and in the original SLA series at the same time). This probability can be
235 calculated empirically through the percentage of extreme values of each component that coincide
236 in time with extreme values of the total SLA series. For each component, a probability
237 distribution function (pdf) of the total SLA is computed using the time intervals during which the
238 component is above its own 99th percentile (i.e. when extreme values of that component are
239 observed). If that pdf is centred around zero, this means that the component has no significant
240 impact on the extremes of total SLA (i.e. extreme values of that component do not lead to
241 extreme total SLA values). Conversely, if the pdf is displaced towards positive values, this
242 means that extreme values of that component coincide with larger positive values of total SLA;
243 that is, extreme values of that component significantly contribute to extreme SLA events.

244 For illustrative purposes, we have constructed a synthetic time series by adding only the tidal and
245 storm surge components isolated from the Ibiza tide gauge. Given the microtidal regime of Ibiza,
246 the extreme values of the total synthetic SLA will coincide with the extreme values of the storm
247 surge component, while being independent of the tidal component. Figure 3 shows the synthetic
248 total SLA pdf corresponding to extreme values of both, the tidal and storm surge components.
249 For the tidal component, the distribution is centred slightly before the 0 level (black line),
250 meaning that extreme values of the tides almost never translate into extremes of total SLA. On
251 the contrary, extreme values of the storm surge component show a high coincidence with
252 positive values of total SLA, and a substantial number of them (those to the right of the 99th
253 percentile denoted by the red line) coincide with extreme values of total SLA. Therefore, in this
254 example the storm surge would be the only responsible for the occurrence of extreme values of
255 total SLA.

256 2.5 The role of wind waves

257 Although the contribution of wind waves to sea level within harbors is practically negligible,
258 their contribution to extreme sea levels in exposed coasts can be very relevant. In order to

259 quantify this contribution, the wave runup 2% (hereafter RU2%), which corresponds to the
260 characteristic value of 2% exceeding probability of individual waves reaching the swash zone
261 during a sea state (Stockdon et al., 2006), was calculated along the coast of Palma Bay.

262 The contribution of waves to coastal sea level depends on the characteristics of the incoming
263 offshore waves, but also (and critically) on the morphology of the coast (Dodet et al., 2019). The
264 characterization of wave effects was carried out in two steps. First, the offshore wave regime of
265 the period 2010 to 2022 was obtained from the SIMAR wave hindcast (Pilar et al., 2008)
266 distributed by Puertos del Estado, which covers from 1958 to present. More specifically, the data
267 belong to the WANA subset, which starts in 2006, and is based on WAM (Hasselmann et al.,
268 1988) and Wavewatch (Tolman, 1991) models, forced by hourly wind fields provided by the
269 Spanish State Meteorological Agency (AEMET). These offshore waves were then propagated up
270 to the coast using the SWAN numerical model. SWAN is a third-generation shallow water model
271 that solves the discrete spectral action balance equation (Booij & Holthuijsen, 1987) and has
272 yielded accurate results in many studies (see e.g. Abu Zed et al., 2022). The model has been set
273 up for the Palma Bay with a 100 x 100 m spatial resolution (Fig. 4), and uses the bathymetry grid
274 obtained from GEBCO, the General Bathymetric Chart Of Oceans (Weatherall et al., 2015).

275 Once the nearshore wave set-up and the wave climate was obtained at the control points (points 1
276 to 20 in Fig. 4), hourly sea state parameters (H_s and T_p) were used to calculate the RU2%. The
277 estimation of RU2% depends on the coastal typology at each control point: where the coast is
278 protected by artificial structures such as dikes or seawalls (magenta dots in Fig. 4), RU2% is
279 estimated using an empirical formulations derived from laboratory experiments (Eurotop, 2018),
280 while on beaches (white dots in Fig. 4) it is estimated using the empirical equation developed by
281 Stockdon et al. (2006) and commonly used in coastal engineering studies (see e.g. Fiedler et al.,
282 2018; Vousdoukas et al., 2012). For the beaches, we use the slope values estimated by Agulles et
283 al. (2021) for the entire Balearic coastline, based on the equilibrium profiles.

284 In order to evaluate the impact of adding the wave contribution, we estimated the potentially
285 flood-prone extension along Palma Bay, considering a mean sea level rise (MSLR) of 0.67 m,
286 the regional value projected for the period 2080-2100 under the RCP8.5 scenario (Agulles et al.,
287 2021; Cherif et al., 2020). On top of this MSLR, we considered 3 extreme sea level scenarios: i)
288 the maximum sea level recorded by the Palma tide gauge (2010-2022), where wave effects are

289 minimal (ESC1); ii) the combination of the maximum recorded sea level (ESC1) with the wave
 290 set-up obtained at the control points (ESC2); iii) the combination of the maximum recorded sea
 291 level (ESC1) with the RU2% contribution obtained at the control points. The area flooded under
 292 each scenario was estimated by combining the “bathtub” approximation algorithm developed by
 293 Enríquez (2022) with the digital terrain elevation model developed by the Spanish National
 294 Geographic Institute, IGN
 295 (https://centrodedescargas.cnig.es/CentroDescargas/locale?request_locale=es). Although the
 296 “bathtub” approximation may be too simplistic to estimate the actual flooding caused by short
 297 events, it provides a useful first approximation to the impact of different definitions of extreme
 298 events.

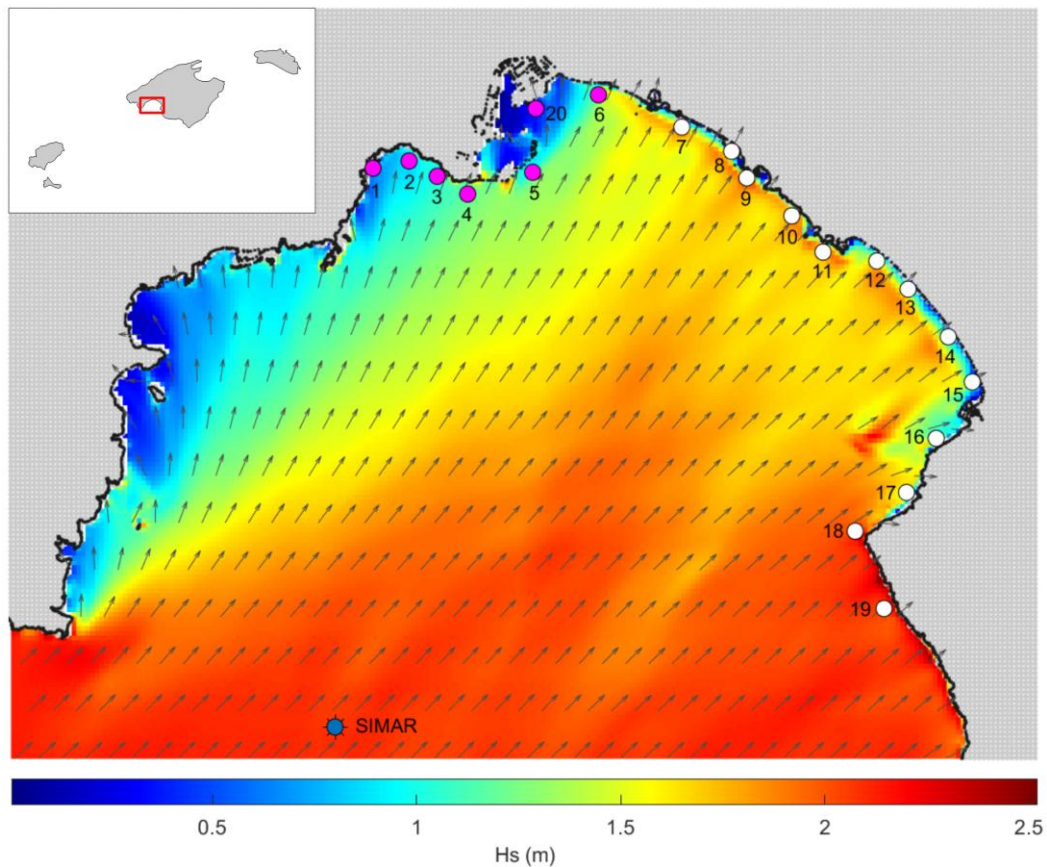


Figure 4: Example of the propagation of an offshore southwesterly sea state given at a SIMAR point (blue dot) towards the coasts of Palma Bay using the SWAN model. The control points where coastal waves are obtained are denoted by numbers from 1 to 20. The wave runup is calculated for artificial coastal protection (magenta dots) and on sandy beaches (white dots).

299 2.6 Spatial scales of the contributors to extreme events

300 To study the characteristic spatial scales of the different processes contributing to extreme sea
 301 level events, we calculated time correlations between the peak events identified at different
 302 stations for each component. But first, the time and intensity of the extreme values of each
 303 component had to be identified; we considered as independent events those separated by a
 304 minimum time lag that was set accordingly to the characteristic time scale of the component: 3
 305 days for the total SLA series, 15 days for the low-frequency atmospheric component, 6 hours for
 306 the storm surge and half an hour for the sub-hourly residuals. Then, time correlation between all
 307 pairs of tide gauges were computed for each component; in order to allow for a certain time lag
 308 (i.e. the expected lag due to a moving storm), we considered the maximum value within a 1-day
 309 window around the date of each event. The result of the process is a set of correlation values
 310 (one for each pair of tide gauges) which are expected to show some dependence with respect to
 311 the separation distance between the instruments. Hence, fitting a spatial correlation function
 312 depending only on the separation distance $\rho(d_{ij})$, a characteristic length-scale L_s can be
 313 estimated. As spatial correlation model we used a Gaussian function (Rasmussen & Williams,
 314 2008; Wilson & Adams, 2013):

$$315 \quad \rho(d_{ij}) = \exp(-0.5 d_{ij}^2 / L_s^2) \quad (3)$$

316 where d_{ij} is the distance between stations i, j .

317 3 Results

318 3.1 Overall characterization of extreme events

319 Figure 5 shows an overview of the peak values of the extreme events identified in the 17 tide
 320 gauge records covering the western sector of the Western Mediterranean and spanning the period
 321 2010-2022 (see Table 1). Most of the medians of the peak values are between 30 and 40 cm, but
 322 they progressively increase for stations close to the Strait of Gibraltar. The reason for this
 323 behaviour is that the tidal regime of the Western Mediterranean is dominated by the M2 tidal
 324 component, which strongly reduces its amplitude after entering the basin through Gibraltar
 325 (Ferrarin et al., 2018). Therefore, the location of the station is expected to play a key role in the
 326 contribution of the tidal component to extreme events.

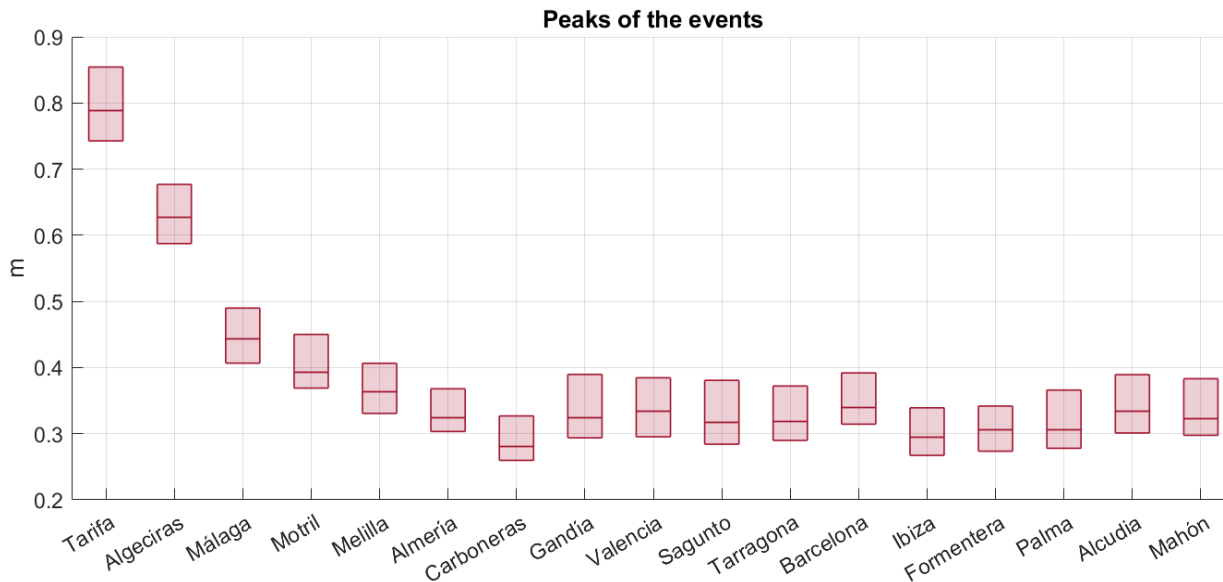


Figure 5: Peak values of the extreme events identified in the 17 tide gauge records spanning the period 2010-2022 (listed in Table 1). Boxplots report the median (inbox solid lines) and the 25th and 75th percentiles (bottom and top limit of the boxes).

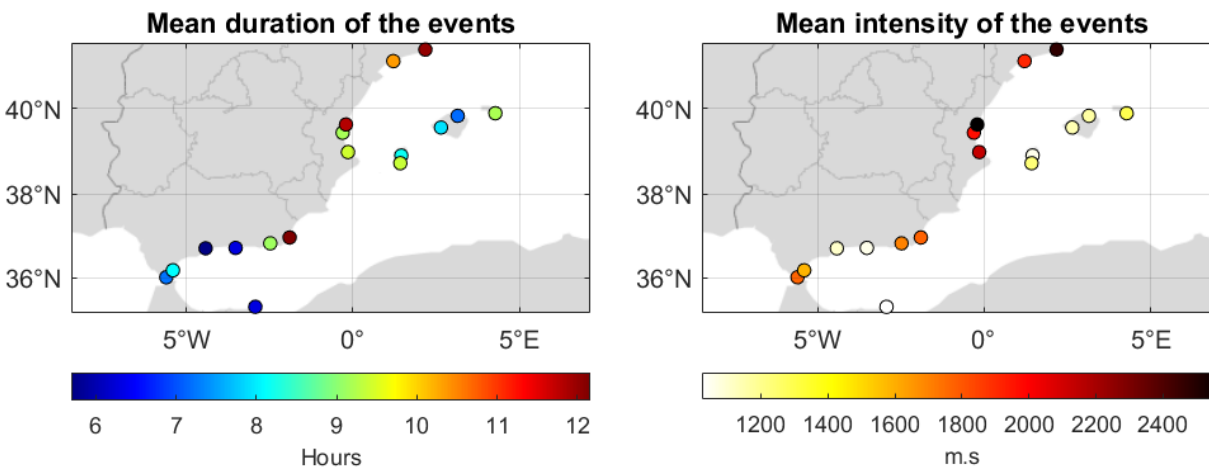


Figure 6: Mean duration (a) and mean intensity (b) of the extreme sea level events identified in the tide gauge records listed in Table 1.

Table 3: Additional information on the extreme sea level events identified in the tide gauge records of Table 1: maximum peak value, 99th percentile of the series, maximum duration, maximum intensity and 15-year return levels computed from hourly and minute series. The values in brackets of the last column are the % of increase with respect to the return levels computed from hourly series.

Station	99th percentile (m)	Maximum level (m)	Maximum duration (days)	Maximum intensity ($\cdot 10^3$ m·s)	Hourly 15-year return levels (m)	Minute 15-year return levels (m)
Tarifa	0.71	1.09	1.21	16.60	1.02	1.07 (5 %)
Algeciras	0.56	0.84	1.75	13.87	0.8	0.84 (5 %)
Málaga	0.39	0.71	3.22	25.59	0.63	0.75 (19 %)
Motril	0.35	0.62	3.12	18.99	0.55	0.66 (20 %)
Melilla	0.31	0.56	3.89	27.57	0.49	0.56 (14 %)
Almería	0.29	0.50	6.15	38.96	0.46	0.52 (13 %)
Carboneras	0.25	0.43	4.42	25.17	0.4	0.43 (8 %)
Gandía	0.27	0.44	6.36	56.78	0.4	0.44 (10 %)
Valencia	0.27	0.44	6.13	55.52	0.4	0.44 (10 %)
Sagunto	0.27	0.43	5.97	55.63	0.41	0.43 (5 %)
Tarragona	0.27	0.45	5.72	52.25	0.42	0.45 (7 %)
Barcelona	0.29	0.45	5.34	47.34	0.43	0.45 (5 %)
Ibiza	0.25	0.45	3.56	14.55	0.38	0.46 (21 %)
Formentera	0.26	0.47	7.33	30.77	0.4	0.46 (15 %)
Palma	0.26	0.46	4.69	18.22	0.41	0.48 (17 %)
Alcudia	0.28	0.49	5.30	24.59	0.43	0.49 (14 %)
Mahón	0.28	0.49	5.08	20.20	0.44	0.49 (11 %)

328 The duration and intensity of the identified extreme events is shown in Fig. 6. The mean duration
329 ranges between 5.7 and 12.2 hours, with the largest values obtained in the northern sector of the
330 Iberian peninsula coasts and the smallest values corresponding to stations near the Strait of
331 Gibraltar (Fig. 6a). The mean intensity shows a similar pattern regarding the largest values,
332 which exceed 2400 m·s for Barcelona and Sagunto stations; the smallest intensities correspond
333 to the stations of the Balearic archipelago and the Alborán Sea (Fig. 6b).

334 Table 3 provides further information on the identified extreme events: the maximum peak value,
335 the 99th percentile of the series, the maximum duration and intensity and the 15-year return
336 levels are reported for each station. As expected, the maximum peak values correspond to the
337 stations close to the Strait of Gibraltar; namely, the largest maximum for the considered period is

338 the 1.1 m obtained in Tarifa. The 99th percentiles, which are used as thresholds to identify
 339 extreme sea level levels, show a distribution similar to that of the maximum values, with a
 340 maximum of 0.71 m at Tarifa and a minimum of 0.25 m at Carboneras (southeast coast of the
 341 Iberian Peninsula). The maximum durations shows that sea level can be above the 99th
 342 percentile for more than 1 week (e.g. in Formentera). As it was the case for the mean duration,
 343 also the maximum durations are shorter close to the Strait of Gibraltar and larger at the northeast
 344 coast of the Iberian peninsula. The maximum intensities correspond to the east coast of the
 345 Iberian Peninsula, more precisely to the Gulf of Valencia, a region that is prone to the
 346 topographic blocking of storms coming from the East.

347 The computation of the monthly distribution of extreme events for each tide gauge of Table 1
 348 (Fig. 7) confirms that they mostly occur in autumn, with October and November accounting for
 349 the highest number of events in almost all stations. The lowest occurrence is observed in late

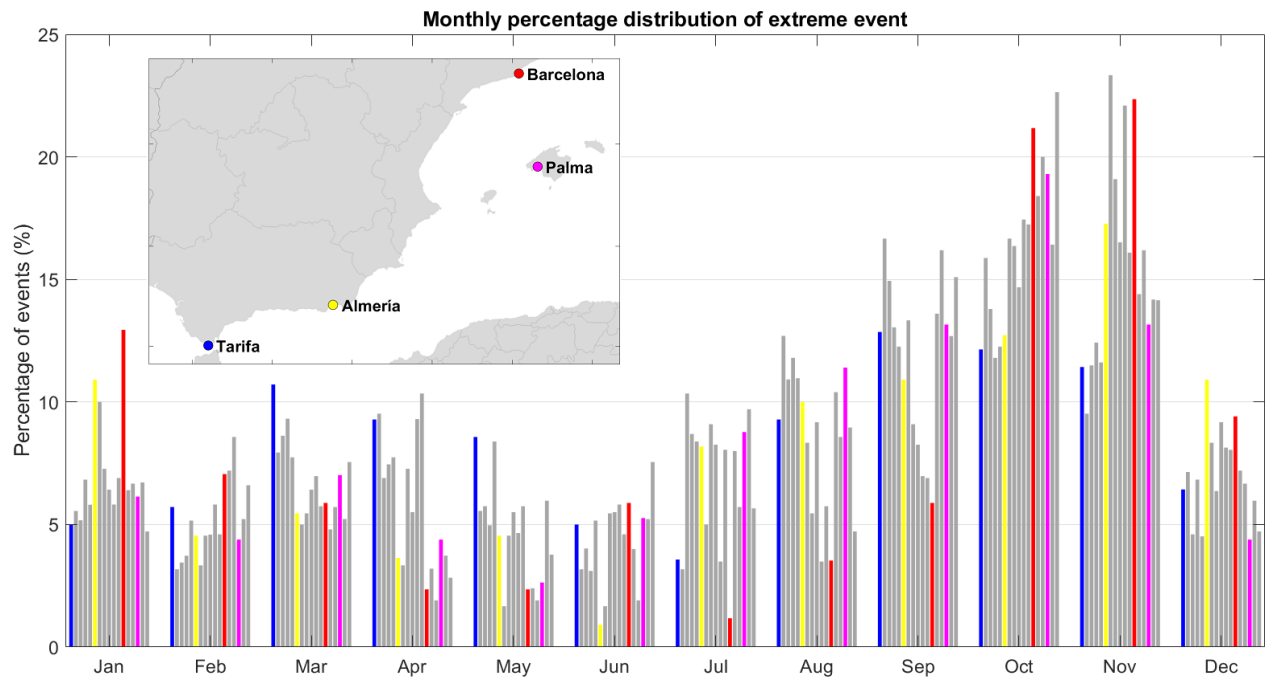


Figure 7: Monthly percentage distribution of extreme events in each tide gauge of Table 1. Four stations distributed throughout the basin (Tarifa, Almería, Barcelona and Palma) have been highlighted in colour.

350 spring and early summer. For the tide gauges located near the Strait of Gibraltar (Tarifa,
 351 Algeciras, Málaga, Motril, and Melilla), autumn is still the main season for extreme events, but
 352 the month with the highest occurrence is September. Moreover, the extreme events identified in
 353 these stations are more uniformly distributed throughout the year than for the stations located in
 354 the east coast of the Iberian Peninsula and the Balearic Islands.

355 A key feature revealed by Table 3 is the importance of using high frequency sea level series for
 356 studying extreme events. Comparing the return levels obtained from the minute and hourly
 357 series, the first exceed the second by an average of 6 cm. In relative terms, the increase in the
 358 return levels when using minute time series ranges between the ~5% of Tarifa, Algeciras,
 359 Sagunto and Barcelona to the ~20% of Málaga, Motril and Ibiza, the average increase being of
 360 about 11%.

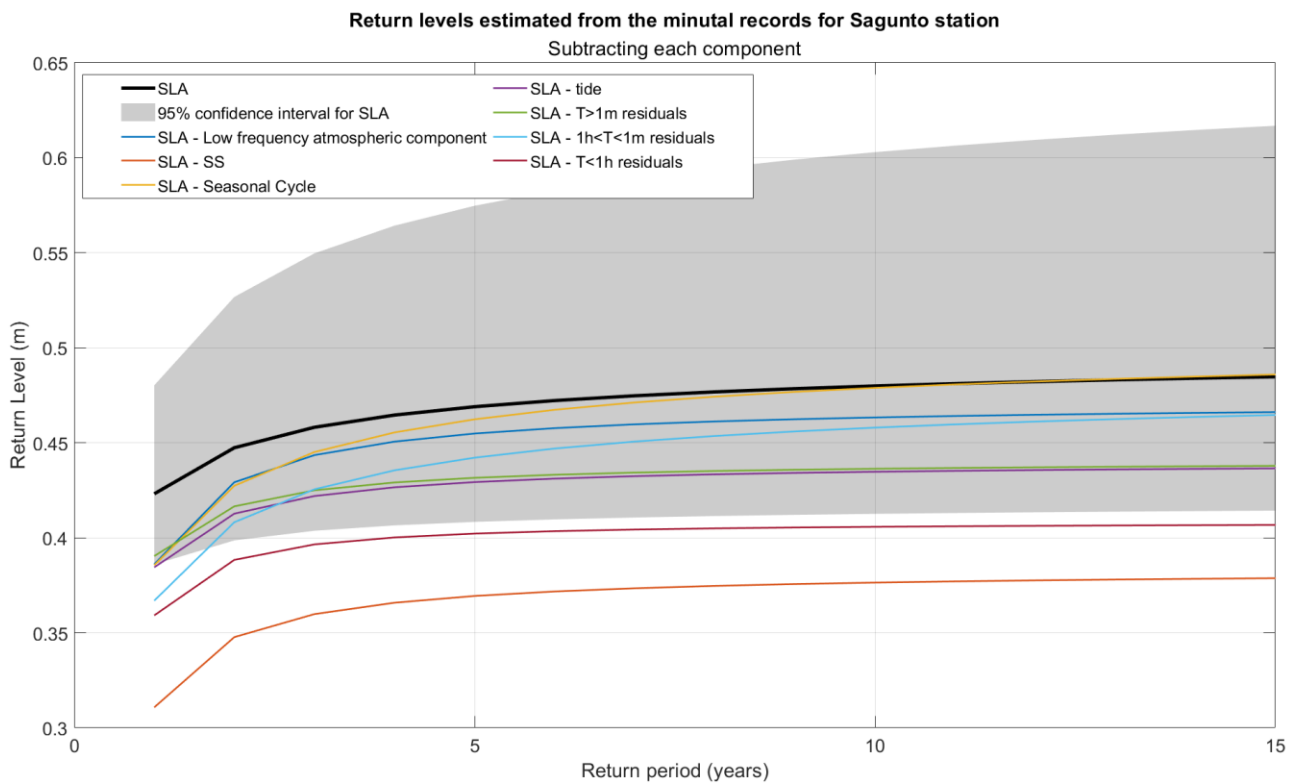


Figure 8: Estimated return levels for the Sagunto tide gauge. They are computed for the total SLA series and for the series resulting after the subtraction of each component. The grey area delimits the 95% confidence intervals of the original series return levels.

361 In order to highlight the importance of high-frequency processes, Fig. 8 shows the return levels
362 computed for Sagunto, a tide gauge reporting large duration and intensity values but with the
363 smallest difference between return levels computed from hourly series and minute series. The
364 figure shows the return levels for the total SLA series and those obtained after subtracting each
365 components from the total series. The decrease in the return levels observed after the subtraction
366 of a components gives an idea of the relevance of that component. The largest reduction, slightly
367 more than 10 cm, is obtained when subtracting the storm surge, and the second one, of the order
368 of 7-8 cm, when subtracting the sub-hourly residuals. Removing the atmospheric signal with $T > 1$
369 month reduces the return levels by about 5 cm, and subtracting the other components results is
370 less relevant reductions. That is, high frequency ($T < 1h$) processes are the second most relevant
371 contributor to return levels even at the station with the smallest difference between return levels
372 computed from hourly series and minute series. In general, the largest reductions in return levels
373 are obtained when subtracting storm surge and high-frequency residuals at stations with a
374 microtidal regime, whereas at those stations with a meso-tidal regime, the originally larger return
375 levels are considerably reduced when subtracting the tide.

376 3.2 Contributors to the extreme events

377 The contribution of the tidal component is obviously very different between the stations with a
378 meso-tidal regime (those located in the Alborán Sea) and the stations with a micro-tidal regime
379 (those located on the eastern Iberian coast and the Balearic Islands). Therefore, when quantifying
380 the different contributions of extreme sea levels the stations have been separated into two groups
381 according to their tidal regime (Fig. 9). For the stations with a microtidal regime the most
382 important contributions are atmospheric: the median values of the low frequency atmospheric
383 contribution account for 5-14% of the peak values, while the median values of the storm surge
384 account for 20-31% of the peak values. The contributions from sub-hourly periods also stands
385 out as a relevant component, accounting for 8-24% of the peak values. For stations with a meso-
386 tidal regime, the tide is by far the most important component, with a contribution that strongly
387 depends on location: from the 88% of Tarifa (located just at the Strait of Gibraltar) to the 38% of
388 Almería (located at the eastern boundary of the Alborán Sea). However, for an extreme event to
389 take place, it is usually necessary that during neap tides some other component has a high value.
390 The median contributions of the other components to peak values are: 1-5% from low frequency

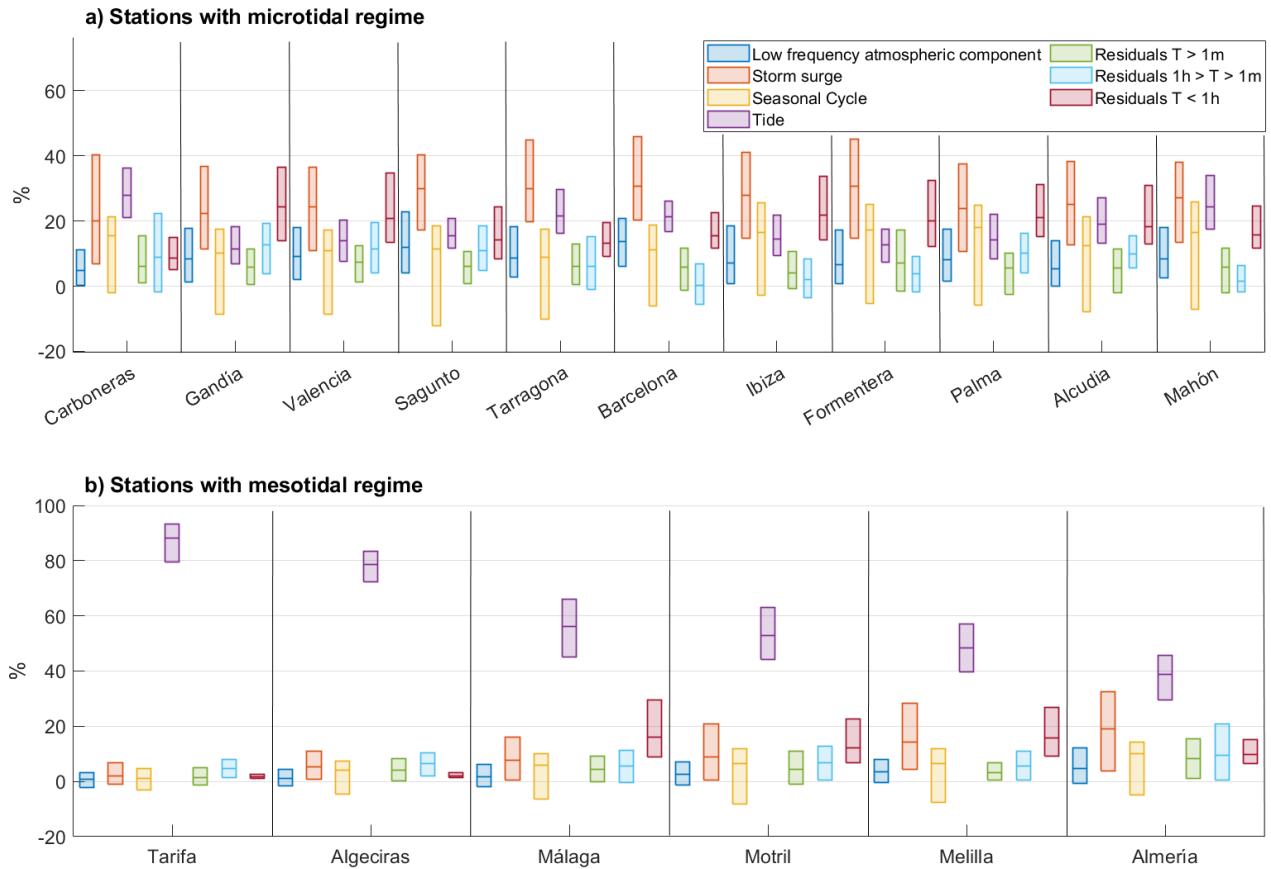


Figure 9: Percentage contributions of each sea level component to the peaks of extreme events identified in: a) tide gauges of Table 1 with a microtidal regime; b) tide gauges of Table 1 with a meso-tidal regime. Boxplots report the median (inbox solid lines) and the 25th and 75th percentiles (bottom and top limit of the boxes).

391 atmospheric processes, 2-19% from storm surges and 2-16% from high frequency (T<1h)
 392 processes.

393 The relevance of each contributor can also be inferred from the probability of extreme joint
 394 events distributions of total SLA and each component. As an example, Fig. 10 shows the pdfs
 395 obtained for Palma de Mallorca, with the 0 level of total SLA marked in black and the 99th
 396 percentile marked in red. For the case of Palma de Mallorca, the probability of having an
 397 extreme value in the total SLA series is larger (18%) when there is an extreme value in the storm
 398 surge component. However, the sub-hourly residuals (T<1h) are the second most important

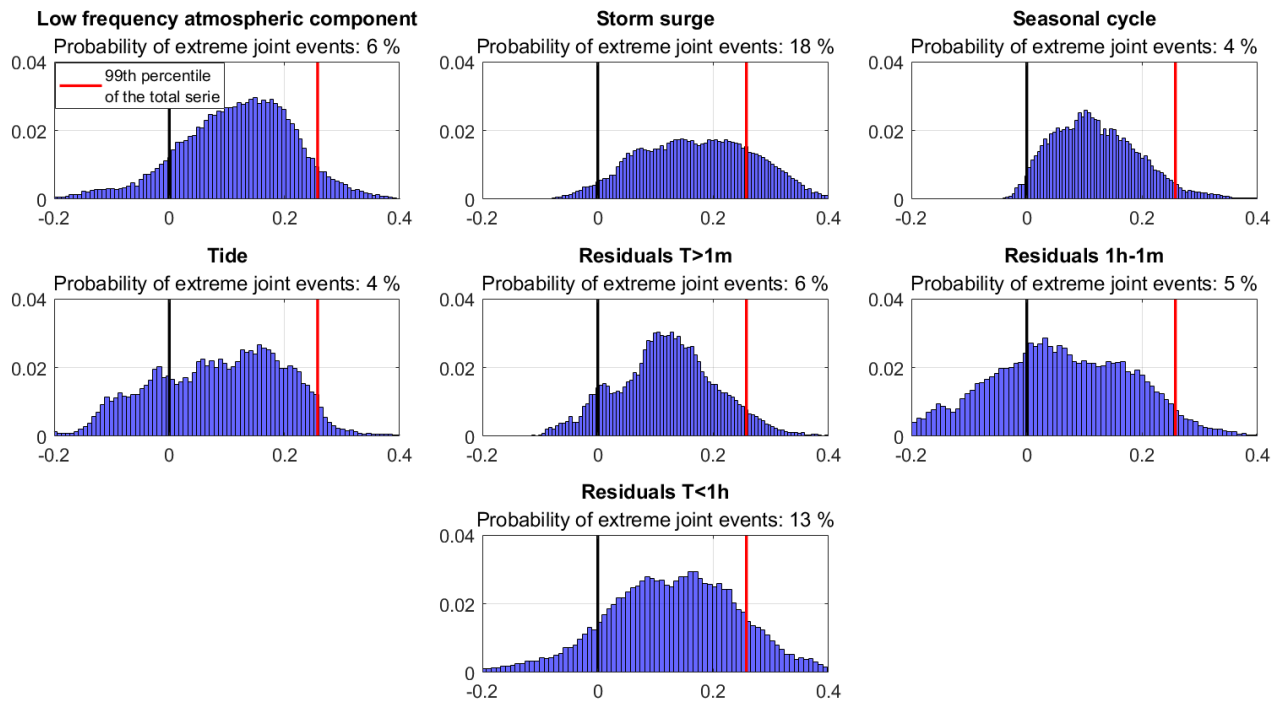


Figure 10: Probability of extreme joint events distributions of total SLA and each component for Palma de Mallorca tide gauge: a) Low-frequency atmospheric component; b) Storm surges; c) Tidal component; d) Seasonal cycle; e) Residuals with $T > 1m$; f) Residuals with $1m < T < 1h$; g) Residuals with $T < 1h$. The black line indicates the 0 level of total SLA marked and the red line indicates the 99th percentile.

399 component, with a probability of 13%. On the other hand, the probability that an extreme in the
 400 total SLA series coincides with an extreme in the tidal and seasonal cycle components is of only
 401 4% in both cases, indicating that these components have a limited impact in this station.
 402 Nevertheless, it is worth noting that the distributions of all components are centred on positive
 403 values, meaning that in general, the presence of extreme values in any component contributes
 404 more or less to having high values in total sea level.

405 Figure 11 shows the results of applying the same analysis to all tide gauges of Table 1. The tidal
 406 contribution is obviously crucial in the occurrence of extreme events near the Strait of Gibraltar.
 407 However, the probability of extreme joint events of this component is about 55% at Tarifa, less

408 than 40% at Algeciras, and smaller at the other stations, indicating that although tides are the
 409 main contributor, high values of other components are also required for an extreme value to
 410 occur. At stations with a microtidal regime, the extremes in the storm surge have the highest
 411 probability of yielding a SLA extreme, with values ranging between 11.2 and 20.2%. The
 412 probability is also significant for subourly residuals, ranging from 5.6 to 13.3% and being
 413 particularly relevant at Gandía, Valencia and the Balearic Islands. The probabilities of the lower
 414 frequency residuals ($T > 1m$ and $1m < T < 1h$) are smaller and have an heterogeneous spatial pattern.

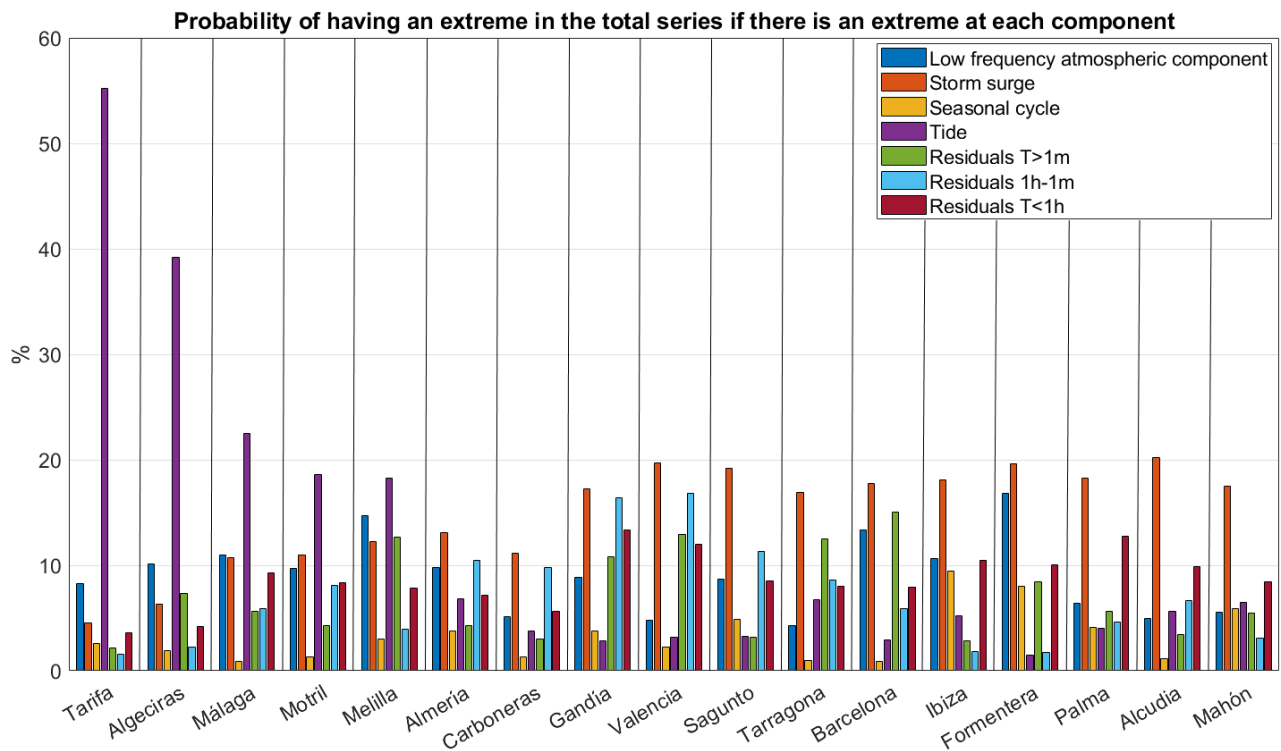


Figure 11: Probability of having an extreme event in the total SLA and simultaneously in one of the different contributors to sea level, estimated for each contributor and each tide gauge of Table 1.

415 3.3 Short-scale spatial variability of extreme events

416 As stated in Section 2, the recent availability of a tide gauge network with an unprecedented
 417 spatial resolution allows some insight into the short-scale spatial variability of extreme events.
 418 The analysis must however be taken with caution, as the short period spanned so far by the series

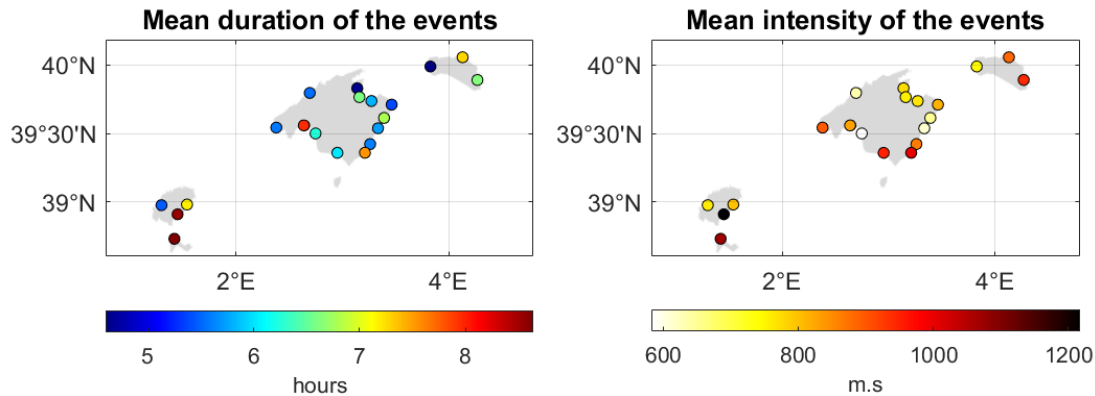


Figure 12: a) Average duration of extreme events in each station of the Balearic Islands, b) Average intensity of extreme events in each station of the Balearic Islands. Note that different colour maps have been used for each variable.

419 (2 years) does not allow a robust extreme value statistics. Figure 12 shows the mean duration
 420 (Fig. 12a) and mean intensity (Fig. 12b) of the extreme events identified for each tide gauge of
 421 Table 2. As a consequence of the short time period considered here, the five stations already used
 422 in Fig. 6 (in that case spanning more than 12 years) show similarities, but also some
 423 differences with respect to Fig. 12. Thus, the mean intensities of the events shown in Fig. 12 are
 424 considerably lower than those of Fig. 6, due to the smaller number of high level events in the
 425 series. Regarding the duration of the events (Fig. 12a), Palma, S'Arenal, Ibiza, and Formentera
 426 stand out, with a mean duration of more than 8 hours. The highest mean intensity corresponds to
 427 Ibiza, and amounts to ~ 1200 m.s. Table 4 shows additional information on the extreme events
 428 identified in each tide gauge record. The 99th percentiles are between 25 and 29 cm for all the
 429 stations, and the highest sea level value recorded in the region during the two-year period is the
 430 73 cm recorded at Ciutadella. That location is well known for the occurrence of large amplitude
 431 sea level oscillations resulting from the resonant response of the harbour to incoming
 432 meteotsunami waves (locally known as “rissaga”, see e.g. Monserrat et al., 2006). The maximum
 433 duration and intensities are very heterogeneous throughout the stations, with the longest event
 434 lasting 3.5 days (in Sa Ràpita) and the most intense event amounting almost $18.7 \cdot 10^3$ m.s (in
 435 Andratx). Since the results obtained so far indicate that the contribution of sub-hourly processes
 436 can be quite relevant, the focus will now be put on the variability of this high-frequency

437 component in the regional context of the Balearic Islands (the domain covered by the dense
438 network of tide gauges).

439 Figure 13 shows the percentage contribution of sub-hourly processes to the peak value of the
440 extreme events identified in each tide gauge. Results show a marked heterogeneity, even for
441 stations separated a few kilometres. The stations with the highest contribution from this

Table 4: Information on the extreme events identified in each series in the Balearic Islands: maximum value reached, 99th percentile of the series, duration of the longest event recorded, and maximum intensity recorded for an event.

Station	99th percentile (m)	Maximum (m)	Maximum duration (days)	Maximum intensity ($\cdot 10^3$ m·s)
Formentera	0.25	0.43	1.9	9.69
Sant Antoni	0.26	0.55	1.58	7.98
Ibiza	0.25	0.48	2	10.47
Santa Eulàlia	0.25	0.54	2.37	7.01
Sa Ràpita	0.26	0.58	3.53	18.46
S'Arenal	0.29	0.49	1.41	2.9
Palma	0.25	0.52	3.04	15.2
Palma	0.28	0.43	1.5	4.44
Andratx	0.26	0.5	3.35	18.67
Port de Sóller	0.28	0.52	1.15	5.19
Alcudia	0.28	0.54	2	12.35
Can Picafort	0.28	0.58	1.18	3.73
Colonia Sant Pere	0.26	0.45	1.89	5.46
Cala Rajada	0.26	0.5	2.05	11.45
Cala Bona	0.27	0.41	1.22	2.81
Porto Cristo	0.27	0.56	1.59	8.46
Portocolom	0.27	0.64	2.61	13.1
Portopetro	0.25	0.47	1.97	9.78
Mahón	0.27	0.51	2.39	11.64
Ciutadella	0.28	0.73	1.57	8.56
Fornells	0.26	0.4	1.55	6.8

442 component are Ciutadella, with a 53.5%, Portocolom with 47.3%, Port de Sóller, with 42.1%,
 443 and Sant Antoni, with 40.7%. All them have at least one event in which the contribution of this
 444 component is greater than 100%, indicating that it is the only responsible for these events (and
 445 that it compensates the negative levels associated with other components). These stations are all
 446 located in sheltered harbours where meteotsunami episodes are relatively frequent (Rabinovich,
 447 2020). On the other hand, there are stations where the contribution of this component is very
 448 small, such as Fornells, Port de Valldemossa or Sa Calobra; these stations are located in places
 449 where neither shelf nor harbour resonance have been reported.

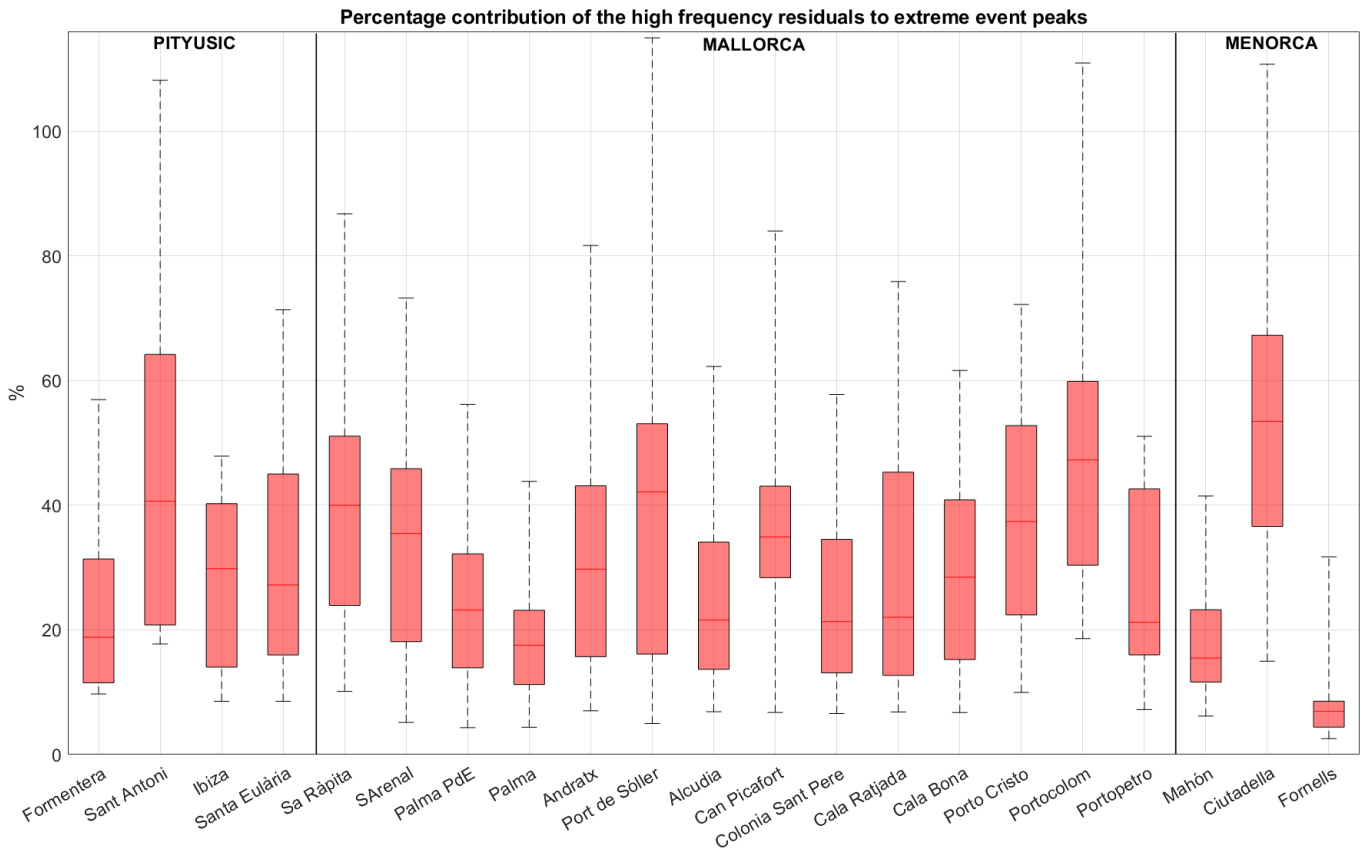


Figure 13: Percentage contributions of high-frequency residuals ($T < 1h$) to extreme sea levels in the Balearic Islands. The stations are separated by islands: Pityusic (Ibiza and Formentera), Mallorca and Menorca. Boxplots report the median (in box solid lines) and the 25th and 75th percentiles (bottom and top limit of the boxes). The whiskers represent the minimum and maximum values of the contribution of this component to the extremes of each series.

450 3.4 Wave contribution to extreme events

451 Here we present the results of the wave contribution to Total Water Level (TWL) at the 20
 452 control points shown in Fig. 4. The maximum value measured by the Palma station operating
 453 with 1-min resolution is 46 cm; the tide gauge is located in the vicinity of point 20 (see Fig. 4),
 454 and it can be considered representative of the sea level of the whole bay without considering the
 455 wave contribution. When the set-up contribution is added, then TWL reaches values between
 456 0.46 and 0.49 m over artificial coastal structures (points 1-6 and 20), and between 0.46 and 0.78
 457 m on the beach (see Table 5). When the RU2% contribution is considered, then TWL reaches

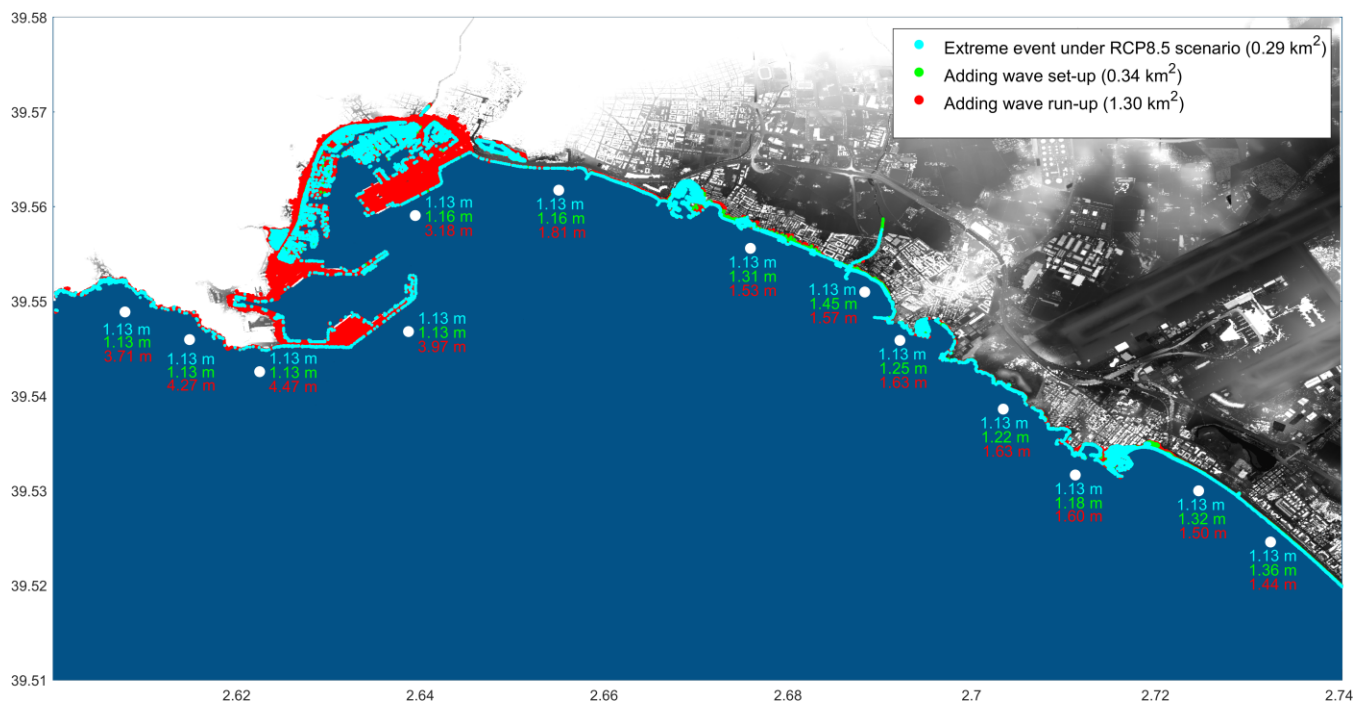


Figure 14: Potentially flood-prone areas of Palma Bay during an intense extreme event occurring under the RCP8.5 scenario projected for the end of the century (2080-2100). Cyan areas are those flooded without considering the wave contribution, green areas are those flooded when considering the wave set-up contribution, and red areas are those impacted when adding the RU2% contribution. The vertical values of sea level at each control point (TWL) are also given with and without the wave contribution.

Table 5: Total Water Level (TWL) at the 20 shore points of Palma Bay shown in Fig. 4. It includes the TWL when adding the wave set-up, provided by the SWAN model, and the TWL calculated when adding the estimated wave run-up contribution, both considering the maximum level recorded at Palma tide gauge (0.46 m); the type of coastal protection and the parameterisation used in the calculation of the RU2% are indicated for each point. Future TWLs would be obtained by adding a mean sea level rise of 0.67m (the regional value projected for 2100 under the RCP8.5 scenario) to present TWLs.

Control point	Coastal typology	TWL when adding set-up (m)	TWL when adding RU2%	
			Source	Value (m)
1	Dike	0.46	Eurotop	3.29
2	Dike	0.46	Eurotop	3.04
3	Dike	0.46	Eurotop	3.60
4	Dike	0.46	Eurotop	3.80
5	Dike	0.46	Eurotop	3.30
6	Dike	0.49	Eurotop	2.51
7	Beach	0.64	ST2006	0.86
8	Beach	0.78	ST2006	0.90
9	Beach	0.58	ST2006	0.96
10	Beach	0.55	ST2006	0.96
11	Beach	0.51	ST2006	0.93
12	Beach	0.65	ST2006	0.83
13	Beach	0.69	ST2006	0.77
14	Beach	0.67	ST2006	0.75
15	Beach	0.63	ST2006	0.73
16	Beach	0.48	ST2006	0.79
17	Beach	0.48	ST2006	0.90
18	Beach	0.46	ST2006	1.00
19	Beach	0.46	ST2006	1.00
20	Vertical	0.49	Eurotop	1.14

458 values between 1.14 and 3.80 m over artificial coastal structures (points 1-6 and 20), and
459 between 0.73 and 1.00 m on the beach. The contribution of waves is therefore very relevant,
460 specially in the artificial parts of the shore, where TWL can exceed the maximum tide gauge
461 value by more than 3 m. It is worth noting that set-up contribution typically lasts as long as the

462 storm duration is (~hours), while the maximum values associated with the RU2% have a
463 duration determined by the wave period (~10 secs).

464 The contributions of the wave set-up and the RU2% have been considered separately, as their
465 durations are different: whereas set-up leads to a more persistent total level rise over the duration
466 of the storm, the RU2% generates a periodic vertical elevation with the period of incoming
467 waves. This makes that the coastal areas reached by the set-up can be effectively flooded;
468 conversely, the flow associated with the RU2% is too small as to flood all the area predicted by
469 the bathtub approximation, even if the effect of the swash in storms can be a major hazard in
470 coastal regions. Under the RCP8.5 scenario, future TWL would be equal to present values plus
471 0.67 m, the mean sea level rise projected for the end of this century. Under that scenario, the
472 potentially floodable areas of Palma Bay during an intense extreme event are shown in Fig. 14.
473 When the contribution of waves is not considered, the floodable area along the bay coast is 0.29
474 km². When adding the estimated wave set-up, the potentially floodable area increases up to 0.34
475 km², that is, an additional 17%. The impacted area when considering the runup is 1.30 km²,
476 which is an increase of almost 350% over the area covered by the still water level.

477 3.5. Spatial scale of main contributors

478 The spatial scales of the extreme sea level events identified in the total series, and of the extreme
479 values of the main contributors to these events are inferred from Fig. 15. This Figure shows, for
480 all station pairs, the correlation between the time sequence of peaks identified at each station.

481 The correlations between station pairs have been computed for the total series (Fig. 15a), the low
482 frequency atmospheric component (Fig. 15b) and the storm surge component (Fig. 15c), and are
483 represented in all cases as a function of the distance between the two stations. The stations
484 considered for the referred components are the 17 tide gauges listed in Table 1, which result in a
485 total of 136 station pairs. For the sub-hourly residuals ($T < 1h$), which are expected to have a
486 shorter spatial scale, the stations considered are the 21 tide gauges located in the Balearic
487 archipelago (listed in Table 2); in this case the number of correlation values between station pairs
488 is 210 (Fig. 15d).

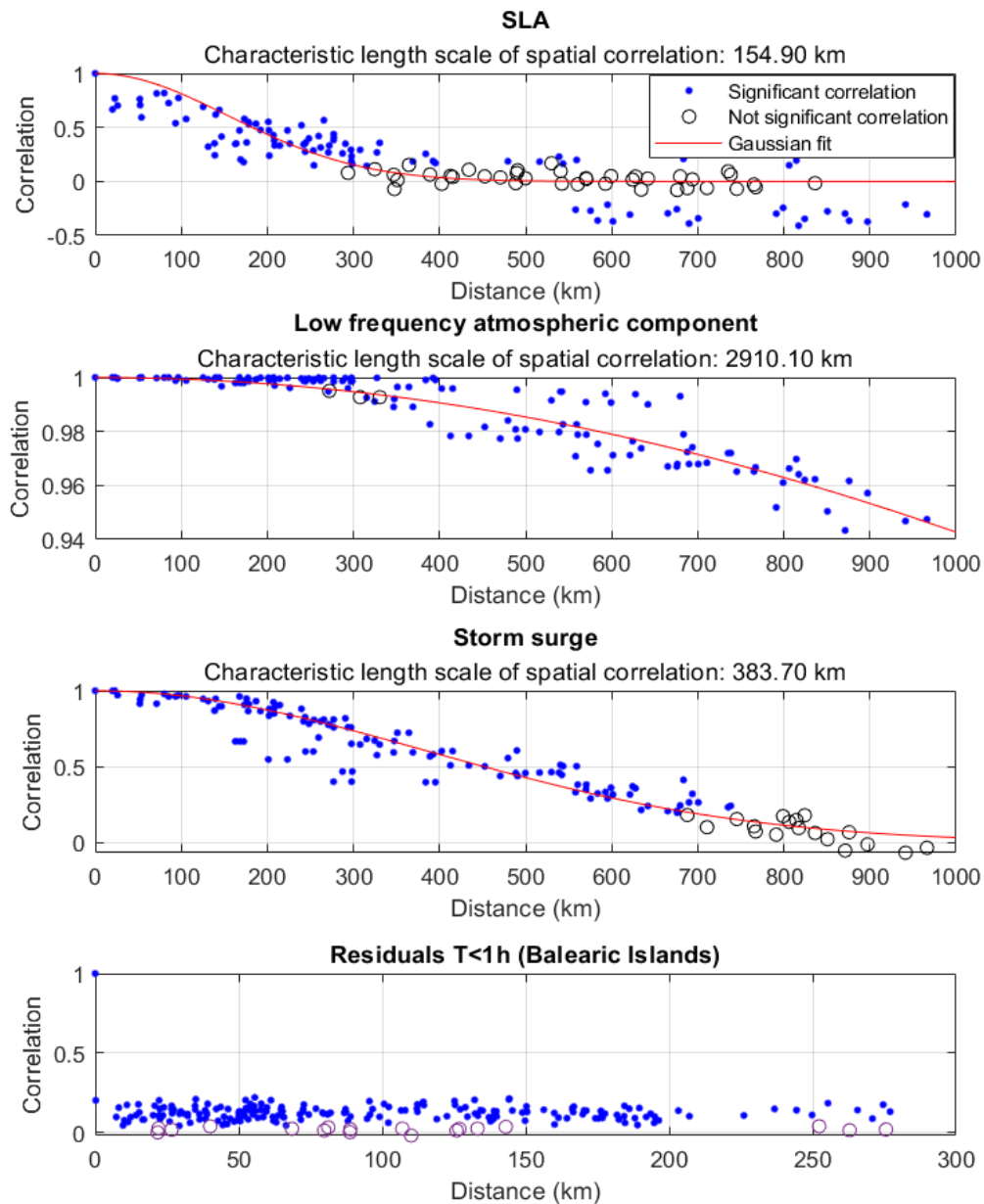


Figure 15: Correlation between the time sequences of peak values identified at each station pair. The correlation value obtained for each station pair is plotted as a function of the distance between the two stations in the form of a blue square (when the correlation is statistically significant) or an empty circle (when the correlation is not statistically significant). The procedure has been applied to the Western Mediterranean tide gauges of Table 1 (spanning the period 2010-2022) for: a) the total SLA series; b) the low frequency atmospheric component; c) the storm surge component; and to the Balearic Island tide gauges of Table 2 (spanning the period 2020-2022) for: d) the subhourly component. Note that the x-axis (distances) of panel d) are different from the other three panels.

489 For the extreme events of the low frequency atmospheric component and of the storm surge
490 component, the fit of Eq. (3) to the significant correlations resulted in characteristic scale values
491 of about 2900 km and 380 km, respectively. These values are consistent with the typical scales of
492 the perturbations generating the extreme sea levels associated with these components. The
493 characteristic scale obtained for total SLA is about 150 km; in this case, extreme values result
494 from the overlapping of different processes with different scales, so that the value of 150 km
495 must be considered a sort of average scale. The correlations obtained for the sub-hourly
496 component are in general very low, regardless of the distance between stations, which prevents
497 the estimation of a meaningful characteristic length scale for this component.

498 **4. Discussion**

499 A major objective of this work was to revisit the characteristics of extreme sea level events in the
500 Western Mediterranean in the light of tide gauge data with a high spatio-temporal resolution. The
501 importance of extreme events in that region is demonstrated by their duration (the time during
502 which sea level remains above the 99th percentile during the event), which can be of more than
503 one week during intense events.

504 The sampling rate of tide gauges has often been a limiting factor for the identification of the
505 actual magnitude of the peaks, since relevant high-frequency processes remain undersampled
506 when using hourly records, for instance. Thus, previous works had already anticipated that the
507 estimated return levels would increase if working with sea level series with a sampling period
508 smaller than 1 hour (Tsimplis et al., 2009). Here we have shown that 15-yr return levels do
509 indeed increase, namely between 5% to 20%, when working with minute series instead of hourly
510 series. In terms of physical processes, missing the contribution of high frequencies to extreme
511 sea levels leads to an overestimation of the importance of other contributions such as storm
512 surges, to the point that the latter are often considered the only process responsible for extreme
513 values.

514 A second, related objective of the work was the quantification of the contribution of different
515 physical processes to extreme events. In many works, the residuals of de-trended and de-tided
516 hourly series are directly considered as storm surges (see e.g. Enríquez et al., 2020; Haigh et al.,
517 2016; Marcos & Woodworth, 2017). Here, we have split the total SLA series into different

518 contributions beyond tides and storm surges, finding that the de-tided residuals of the series after
519 removing the steric and the atmospheric component can significantly contribute to the extreme
520 levels, at least in some cases and at some stations. In fact, at many coastal sites with a micro-tidal
521 regime (the whole Western Mediterranean except the Alborán Sea), sub-hourly processes (which
522 include for instance meteotsunamis and shelf waves) are the second most important contributor
523 to extreme levels, storm surges being always the main contributor. It is also worth noting, that
524 even if storm surges are the main contributor, they contribute to 20-30 % of the peak level,
525 which enforces the idea that extreme events require multiple contributions from different
526 mechanisms.

527 The deployment in the Balearic Islands of a tide gauge network with an unprecedented spatio-
528 temporal resolution has allowed a further insight into the contribution of sub-hourly residuals to
529 extreme levels. It has been shown that high frequency processes ($T < 1$ h) are a key factor in the
530 occurrence of extreme events in some ports, and that they are often absolutely local processes. In
531 this sense it is worth noting that the conventional tide gauge networks (i.e. with less spatial
532 resolution), may be unadequate to assess the importance of those events.

533 A third key feature of the study has been the evaluation of the impact that waves can have on
534 total sea levels measured at the coast. The contribution of waves is highly dependent on the
535 morphology of the coast (e.g., the estimated wave runup is considerably higher in the presence of
536 rigid structures than on beaches) and on the orientation of the coastline with respect to the
537 direction of the waves. Namely, our case study for the Bay of Palma has shown that during an
538 intense event, sea level at coastal sites with artificial structures can be up to 2.5 m higher than in
539 neighbouring sites with a beach-type morphology. Therefore, the approach followed in some
540 works in which the wave runup is quantified without a detailed consideration of the coastline or
541 coastal structure (see e.g. Melet et al., 2018; Sayol & Marcos, 2018) may be too simplistic. On
542 the other hand, it should also be noted that those extreme values would occur over short periods
543 (~secs), as they are associated to the swash part of the wave runup. Thus, the flood-prone areas
544 shown in Fig. 14 constitute only a first illustrative approximation, as the bathtub approach tends
545 to overestimate the extent of the flooded area.

546 Finally, regarding the characteristic spatial scale of the main contributors to extreme levels, it
547 seems clear that the atmospheric contribution operates over a wide range of spatial scales: from

548 ~3000 km in the case of the low frequency atmospheric component to a few km in the case of the
549 resonant response of shelves and harbours. In fact, the inference of a characteristic scale for the
550 subhourly residuals has not been possible, even using a tide gauge network with a mean
551 separation distance of ~10 km in large parts of the domain. The characteristic scale of storm
552 surges has been quantified in 380 km, a value that differs significantly from the results given in
553 other studies. Thus, Enríquez et al. (2020), who also estimated the spatial footprints of storm
554 surges in the Western Mediterranean, obtained a coastal correlation length of 830 km (using a
555 clustering analysis technique) and cluster lengths between 2000 and 3500 km (using the match
556 level analysis and copula analysis methods). The differences are likely due to the fact that
557 Enríquez et al. (2020) considered as storm surge all non-tidal residuals; this includes the low-
558 frequency atmospheric component, which has been analysed separately in our work and for
559 which we have obtained a characteristic scale of a few thousand km.

560 **5. Conclusions**

561 In this work we have provided a detailed description of the extreme events observed by tide
562 gauges deployed on the coasts of the Western Mediterranean basin. We have analysed different
563 time scales separately, in order to characterise and quantify the different processes that contribute
564 to the occurrence of extreme sea levels on the coast. The different tidal regimes of the analysed
565 domain condition the magnitude of extreme levels and determine at least in part the relative
566 importance of the different components of extreme events. A feature common to the whole
567 domain is that Autumn is clearly the season with the highest occurrence of extreme events.

568 A main conclusion of this work is that the availability of sea level records with a high sampling
569 rate is of paramount importance for the study of extreme levels. Records with a 1-minute
570 sampling interval allow a better identification of the contributors to coastal extreme sea level and
571 a more accurate estimation of the maximum value of the peaks. In fact, they allow taking into
572 account processes that are usually not considered in previous works using hourly time series.

573 For the stations of the Western Mediterranean with a microtidal regime, the main contributors to
574 the extreme values are the storm surge, the low frequency component of the atmospheric
575 contribution, and the sub-hourly processes. The tidal contribution is more important close to the
576 Strait of Gibraltar, but still requires peaks in other components for an extreme to occur. The high

577 spatio-temporal resolution resulting from the deployment of the VENOM tide gauges (altogether
578 with the tide gauges operated by other institutions in the Balearic Islands) has allowed a further
579 insight into the contributions of sub-hourly processes to extreme sea levels. We have shown that
580 these processes have a very small spatial scale, but they can nevertheless be very important at
581 certain locations, becoming eventually the main contribution. The ports where this contribution
582 is most important coincide with those places where meteotsunamis are usually reported,
583 indicating that these phenomena are the dominant processes of the sub-hourly domain.

584 Finally, we have shown that waves can play a key role in the total water level reached during
585 extreme events, as they can lead to a rise of several meters. The contribution of waves to coastal
586 sea level is highly dependent on the type of coastal structure, reaching considerably higher
587 values when they imping on rigid protections. As an application, we have obtained a first
588 approximation to potentially flood-prone areas of the Bay of Palma during extreme events. The
589 methodology applied to propagate the waves and obtain the flooding areas could be extrapolated
590 to other regions. By adding the mean sea level rise projected under future climate scenarios, they
591 constitutes a useful tool for stakeholders dealing with the coastal adaptation to climate change.

592 **Acknowledgments**

593 This work is part of the R+D+I coordinated project VENOM (PGC2018-099285-B-C21,
594 PGC2018-099285-B-C22) and the project UNCHAIN (PCI2019-103680), both funded by
595 MCIN/AEI/10.13039/501100011033 and by the ERDF (A way of making Europe). This research
596 has been supported by the Ministerio de Ciencia e Innovación and the European Regional
597 Development Fund, Interreg. We thank the data providers (Puertos del Estado, SOCIB and Ports-
598 IB) for making their datasets freely available. We also want to thank the support of the Balearic
599 Holding of Harbours (Ports-IB) to the deployment of the VENOM tide gauge network and all the
600 members of the Sea Level and Climate group that have participated in the design, installation and
601 maintenance of the network, particularly Joan Puigdefabregas, Aida Frank-Comas, Joan
602 Villalonga, Joaquim Tomàs-Ferrer, Albert Font and Javier Soto-Navarro.

603

604 **Open Research**

605 The data of the REDMAR tide gauges network of Puertos del Estado are accessible through its
 606 web catalogue (<https://opendap.puertos.es/thredds/catalog.html>, last accessed 9 february 2023,
 607 Pérez et al., 2013). In the same catalogue the outputs of the NIVMAR forecasting system
 608 (https://opendap.puertos.es/thredds/catalog/nivmar_large_nivmar/catalog.html, last accessed 9
 609 february 2023, Álvarez Fanjul et al., 2001) are also available. The wave parameters of the
 610 SIMAR wave hindcast can be consulted on the web page of Puertos del Estado
 611 (<https://www.puertos.es/es-es/oceanografia/Paginas/portus.aspx>, last accessed 9 february 2023,
 612 Pilar et al., 2008). The bathymetric grid used for the shoreward wave propagation was obtained
 613 from the GEBCO website (<https://www.gebco.net/>, last accessed 9 february 2023, Weatherall et
 614 al., 2015). The code developed to identify and analyse the extreme events of the tide gauge series
 615 can be accessed at <https://doi.org/10.5281/zenodo.7848818> (Ramos-Alcántara et al., 2023).

616 **References**

- 617 Abu Zed, A. A., Kansoh, R. M., Iskander, M. M., & Elkholy, M. (2022). Wind and wave climate
 618 southeastern of the Mediterranean Sea based on a high-resolution SWAN model.
 619 *Dynamics of Atmospheres and Oceans*, 99, 101311.
 620 <https://doi.org/10.1016/j.dynatmoce.2022.101311>
- 621 Agulles, M., Jordà, G., & Lionello, P. (2021). Flooding of Sandy Beaches in a Changing
 622 Climate. The Case of the Balearic Islands (NW Mediterranean). *Frontiers in Marine*
 623 *Science*, 8, 760725. <https://doi.org/10.3389/fmars.2021.760725>
- 624 Álvarez Fanjul, E., Pérez Gómez, B., & Rodríguez Sánchez Arévalo, I. (2001). Nivmar: A storm
 625 surge forecasting system for Spanish waters. *Scientia Marina*, 65(S1), 145–154.
 626 <https://doi.org/10.3989/scimar.2001.65s1145>
- 627 Amores, A., Marcos, M., Carrió, D. S., & Gómez-Pujol, L. (2020). Coastal impacts of Storm
 628 Gloria (January 2020) over the north-western Mediterranean. *Natural Hazards and Earth*
 629 *System Sciences*, 20(7), 1955–1968. <https://doi.org/10.5194/nhess-20-1955-2020>
- 630 Backhaus, J. O. (1985). A three-dimensional model for the simulation of shelf sea dynamics.
 631 *Deutsche Hydrographische Zeitschrift*, 38(4), 165–187.
 632 <https://doi.org/10.1007/BF02328975>

- 633 Booij, N., & Holthuijsen, L. H. (1987). Propagation of ocean waves in discrete spectral wave
634 models. *Journal of Computational Physics*, *68*(2), 307–326.
635 [https://doi.org/10.1016/0021-9991\(87\)90060-X](https://doi.org/10.1016/0021-9991(87)90060-X)
- 636 Calafat, F. M., Avgoustoglou, E., Jordà, G., Flocas, H., Zodiatis, G., Tsimplis, M. N., &
637 Kouroutzoglou, J. (2014). The ability of a barotropic model to simulate sea level
638 extremes of meteorological origin in the Mediterranean Sea, including those caused by
639 explosive cyclones. *Journal of Geophysical Research: Oceans*, *119*(11), 7840–7853.
640 <https://doi.org/10.1002/2014JC010360>
- 641 Calafat, F. M., Gomis, D., & Marcos, M. (2009). Comparison of Mediterranean sea level fields
642 for the period 1961–2000 as given by a data reconstruction and a 3D model. *Global and
643 Planetary Change*, *68*(3), 175–184. <https://doi.org/10.1016/j.gloplacha.2009.04.003>
- 644 Callahan, J. A., & Leathers, D. J. (2021). Estimation of Return Levels for Extreme Skew Surge
645 Coastal Flooding Events in the Delaware and Chesapeake Bays for 1980–2019. *Frontiers
646 in Climate*, *3*, 684834. <https://doi.org/10.3389/fclim.2021.684834>
- 647 Cherif, S., Doblus-Miranda, E., Lionello, P., Borrego, C., Giorgi, F., Iglesias, A., Jebari, S.,
648 Mahmoudi, E., Moriondo, M., Pringault, O., Rilov, G., Somot, S., Tsikliras, A., Vila, M.,
649 & Zittis, G. (2020). Drivers of Change. In W. Cramer, J. Guiot, & K. Marini (Eds.),
650 *Climate and Environmental Change in the Mediterranean Basin – Current Situation and
651 Risks for the Future. First Mediterranean Assessment Report* (pp. 59–180). Union for the
652 Mediterranean, Plan Bleu, UNEP/MAP. 10.5281/zenodo.7100601
- 653 Cid, A., Menéndez, M., Castanedo, S., Abascal, A. J., Méndez, F. J., & Medina, R. (2016).
654 Long-term changes in the frequency, intensity and duration of extreme storm surge
655 events in southern Europe. *Climate Dynamics*, *46*(5–6), 1503–1516.
656 <https://doi.org/10.1007/s00382-015-2659-1>
- 657 Codiga, D. (2023). UTide Unified Tidal Analysis and Prediction Functions. [Software].
658 Mathworks. [https://www.mathworks.com/matlabcentral/fileexchange/46523-utide-
659 unified-tidal-analysis-and-prediction-functions](https://www.mathworks.com/matlabcentral/fileexchange/46523-utide-unified-tidal-analysis-and-prediction-functions)
- 660 de Alfonso, M., Lin-Ye, J., García-Valdecasas, J. M., Pérez-Rubio, S., Luna, M. Y., Santos-
661 Muñoz, D., Ruiz, M. I., Pérez-Gómez, B., & Álvarez-Fanjul, E. (2021). Storm Gloria:
662 Sea State Evolution Based on in situ Measurements and Modeled Data and Its Impact on

- 663 Extreme Values. *Frontiers in Marine Science*, 8, 646873.
664 <https://doi.org/10.3389/fmars.2021.646873>
- 665 Del-Rosal-Salido, J., Folgueras, P., Bermúdez, M., Ortega-Sánchez, M., & Losada, M. Á.
666 (2021). Flood management challenges in transitional environments: Assessing the effects
667 of sea-level rise on compound flooding in the 21st century. *Coastal Engineering*, 167,
668 103872. <https://doi.org/10.1016/j.coastaleng.2021.103872>
- 669 Dey, A. K., & Das, K. P. (2016). Modeling Extreme Hurricane Damage Using the Generalized
670 Pareto Distribution. *American Journal of Mathematical and Management Sciences*,
671 35(1), 55–66. <https://doi.org/10.1080/01966324.2015.1075926>
- 672 Dodet, G., Melet, A., Ardhuin, F., Bertin, X., Idier, D., & Almar, R. (2019). The Contribution of
673 Wind-Generated Waves to Coastal Sea-Level Changes. *Surveys in Geophysics*, 40(6),
674 1563–1601. <https://doi.org/10.1007/s10712-019-09557-5>
- 675 Dupuis, D. J. (1999). Exceedances over High Thresholds: A Guide to Threshold Selection.
676 *Extremes*, 1, 251–261. <https://doi.org/10.1023/A:1009914915709>
- 677 Enríquez, A. R. (2022). MatFlood. [Software]. Zenodo. <https://doi.org/10.5281/zenodo.7448967>
- 678 Enríquez, A. R., Wahl, T., Marcos, M., & Haigh, I. D. (2020). Spatial Footprints of Storm Surges
679 Along the Global Coastlines. *Journal of Geophysical Research: Oceans*, 125(9).
680 <https://doi.org/10.1029/2020JC016367>
- 681 Eurotop, Van der Meer, J. W., Allsop, N. W. H., Bruce, T., De Rouck, J., Kortenhaus, A., Pullen,
682 T., Schüttrumpf, H., Troch, P., & Zanuttigh, B. (2018). *Manual on wave overtopping of
683 sea defences and related structures. An overtopping manual largely based on European
684 research, but for worldwide application.* www.overtopping-manual.com
- 685 Ferrarin, C., Bellafiore, D., Sannino, G., Bajo, M., & Umgiesser, G. (2018). Tidal dynamics in
686 the inter-connected Mediterranean, Marmara, Black and Azov seas. *Progress in
687 Oceanography*, 161, 102–115. <https://doi.org/10.1016/j.pocean.2018.02.006>
- 688 Fiedler, J. W., Smit, P. B., Brodie, K. L., McNinch, J., & Guza, R. T. (2018). Numerical
689 modeling of wave runup on steep and mildly sloping natural beaches. *Coastal
690 Engineering*, 131, 106–113. <https://doi.org/10.1016/j.coastaleng.2017.09.004>
- 691 García-Valdecasas, J., Pérez Gómez, B., Molina, R., Rodríguez, A., Rodríguez, D., Pérez, S.,
692 Campos, Á., Rodríguez Rubio, P., Gracia, S., Ripollés, L., Terrés Nicoli, J. M., de los
693 Santos, F. J., & Álvarez Fanjul, E. (2021). *Operational tool for characterizing high*

- 694 *frequency sea level oscillations*. *106*, 1149–1167.
695 <https://doi.org/10.3989/scimar.2001.65s1145>
- 696 Gomis, D., Tsimplis, M., Marcos, M., Fenoglio-Marc, L., Pérez, B., Raicich, F., Vilibić, I.,
697 Wöppelmann, G., & Monserrat, S. (2012). Mediterranean Sea-Level Variability and
698 Trends. In P. Lionello (Ed.), *The Climate of the Mediterranean Region* (pp. 257–299).
699 Elsevier. <https://doi.org/10.1016/B978-0-12-416042-2.00004-5>
- 700 Haigh, I. D., Wadey, M. P., Wahl, T., Ozsoy, O., Nicholls, R. J., Brown, J. M., Horsburgh, K., &
701 Gouldby, B. (2016). Spatial and temporal analysis of extreme sea level and storm surge
702 events around the coastline of the UK. *Scientific Data*, *3*(1), 160107.
703 <https://doi.org/10.1038/sdata.2016.107>
- 704 Hasselmann, S., Hasselmann, K., Bauer, E., Janssen, P. A. E., Komen, G. J., Bertotti, L.,
705 Lionello, P., Guillaume, A., Cardone, V. C., Greenwood, J. A., Reistad, M., Zambresky,
706 L., & Ewing, J. A. (1988). The WAM Model—A Third Generation Ocean Wave
707 Prediction Model. *Journal of Physical Oceanography*, *18*(12), 1775–1810.
- 708 Holthuijsen, L. H. (2007). *Waves in Oceanic and Coastal Waters*.
- 709 Horsburgh, K. J., & Wilson, C. (2007). Tide-surge interaction and its role in the distribution of
710 surge residuals in the North Sea. *Journal of Geophysical Research*, *112*(C8), C08003.
711 <https://doi.org/10.1029/2006JC004033>
- 712 Huthnance, J. M., Mysak, L. A., & Wang, D.-P. (1986). Coastal trapped waves. In C. N. K.
713 Mooers (Ed.), *Coastal and Estuarine Sciences* (Vol. 3, pp. 1–18). American Geophysical
714 Union. <https://doi.org/10.1029/CO003p0001>
- 715 Lambert, E., Rohmer, J., Le Cozannet, G., & van de Wal, R. S. W. (2020). Adaptation time to
716 magnified flood hazards underestimated when derived from tide gauge records.
717 *Environmental Research Letters*, *15*(7), 074015. [https://doi.org/10.1088/1748-](https://doi.org/10.1088/1748-9326/ab8336)
718 [9326/ab8336](https://doi.org/10.1088/1748-9326/ab8336)
- 719 Larnicol, G., Ayoub, N., & Le Traon, P. Y. (2002). Major changes in Mediterranean Sea level
720 variability from 7 years of TOPEX/Poseidon and ERS-1/2 data. *Journal of Marine*
721 *Systems*, *33–34*, 63–89. [https://doi.org/10.1016/S0924-7963\(02\)00053-2](https://doi.org/10.1016/S0924-7963(02)00053-2)
- 722 Marcos, M., Tsimplis, M. N., & Shaw, A. G. P. (2009). Sea level extremes in southern Europe.
723 *Journal of Geophysical Research*, *114*(C1), C01007.
724 <https://doi.org/10.1029/2008JC004912>

- 725 Marcos, M., & Woodworth, P. L. (2017). Spatiotemporal changes in extreme sea levels along the
726 coasts of the North Atlantic and the Gulf of Mexico. *Journal of Geophysical Research:
727 Oceans*, 122(9), 7031–7048. <https://doi.org/10.1002/2017JC013065>
- 728 Melet, A., Meyssignac, B., Almar, R., & Le Cozannet, G. (2018). Under-estimated wave
729 contribution to coastal sea-level rise. *Nature Climate Change*, 8(3), 234–239.
730 <https://doi.org/10.1038/s41558-018-0088-y>
- 731 Menéndez, M., & Woodworth, P. L. (2010). Changes in extreme high water levels based on a
732 quasi-global tide-gauge data set. *Journal of Geophysical Research: Oceans*, 115(C10),
733 2009JC005997. <https://doi.org/10.1029/2009JC005997>
- 734 Middleton, J. F., & Thompson, K. R. (1986). Return periods of extreme sea levels from short
735 records. *Journal of Geophysical Research*, 91(C10), 11707.
736 <https://doi.org/10.1029/JC091iC10p11707>
- 737 Monserrat, S., Vilibić, I., & Rabinovich, A. B. (2006). Meteotsunamis: Atmospherically induced
738 destructive ocean waves in the tsunami frequency band. *Natural Hazards and Earth
739 System Sciences*, 6(6), 1035–1051. <https://doi.org/10.5194/nhess-6-1035-2006>
- 740 Muis, S., Verlaan, M., Winsemius, H. C., Aerts, J. C. J. H., & Ward, P. J. (2016). A global
741 reanalysis of storm surges and extreme sea levels. *Nature Communications*, 7(1), 11969.
742 <https://doi.org/10.1038/ncomms11969>
- 743 Nicholls, R. J., Hanson, S. E., Lowe, J. A., Warrick, R. A., Lu, X., & Long, A. J. (2014).
744 Sea-level scenarios for evaluating coastal impacts. *WIREs Climate Change*, 5(1), 129–
745 150. <https://doi.org/10.1002/wcc.253>
- 746 Noji, E. K. (1991). Natural Disasters. *Critical Care Clinics*, 7(2), 271–292.
747 [https://doi.org/10.1016/S0749-0704\(18\)30306-3](https://doi.org/10.1016/S0749-0704(18)30306-3)
- 748 Pérez, B., Álvarez Fanjul, E., Pérez, S., de Alfonso, M., & Vela, J. (2013). Use of tide gauge data
749 in operational oceanography and sea level hazard warning systems. *Journal of
750 Operational Oceanography*, 6(2), 1–18.
751 <https://doi.org/10.1080/1755876X.2013.11020147>
- 752 Pérez Gómez, B., Vilibić, I., Šepić, J., Međugorac, I., Ličer, M., Testut, L., Fraboul, C., Marcos,
753 M., Abdellaoui, H., Álvarez Fanjul, E., Barbalić, D., Casas, B., Castaño-Tierno, A.,
754 Čupić, S., Drago, A., Fraile, M. A., Galliano, D. A., Gauci, A., Gloginja, B., ... Zodiatis,

- 755 G. (2022). Coastal sea level monitoring in the Mediterranean and Black seas. *Ocean*
756 *Science*, 18(4), 997–1053. <https://doi.org/10.5194/os-18-997-2022>
- 757 Pilar, P., Soares, C. G., & Carretero, J. C. (2008). 44-year wave hindcast for the North East
758 Atlantic European coast. *Coastal Engineering*, 55(11), 861–871.
759 <https://doi.org/10.1016/j.coastaleng.2008.02.027>
- 760 Rabinovich, A. B. (2020). Twenty-Seven Years of Progress in the Science of Meteorological
761 Tsunamis Following the 1992 Daytona Beach Event. *Pure and Applied Geophysics*,
762 177(3), 1193–1230. <https://doi.org/10.1007/s00024-019-02349-3>
- 763 Raby, A. (2003). *Extreme Waves, Overtopping and Flooding at Sea Defences* [University of
764 Oxford]. <https://ora.ox.ac.uk/objects/uuid:82fcc770-8838-4f9b-9abe-32eecd05f9a>
- 765 Ramos-Alcántara, J., Agulles, M., Villalonga, J., Gomis, D., & Jordà, G. (2023). Sea Level
766 Extremes Analysis [Software]. Zenodo. <https://doi.org/10.5281/zenodo.7848818>
- 767 Rasmussen, C. E., & Williams, C. K. I. (2008). *Gaussian processes for machine learning* (3.
768 print). MIT Press.
- 769 Reek, T., Doty, S. R., & Owen, T. W. (1992). A Deterministic Approach to the Validation of
770 Historical Daily Temperature and Precipitation Data from the Cooperative Network.
771 *Bulletin of the American Meteorological Society*, 73(6), 753–762.
772 [https://doi.org/10.1175/1520-0477\(1992\)073<0753:ADATTV>2.0.CO;2](https://doi.org/10.1175/1520-0477(1992)073<0753:ADATTV>2.0.CO;2)
- 773 Ruggiero, P., Komar, P. D., McDougal, W. G., Marra, J. J., & Beach, R. A. (2001). Wave
774 Runup, Extreme Water Levels and the Erosion of Properties Backing Beaches. *Journal of*
775 *Coastal Research*, 17(2), 407–419.
- 776 Sayol, J. M., & Marcos, M. (2018). Assessing Flood Risk Under Sea Level Rise and Extreme
777 Sea Levels Scenarios: Application to the Ebro Delta (Spain). *Journal of Geophysical*
778 *Research: Oceans*, 123(2), 794–811. <https://doi.org/10.1002/2017JC013355>
- 779 Smyth, G. K. (2005). Numerical Integration. In P. Armitage & T. Colton (Eds.), *Encyclopedia of*
780 *Biostatistics* (p. b2a14026). John Wiley & Sons, Ltd.
781 <https://doi.org/10.1002/0470011815.b2a14026>
- 782 Soto-Navarro, J., Criado-Aldeanueva, F., García-Lafuente, J., & Sánchez-Román, A. (2010).
783 Estimation of the Atlantic inflow through the Strait of Gibraltar from climatological and
784 in situ data. *Journal of Geophysical Research: Oceans*, 115(C10), 2010JC006302.
785 <https://doi.org/10.1029/2010JC006302>

- 786 Stockdon, H. F., Holman, R. A., Howd, P. A., & Sallenger, A. H. (2006). Empirical
787 parameterization of setup, swash, and runup. *Coastal Engineering*, *53*(7), 573–588.
788 <https://doi.org/10.1016/j.coastaleng.2005.12.005>
- 789 Tintoré, J., Vizoso, G., Casas, B., Heslop, E., Pascual, A., Orfila, A., Ruiz, S., Martínez-
790 Ledesma, M., Torner, M., Cusí, S., Diedrich, A., Balaguer, P., Gómez-Pujol, L., Álvarez-
791 Ellacuria, A., Gómara, S., Sebastian, K., Lora, S., Beltrán, J. P., Renault, L., ...
792 Manriquez, M. (2013). SOCIB: The Balearic Islands Coastal Ocean Observing and
793 Forecasting System Responding to Science, Technology and Society Needs. *Marine*
794 *Technology Society Journal*, *47*(1), 101–117. <https://doi.org/10.4031/MTSJ.47.1.10>
- 795 Tolman, H. L. (1991). A third-generation model for wind waves on slowly varying, unsteady,
796 and inhomogeneous depths and currents. *Journal of Physical Oceanography*, *21*(6), 782–
797 797. [https://doi.org/10.1175/1520-0485\(1991\)021<0782:ATGMFW>2.0.CO;2](https://doi.org/10.1175/1520-0485(1991)021<0782:ATGMFW>2.0.CO;2)
- 798 Tsimplis, M. N., Calafat, F. M., Marcos, M., Jordà, G., Gomis, D., Fenoglio-Marc, L., Struglia,
799 M. V., Josey, S. A., & Chambers, D. P. (2013). The effect of the NAO on sea level and
800 on mass changes in the Mediterranean Sea: NAO effects on Mediterranean Sea level.
801 *Journal of Geophysical Research: Oceans*, *118*(2), 944–952.
802 <https://doi.org/10.1002/jgrc.20078>
- 803 Tsimplis, M. N., Marcos, M., Pérez, B., Challenor, P., Garcia-Fernandez, M. J., & Raicich, F.
804 (2009). On the effect of the sampling frequency of sea level measurements on return
805 period estimate of extremes—Southern European examples. *Continental Shelf Research*,
806 *29*(18), 2214–2221. <https://doi.org/10.1016/j.csr.2009.08.015>
- 807 Tsimplis, M. N., & Shaw, A. G. P. (2010). Seasonal sea level extremes in the Mediterranean Sea
808 and at the Atlantic European coasts. *Natural Hazards and Earth System Sciences*, *10*(7),
809 1457–1475. <https://doi.org/10.5194/nhess-10-1457-2010>
- 810 Tsimplis, M. N., & Woodworth, P. L. (1994). The global distribution of the seasonal sea level
811 cycle calculated from coastal tide gauge data. *Journal of Geophysical Research*, *99*(C8),
812 16031. <https://doi.org/10.1029/94JC01115>
- 813 Vilibić, I., & Šepić, J. (2017). Global mapping of nonseismic sea level oscillations at tsunami
814 timescales. *Scientific Reports*, *7*(1), 40818. <https://doi.org/10.1038/srep40818>

- 815 Vousdoukas, M. I., Wziatek, D., & Almeida, L. P. (2012). Coastal vulnerability assessment
816 based on video wave run-up observations at a mesotidal, steep-sloped beach. *Ocean
817 Dynamics*, 62(1), 123–137. <https://doi.org/10.1007/s10236-011-0480-x>
- 818 Wahl, T., Haigh, I. D., Nicholls, R. J., Arns, A., Dangendorf, S., Hinkel, J., & Slangen, A. B. A.
819 (2017). Understanding extreme sea levels for broad-scale coastal impact and adaptation
820 analysis. *Nature Communications*, 8(1), 16075. <https://doi.org/10.1038/ncomms16075>
- 821 Weatherall, P., Marks, K. M., Jakobsson, M., Schmitt, T., Tani, S., Arndt, J. E., Rovere, M.,
822 Chayes, D., Ferrini, V., & Wigley, R. (2015). A new digital bathymetric model of the
823 world's oceans. *Earth and Space Science*, 2(8), 331–345.
824 <https://doi.org/10.1002/2015EA000107>
- 825 Williams, J., Matthews, A., & Jevrejeva, S. (2019). Development of an automatic tide gauge
826 processing system. *National Oceanography Centre Research and Consultancy Report*,
827 64, 26.
- 828 Wilson, A. G., & Adams, R. P. (2013). Gaussian Process Kernels for Pattern Discovery and
829 Extrapolation. *Proceedings of the 30th International Conference on Machine Learning*,
830 28(3), 1067–1075.
- 831 Wolf, J. (2009). Coastal flooding: Impacts of coupled wave–surge–tide models. *Natural
832 Hazards*, 49(2), 241–260. <https://doi.org/10.1007/s11069-008-9316-5>
- 833 Woodworth, P. L., Melet, A., Marcos, M., Ray, R. D., Wöppelmann, G., Sasaki, Y. N., Cirano,
834 M., Hibbert, A., Huthnance, J. M., Monserrat, S., & Merrifield, M. A. (2019). Forcing
835 Factors Affecting Sea Level Changes at the Coast. *Surveys in Geophysics*, 40(6), 1351–
836 1397. <https://doi.org/10.1007/s10712-019-09531-1>
- 837